Physics Reports 1026 (2023) 1–63

Contents lists available at ScienceDirect

Physics Reports

journal homepage: www.elsevier.com/locate/physrep

Perturbative light–matter interactions; from first principles to inverse design

Niclas Westerberg, Robert Bennett *

School of Physics & Astronomy, University of Glasgow, Glasgow, G12 8QQ, United Kingdom

ARTICLE INFO

Article history:
Received 31 August 2022
Received in revised form 24 May 2023
Accepted 24 July 2023
Available online 31 July 2023
Editor: Andreas Buchleitner

Keywords:
Light–matter interaction
Quantum electrodynamics
Macroscopic QED
Inverse design
Dyadic Green's tensor

ABSTRACT

Our experience of the world around us is governed almost entirely by light–matter interactions. At the most fundamental level, such interactions are described by quantum electrodynamics (QED), a well-established theory that has stood up to decades of experimental testing to remarkable degrees of precision. However, the complexity of real systems almost always means that the quantum electrodynamical equations describing a given scenario are often infeasible or impractical to solve. Thus, a sequence of approximations and idealisations are made, in order to build up from the simple case of an isolated electron interacting with a gauge field leading to the deceptively simple laws governing reflection and refraction at mirrors and lenses. This review provides a pedagogical overview of this journey, concentrating on cases where external boundary conditions can be used as a control method. Beginning from the fundamental Lagrangian, topics include gauge freedom, perturbative macroscopic QED descriptions of spontaneous decay, Casimir–Polder forces, resonant energy transfer, interatomic Coulombic decay, all of which are described in terms of the dyadic Green's tensor that solves the Helmholtz equation. We discuss in detail how to calculate this tensor in practical situations before outlining new techniques in the design and optimisation of perturbative light–matter interactions, highlighting some recent advances in free-form, unconstrained inverse design of optical devices. Finally, an outlook towards the frontiers in the interaction of quantum light with matter is given, including its interface with chemical reactivity via polaritonic chemistry and quantum chemistry via quantum electrodynamical density functional theory (QEDFT).

Contents

* Corresponding author.
E-mail address: robert.bennett@glasgow.ac.uk (R. Bennett).

https://doi.org/10.1016/j.physrep.2023.07.005

1. Introduction

Light–matter interactions as governed by the theory of quantum electrodynamics are at the heart of physics, being responsible for a large majority of everyday physical phenomena (with the notably exception of gravity). The theory of quantum electrodynamics is well-understood — indeed it results in some of the most precisely-tested quantities in all the sciences [1]. So why is quantum electrodynamics still an active field of research? The answer lies in the complexity frontier — while the fundamental interactions are known, solving the resulting equations is either infeasible or impossible in many practical situations. For example, using quantum electrodynamics to predict the properties of a macroscopic object will, at the fundamental level, involve computing the mutual interactions of upwards of very roughly 10^{23} particles. This should contextualised against idealised few-body systems where predictions of properties for even a handful of particles proves computationally highly non-trivial (see, e.g., [2], meaning that a fully quantum-electrodynamical description of a macroscopic object is simply beyond reach.

Physics has, of course, developed ways to deal with this issue. These rely on abstracting away much of the complexity of the underlying system and concentrating on effective quantities, often with those actually being described before the underlying structure was discovered. For example, Newtonian mechanics is more than capable making accurate physical predictions within its realm of validity without considering the constituent atoms that make up macroscopic objects.

In this review we will consider the 'mixed' situation, where a quantum object such as an atom or molecule is influence by macroscopic objects in its surroundings. We will begin from first principles and stick to the perturbative case, where the quantum object can be considered to be weakly coupled to the electromagnetic field.

We begin in Section 2 with the fundamental Lagrangian for quantum electrodynamics as a gauge theory, verifying that this reproduces Maxwell's equations regardless of a choice of gauge. We then introduce the charge and current

densities relevant to an atom, and address the question of gauge choice. Using an arbitrary-gauge Lagrangian, we introduce Coulomb gauge then demonstrate in detail that an alternative gauge choice leads to the multipolar Hamiltonian usually most convenient for describing the interaction of atoms (or any other kind of quantum emitter) with light. The long-wavelength limit of this leads to the dipolar Hamiltonian that finds extensive use in cavity quantum electrodynamics and related fields.

In Section 3 we address the question of how the quantum theory of light and matter can be adapted and extended to deal with macroscopic objects made up of overwhelmingly large numbers of atoms. After discussing the advantages and drawbacks of various macroscopic quantisation methods, we explicitly carry out the quantisation of macroscopic quantum electrodynamics, arriving at electromagnetic fields expressed in terms of a set of polariton-like creation and annihilation operators and the (classical) dyadic Green's tensor summarising the effect of the electromagnetic environment. Section 4 covers how the environment-dependent theory of electromagnetism can be used to yield observable quantities such as forces and decay rates, as well as how it can be used to predict the parameters entering into quantum models of light–matter interaction such as the Jaynes–Cummings model.

The goal of Section 5 is to delve further into the actual calculation of the dyadic Green's tensors that the preceding two sections will have demonstrated to be central to describing perturbative environment-modified light–matter interactions. Particular attention is given to the Green's tensor for a dielectric half-space with its form, approximations and evaluation via contour integration discussed in significant detail. This section closes with an account of how Green's tensors can be calculated numerically, and how such quantities can be accessed experimentally.

Having discussed the consequences of choosing a particular Green's tensor to calculate in Section 5, Section 6 reverses the logic entirely to ask the question; what Green's tensor is needed in order to realise a given goal specified by a merit function? This is the realm of inverse design, which is a rapidly-expanding subfield of nanophotonics where structures can be wavelength or sub-wavelength scale, dramatically complicating their design. Remarkable theoretical, computational and experimental results are summarised as an invitation, before moving onto an examination of the underlying methods that make inverse design feasible. Taking spontaneous decay as an example, a merit function is explicitly calculated before a brief summary of popular methods of implementing inverse design algorithms.

This review ends with Section 7, which discusses relation of the material in the preceding sections to some aspects of the current state of the art in light–matter interactions, namely polaritonic chemistry and quantum electrodynamical density functional theory.

Throughout this review two additional goals are kept in mind. Firstly, as far as possible this work aims to be pedagogical, especially in Sections 2, 3 and 5. The remaining parts present more of an overview of developments, with only some simple examples explicitly derived. Nevertheless, the focus is kept on a pedagogical explanation of 'real-world' techniques the reader would need in order to actually reproduce and expand upon such results, as well as acknowledging issues with overlapping and confusing terminology that often cause unnecessary stumbling blocks to those beginning in this field.

2. Fundamentals

The history of electromagnetism has been characterised by a gradual process of unification — beginning with Maxwell's unification of the entirely unrelated phenomenologies of electric and magnetic fields, all the way up to the modern viewpoint of electromagnetism as a gauge theory and its unification with the weak force. All of these viewpoints are still of use today, the choice of which statement of the theory is most appropriate depends on the conditions and requirements of a particular calculation. Here we will begin from the quantum electrodynamical Lagrangian at its most fundamental level, and gradually introduce approximations which bring the theory closer and closer to our everyday experience.

The symmetry law underlying quantum electrodynamics (QED) is that the theory should be invariant under a $U(1)$ rotation, corresponding to rotation of the field in the complex plane. Up to operators of mass dimension 4, the most general Lagrangian density that can be written that obeys such a symmetry is (see, for example, [3]):

$$\mathscr{L} = i\hbar c\bar{\psi}\gamma^{\mu}D_{\mu}\psi - mc^2\bar{\psi}\psi - \frac{1}{4\mu_0}F_{\mu\nu}F^{\mu\nu}, \tag{1}$$

with, in the $(+,-,-,-)$ metric convention:

$$D_{\mu} = \partial_{\mu} + i\frac{q}{\hbar}A_{\mu}, \qquad \bar{\psi} = \psi^{\dagger}\gamma^{0}, \qquad F_{\mu\nu} = \partial_{\mu}A_{\nu} - \partial_{\nu}A_{\mu},$$

where ψ is a complex four component spinor representing matter, γ are matrices obeying $\{\gamma^{\mu},\gamma^{\nu}\} = 2\eta^{\mu\nu}$ with η the Minkowski metric, A is the gauge potential (ultimately leading to electric and magnetic fields), m is the mass of the electron and q is its charge. As usual $\hbar$ is the reduced Planck constant, c is the speed of light and μ_0 is the vacuum permeability, related to the vacuum permittivity ε_0 and the speed of light via $c^2 = 1/(\varepsilon_0\mu_0)$.

The statement (1) of QED is almost never used outside high-energy physics, since it has little clear relation to the observables of low-energy settings such as electric and magnetic fields or particle positions and momenta. In order to bring this theory into a form more useful for everyday laboratory situations, we make some manipulations and approximations.

2.1. Matter field

The Euler–Lagrange equation arising from variation of $\mathscr{L}$ with respect to $\bar{\psi}$ results in the Dirac equation;

$$\left[i\hbar c\gamma^\mu\left(\partial_\mu + i\frac{q}{\hbar}A_\mu\right) - mc^2\right]\psi = 0, \tag{2}$$

while varying ψ results in the adjoint Dirac equation;

$$\bar{\psi}\left[i\hbar c\left(\overleftarrow{\partial_\mu}\gamma^\mu - i\frac{q}{\hbar}A_\mu\right) - mc^2\right] = 0, \tag{3}$$

where $\overleftarrow{\partial_\mu}$ denotes a derivative acting to the left. Multiplying the Dirac Eq. (2) by $\bar{\psi}$ from the left, the adjoint Dirac Eq. (3) by ψ from the right and adding the two equations together causes all terms without derivatives to cancel:

$$\bar{\psi}(\gamma^\mu\partial_\mu + \overleftarrow{\partial_\mu}\gamma^\mu)\psi = \bar{\psi}\gamma^\mu\partial_\mu\psi + (\partial_\mu\psi)\gamma^\mu\psi = 0, \tag{4}$$

or equivalently;

$$\partial_\mu(\bar{\psi}\gamma^\mu\psi) = 0, \tag{5}$$

showing that $\bar{\psi}\gamma^\mu\psi$ is a conserved quantity. We define the conserved current as;

$$J^\mu = qc\bar{\psi}\gamma^\mu\psi. \tag{6}$$

A factor qc has been introduced for later convenience [which of course does not affect the current's defining property (5)], this means the current above may looks slightly different to textbook versions where different conventions are used.

The standard textbook method of finding the non-relativistic approximation to the Dirac Lagrangian uses the equations of motion (2) and (3), and highlights its coupling to the field as a demonstration of the emergence of the coupling of the spin to the magnetic field. Here we are considering the matter part only and would like to stay in the Lagrangian formalism as much as possible. We therefore take a different route along the same lines as Ref. [4]. The non-relativistic approximation is based on the principle that one component of the energy–momentum four vector (the rest mass) should dominate over the others, so it makes sense to separate the matter-field Lagrangian density

$$\mathscr{L}_M = i\hbar c\bar{\psi}\gamma^\mu\partial_\mu\psi - mc^2\bar{\psi}\psi \tag{7}$$

into its scalar and three-vector parts, giving;

$$\mathscr{L}_M = i\hbar\psi^\dagger\partial_t\psi + i\hbar c\psi^\dagger\alpha^i\partial_i\psi - mc^2\psi^\dagger\beta\psi, \tag{8}$$

where $\alpha^i \equiv \gamma^0\gamma^i$ and $\gamma^0 \equiv \beta$, and the property $\gamma^0\gamma^0 = 1$ has been used. In the Dirac representation of the gamma matrices

$$\gamma^0 = \begin{pmatrix}\mathbb{I}_2 & 0\\ 0 & -\mathbb{I}_2\end{pmatrix} = \beta, \quad \gamma^i = \begin{pmatrix}0 & \sigma^i\\ -\sigma^i & 0\end{pmatrix}, \tag{9}$$

the α^i take the explicit form

$$\alpha^i \equiv \gamma^0\gamma^i = \begin{pmatrix}0 & \sigma^i\\ \sigma^i & 0\end{pmatrix}. \tag{10}$$

Splitting the four-spinor ψ into its upper and lower components φ and χ

$$\psi = \begin{pmatrix}\varphi\\ \chi\end{pmatrix} \tag{11}$$

and expanding out the matter-field Lagrangian density (7), one has;

$$\mathscr{L}_M = i\hbar(\varphi^\dagger\partial_t\varphi + \chi^\dagger\partial_t\chi) + i\hbar c(\varphi^\dagger\sigma^i\partial_i\chi + \chi^\dagger\sigma^i\partial_i\varphi) - mc^2(\phi^\dagger\varphi - \chi^\dagger\chi) \tag{12}$$

In a non-relativistic approximation, mc^2 can be taken to be much larger than any other quantity. This suggests making the following transformation;

$$\begin{pmatrix}\varphi\\ \chi\end{pmatrix} = e^{-imc^2t/\hbar}\begin{pmatrix}\varphi_0\\ \chi_0\end{pmatrix} \tag{13}$$

where φ_0 and χ_0 are still time-dependent, but will eventually be considered as slowly varying compared to the rapidly-oscillating factor $e^{-imc^2t/\hbar}$. Applying this to the Lagrangian $\mathscr{L}_M$, one finds;

$$\mathscr{L}_M = i\hbar(\varphi_0^\dagger\partial_t\varphi_0 + \chi_0^\dagger\partial_t\chi_0) + i\hbar c(\varphi_0^\dagger\sigma^i\partial_i\chi_0 + \chi_0^\dagger\sigma^i\partial_i\varphi_0) + 2mc^2\chi_0^\dagger\chi_0 \tag{14}$$

where, importantly, the term proportional to $\varphi^\dagger\varphi$ cancelled out with one of the terms coming from applying the product rule to the time derivative of the transformed spinors on the right hand side of (13). Similarly to the textbook approach (see, e.g. [5]), we can here use the approximate equations of motion to write the lower spinor as

$$\chi_0 = -\frac{i\hbar}{2mc}\sigma^i\partial_i\varphi_0. \tag{15}$$

Substituting this into the Lagrangian density (14) and using the Pauli matrix property that $\sigma_i\sigma_i = \delta_{ij} + i\epsilon_{ijk}\sigma_k$ one finds;

$$\mathscr{L}_M = i\hbar\varphi_0^\dagger\partial_t\varphi_0 + \frac{i\hbar^3}{4m^2c^2}(\partial_i\varphi_0^\dagger)(\partial_i\partial_t\varphi_0^\dagger) + \frac{\hbar^2}{2m}\varphi_0^\dagger\partial_i\partial_i\varphi_0 - \frac{\hbar^2}{2m}(\partial_i\varphi_0^\dagger)(\partial_i\varphi_0) + \frac{\hbar^2}{2m}(\partial_i\varphi_0^\dagger)(\partial_i\varphi_0) \tag{16}$$

in which the final two terms cancel. Keeping terms only up to order $1/m$ and switching to vector notation gives the non-relativistic matter Lagrangian

$$\mathscr{L}_M \approx i\hbar\varphi_0^\dagger\partial_t\varphi_0 + \frac{\hbar^2}{2m}\varphi_0^\dagger\nabla^2\varphi_0 \tag{17}$$

reversing the transformation (13) gives the final Lagrangian

$$\mathscr{L}_M = i\hbar\varphi^\dagger\partial_t\varphi - \frac{\hbar^2}{2m}\varphi^\dagger\nabla^2\varphi - mc^2\varphi^\dagger\varphi \tag{18}$$

Varying $\varphi^\dagger$ gives the Schrödinger equation with a rest mass term;

$$i\hbar\partial_t\varphi = -\frac{\hbar^2\nabla^2}{2m}\varphi + mc^2\varphi \tag{19}$$

as expected in a non-relativistic approximation. This is the so-called Schrödinger field, after subtracting off the constant mass-energy. Finally, we transform to the particle picture (first quantisation), as opposed to working with fields (second quantisation). In this picture, this is the Schrödinger equation for a free non-relativistic point-particle with Lagrangian

$$\mathscr{L}_M = \frac{\mathbf{p}^2}{2m}. \tag{20}$$

2.2. Photon field

The Lagrangian (1) can be rewritten as;

$$\mathscr{L} = i\hbar c\bar{\psi}\gamma^\mu\partial_\mu\psi - mc^2\bar{\psi}\psi - \frac{1}{4\mu_0}F_{\mu\nu}F^{\mu\nu} - A_\mu J^\mu, \tag{21}$$

where we have used the conserved current $J^\mu = cq\bar{\psi}\gamma^\mu\psi$ defined in Eq. (6). When considering the photon field there is no hope or reason to attempt a non-relativistic approximation like in the previous section since the photon is intrinsically relativistic as it has no mass. Instead, we will have to directly vary the gauge field A in the full statement of the Lagrangian density (21) in order to get its equations of motion.

Before progressing we note that the Lagrangian density (21) contains some redundancy which can be eliminated. Defining an arbitrary spacetime function χ (known as a gauge generating function) and applying a transformation of the form

$$A_\mu \to A_\mu + \partial_\mu\chi \tag{22}$$

to the Lagrangian density (21), the first two terms are unaffected but the second two terms become;

$$F_{\mu\nu} = \partial_\mu A_\nu - \partial_\nu A_\mu \to \partial_\mu(A_\nu + \partial_\nu\chi) - \partial_\nu(A_\mu + \partial_\mu\chi) = \partial_\mu A_\nu - \partial_\nu A_\mu + \partial_\mu\partial_\nu\chi - \partial_\nu\partial_\mu\chi = F_{\mu\nu}\,, \tag{23}$$

and

$$J^\mu A_\mu \to J^\mu(A_\mu + \partial_\mu\chi) = J^\mu A_\mu + J^\mu\partial_\mu\chi = J^\mu A_\mu + \partial_\mu(J^\mu\chi) - \chi\partial_\mu J^\mu. \tag{24}$$

The final term in (24) is zero by current conservation [see Eqs. (5) and (6)], and the penultimate term is a total divergence so can be eliminated from the Lagrangian via the divergence theorem (assuming, as always, that all fields vanish at infinity). Eqs. (23) and (24) therefore demonstrate that the Lagrangian density (21) remains unchanged by a transformation of the form (22) — in other words there is more than one choice of the gauge field A that leads to the same Lagrangian density. That this must happen perhaps should have been obvious from the start — the Lagrangian density (21) does not contain the time-derivative of A^0 ($F_{\mu\nu}$ is antisymmetric in its indices), meaning that this field component has no canonically conjugate momentum and no dynamics.

We will postpone choosing a gauge as long as possible in order to emphasise that the equations of motion for the field A are Maxwell's equations, independent of a particular choice of gauge. We begin by expanding the free photon term in

the Lagrangian density (21) into scalar and three-vector components:

$$\begin{aligned}-\frac{1}{4}F_{\mu\nu}F^{\mu\nu} &= -\frac{1}{2}(\partial^\mu A^\nu)(\partial_\mu A_\nu) + \frac{1}{2}(\partial^\mu A^\nu)(\partial_\nu A_\mu)\\ &= \frac{1}{2}(\partial_i A_0)^2 + \frac{1}{2}(\partial_0 A_i)^2 - \frac{1}{2}(\partial_i A_j)^2 + (\partial_i A_0)(\partial_0 A_i) + \frac{1}{2}(\partial_i A_j)(\partial_j A_i)\\ &= \frac{1}{2}(\partial_i A_0 + \partial_0 A_i)^2 - \frac{1}{2}(\partial_i A_j)^2 + \frac{1}{2}(\partial_i A_j)(\partial_j A_i)\,.\end{aligned}$$

Restoring the factor $1/\mu_0$ and adding back the term $-A_\mu J^\mu$, we have an expanded version of all the A-dependent terms in the Lagrangian density (21)

$$-\frac{1}{4\mu_0}F_{\mu\nu}F^{\mu\nu} - A_\mu J^\mu = \frac{1}{2\mu_0}(\partial_i A_0 + \partial_0 A_i)^2 - \frac{1}{2\mu_0}(\partial_i A_j)^2 + \frac{1}{2\mu_0}(\partial_i A_j)(\partial_j A_i) - A_0 J^0 + A_i J^i, \tag{25}$$

from which we can find the equations of motion for the gauge field A. First considering the scalar part A_0, the relevant Euler–Lagrange equations are

$$\frac{\partial \mathscr{L}}{\partial A_0} - \partial_i \frac{\partial \mathscr{L}}{\partial(\partial_i A_0)} = 0, \tag{26}$$

from which one finds

$$-J_0 - \frac{1}{\mu_0}\partial_i(\partial_i A_0 + \partial_0 A_i) = 0. \tag{27}$$

Identifying the charge density ρ as J_0/c and the electromagnetic scalar potential as $\phi = A_0 c$, this becomes

$$-c\rho - \frac{1}{c\mu_0}\partial_i(\partial_i \phi + \partial_t A_i) = 0, \tag{28}$$

or, switching to vector notation;

$$-\nabla^2\phi - \nabla\cdot\dot{\mathbf{A}} = \frac{\rho}{\varepsilon_0} \tag{29}$$

where $c^2 = 1/(\varepsilon_0\mu_0)$ was used. Here we have suppressed the arguments $(\mathbf{r}, t)$ in order to keep the notation compact, this will be done throughout unless multiple positions/times are involved in an expression.

Moving on to the equations of motion for the field $\mathbf{A}$, we note that since $\mathscr{L}$ depends on the derivatives of $\mathbf{A}$ with respect to both space and time, its corresponding Euler–Lagrange equations are

$$\frac{\partial \mathscr{L}}{\partial A_j} - \partial_i \frac{\partial \mathscr{L}}{\partial(\partial_i A_j)} - \partial_0 \frac{\partial \mathscr{L}}{\partial(\partial_0 A_j)} = 0, \tag{30}$$

giving

$$\mu_0 J_i + \partial_j\partial_j A_i - \partial_j\partial_i A_j - \partial_0\partial_0 A_i + \partial_0\partial_i A_0 = 0, \tag{31}$$

or, in vector notation;

$$\frac{1}{c^2}\nabla\dot{\phi} + \frac{1}{c^2}\ddot{\mathbf{A}} - \nabla^2\mathbf{A} + \nabla(\nabla\cdot\mathbf{A}) = \mu_0\mathbf{J}\,. \tag{32}$$

Two quantities can be defined from the potentials $\mathbf{A}$ and ϕ, the familiar electric field $\mathbf{E}$ and magnetic field $\mathbf{B}$

$$\mathbf{E} = -\dot{\mathbf{A}} - \nabla\phi, \qquad \mathbf{B} = \nabla\times\mathbf{A}, \tag{33}$$

which by construction immediately implies two of Maxwell's equations;

$$\nabla\cdot\mathbf{B} = 0 \quad \text{(Gauss's law for magnetism)}, \tag{34}$$

$$\nabla\times\mathbf{E} = -\dot{\mathbf{B}} \quad \text{(Faraday's law of induction)}. \tag{35}$$

Taking the divergence of the definition (33) of the electric field gives another of Maxwell's equations;

$$\nabla\cdot\mathbf{E} = -\nabla\cdot\dot{\mathbf{A}} - \nabla^2\phi = \frac{\rho}{\varepsilon_0} \quad \text{(Gauss's law)}. \tag{36}$$

The fourth and final Maxwell equation can be found by taking the curl of the definition (33) of the magnetic field;

$$\nabla\times\mathbf{B} = \nabla\times\nabla\times\mathbf{A} = \nabla(\nabla\cdot\mathbf{A}) - \nabla^2\mathbf{A}, \tag{37}$$

using the equation of motion for $\mathbf{A}$

$$\nabla\times\mathbf{B} = \mu_0\mathbf{J} - \frac{1}{c^2}\nabla\dot{\phi} - \frac{1}{c^2}\ddot{\mathbf{A}} = \mu_0\mathbf{J} + \frac{1}{c^2}\frac{\partial}{\partial t}\left(-\nabla\phi - \dot{\mathbf{A}}\right), \tag{38}$$

and the definition (33) of **E**, giving

$$\nabla \times \mathbf{B} = \mu_0 \mathbf{J} + \varepsilon_0 \mu_0 \dot{\mathbf{E}} \qquad \text{(Ampere's law)}. \tag{39}$$

We have derived all four of Maxwell's equations from the Lagrangian (1), without specifying a gauge. This of course is to be expected as Maxwell's equations depend only on the gauge-invariant fields **E** and **B**. We could also have written the free photon Lagrangian density in terms of gauge invariant quantities. Note that for any vector field;

$$(\nabla \times \mathbf{V})^2 = (\partial_i V_j)^2 - (\partial_i V_j)(\partial_j V_i), \tag{40}$$

so;

$$-\frac{1}{4\mu_0} F_{\mu\nu} F^{\mu\nu} = \frac{1}{2\mu_0 c^2} (\nabla\phi + \dot{\mathbf{A}})^2 - \frac{1}{2\mu_0} (\nabla \times \mathbf{A})^2 = \frac{1}{2\mu_0} \left(\frac{1}{c^2} \mathbf{E} \cdot \mathbf{E} - \mathbf{B} \cdot \mathbf{B} \right). \tag{41}$$

It is important to note that the appearance of **E** and **B** in this form of the Lagrangian density should be understood only as a shorthand for the version written in terms of ϕ and **A** — the latter in particular is one of the dynamical variables of the theory which will later be used to identify canonical momenta and carry out a quantisation.

2.3. Atoms and photons

In order to more closely study the interaction of light and matter, we look at the two coupling terms in the Lagrangian density (21),

$$-\frac{1}{4\mu_0} F_{\mu\nu} F^{\mu\nu} - A_\mu J^\mu = \frac{1}{2\mu_0} \left(\frac{1}{c^2} (\dot{\mathbf{A}} + \nabla\phi)^2 - (\nabla \times \mathbf{A})^2 \right) - \phi\rho + \mathbf{A} \cdot \mathbf{J}\,, \tag{42}$$

where again we have identified the charge density ρ as J_0/c and the electromagnetic scalar potential as $\phi = A_0 c$. Since we are interested in the interaction of matter with bound collections of charged particles (chiefly atoms), we specify the charge density as a bound charge density $\rho = \rho_b$ via

$$\rho_b(\mathbf{r}) = -e\delta(\mathbf{r} - \mathbf{q}) + e\delta(\mathbf{r}), \tag{43}$$

where **q** is the coordinate of an electron bound to a nucleus fixed at $\mathbf{r} = \mathbf{0}$. The corresponding current density is

$$\mathbf{J}_b(\mathbf{r}) = -e\dot{\mathbf{q}}\delta(\mathbf{r} - \mathbf{q}). \tag{44}$$

We can additionally use these in the matter-only Lagrangian density [see Eq. (20)] to find the total Lagrangian L;

$$L = \frac{1}{2} m\dot{\mathbf{q}}^2 - \int d^3r \mathscr{L}(\mathbf{A}, \phi), \tag{45}$$

with

$$\begin{aligned} \mathscr{L}(\mathbf{A}, \phi) &= \frac{\varepsilon_0}{2} \left[(\dot{\mathbf{A}} + \nabla\phi)^2 - c^2 (\nabla \times \mathbf{A})^2 \right] - \phi\rho + \mathbf{A} \cdot \mathbf{J} \\ &= \frac{\varepsilon_0}{2} \left[(\dot{\mathbf{A}}(\mathbf{r}) + \nabla\phi(\mathbf{r}))^2 - c^2 (\nabla \times \mathbf{A}(\mathbf{r}))^2 \right] \\ &\qquad + e\phi(\mathbf{r})\delta(\mathbf{r} - \mathbf{q}) + e\phi(\mathbf{r})\delta(\mathbf{r}) - e\mathbf{A}(\mathbf{r}) \cdot \dot{\mathbf{q}}\delta(\mathbf{r} - \mathbf{q}) \end{aligned} \tag{46}$$

as our final non-relativistic Lagrangian using which the interaction with atoms can be studied.

Following [6] we will adopt **q** and **A** as the independent dynamical variables of the theory. The momenta conjugate to **q** and **A** are;

$$\mathbf{p} = \frac{\partial L}{\partial \dot{\mathbf{q}}} = m\dot{\mathbf{q}} - e\mathbf{A}(\mathbf{q}) \equiv \mathbf{p}(\mathbf{q}), \tag{47}$$

$$\boldsymbol{\Pi} = \frac{\partial \mathscr{L}}{\partial \dot{\mathbf{A}}} = \varepsilon_0 (\dot{\mathbf{A}} + \nabla\phi) = -\varepsilon_0 \mathbf{E}(\mathbf{r}) \equiv \boldsymbol{\Pi}(\mathbf{r}). \tag{48}$$

from which the Hamiltonian can be obtained via the Legendre transform

$$H = \mathbf{p} \cdot \dot{\mathbf{q}} + \int \mathrm{d}^3 r \boldsymbol{\Pi}(\mathbf{r}) \cdot \dot{\mathbf{A}}(\mathbf{r}) - L\,. \tag{49}$$

Carrying out the integral in the final term of (46), we have for all the terms in (49) that are not under an integral;

$$\mathbf{p} \cdot \dot{\mathbf{q}} - \frac{m\dot{\mathbf{q}}^2}{2} + e\dot{\mathbf{q}} \cdot \mathbf{A}(\mathbf{q}) = m\dot{\mathbf{q}}^2 - e\mathbf{A}(\mathbf{q}) \cdot \dot{\mathbf{q}} - \frac{m\dot{\mathbf{q}}^2}{2} + e\dot{\mathbf{q}} \cdot \mathbf{A}(\mathbf{q}) = \frac{m\dot{\mathbf{q}}^2}{2}, \tag{50}$$

giving

$$H = \frac{m\dot{\mathbf{q}}^2}{2} + \int \mathrm{d}^3 r \boldsymbol{\Pi}(\mathbf{r}) \cdot [\boldsymbol{\Pi}(\mathbf{r}) - \nabla\phi(\mathbf{r})] - \frac{1}{2}\int \mathrm{d}^3 r \left[\boldsymbol{\Pi}^2(\mathbf{r}) - \mathbf{B}^2(\mathbf{r}) - \rho_b(\mathbf{r})\phi(\mathbf{r})\right]$$
$$= \frac{1}{2m}\left[\mathbf{p} + e\mathbf{A}(\mathbf{q})\right]^2 + \frac{1}{2}\int \mathrm{d}^3 r \left\{\boldsymbol{\Pi}^2(\mathbf{r}) + \mathbf{B}^2(\mathbf{r}) + [\rho_b(\mathbf{r}) + \nabla\cdot\boldsymbol{\Pi}(\mathbf{r})]\phi(\mathbf{r})\right\}, \tag{51}$$

where Eq. (47) has been used and the term proportional to $\nabla\phi$ has been integrated by parts. The terms proportional to ϕ can be eliminated by noting that;

$$\nabla\cdot\boldsymbol{\Pi} + \rho_b = 0 \tag{52}$$

which follows from Eqs. (36) and (48). In this, ϕ acts as a Lagrange multiplier that allows us to fix Gauss's law as a primary constraint at a classical level. At this point, we will leave ϕ unspecified, noting that it depends on the particular chosen gauge. This leaves

$$H = \frac{1}{2m}\left[\mathbf{p} + e\mathbf{A}(\mathbf{q})\right]^2 + \frac{1}{2}\int \mathrm{d}^3 r \left[\boldsymbol{\Pi}^2(\mathbf{r}) + \mathbf{B}^2(\mathbf{r})\right], \tag{53}$$

as the Hamiltonian, together with the Poisson brackets $\{\mathbf{A}(\mathbf{r}), \boldsymbol{\Pi}(\mathbf{r}')\} = \delta_\perp(\mathbf{r} - \mathbf{r}')$[1] and $\{\mathbf{q}_i, \mathbf{p}_j\} = \delta_{ij}$, which we will ultimately use to describe atom-light interactions after redundant degrees of freedom have been eliminated by choosing a gauge.

2.4. Gauges

We already saw that the Lagrangian is invariant under a gauge transformation (22). In order to continue postponing the choice of gauge as long as possible, here we will continue to follow [6] and take a very general form of the gauge generating function, introducing a gauge density $\tilde{\chi}$

$$\chi(\mathbf{r}) = \int \mathrm{d}^3 r' \tilde{\chi}(\mathbf{r}, \mathbf{r}', \mathbf{A}(\mathbf{r}')) \equiv \int \mathrm{d}^3 r' \tilde{\chi}(\mathbf{r}, \mathbf{r}'). \tag{54}$$

The Lagrangian (46) in the new gauge is given simply by replacing the original potentials with their transformed counterparts:

$$L' = L(\mathbf{A}', \phi') = L(\mathbf{A} - \nabla\chi, \phi + \dot{\chi}). \tag{55}$$

Recalling that the square-bracketed terms in (46) are gauge invariant [see Eqs. (23) and (24)], the new Lagrangian can be written in terms of the original fields as;

$$L' = L - \int \mathrm{d}r \rho_b(\mathbf{r})\dot{\chi}(\mathbf{r}) - \int \mathrm{d}r \mathbf{J}_b(\mathbf{r})\cdot\nabla\chi(\mathbf{r}) = L - \int \mathrm{d}r \rho_b(\mathbf{r})\dot{\chi}(\mathbf{r}) + e\dot{\mathbf{q}}\cdot\nabla\chi(\mathbf{q}). \tag{56}$$

Since χ depends on time only via its dependence on the time-dependent quantity $\mathbf{A}$, we have;

$$\dot{\chi}(\mathbf{r}) = \int \mathrm{d}r' \dot{\mathbf{A}}(\mathbf{r}')\cdot\frac{\partial\chi(\mathbf{r}, \mathbf{r}')}{\partial\mathbf{A}(\mathbf{r}')}, \tag{57}$$

giving for the second term of (56);

$$\int \mathrm{d}^3 r \rho_b(\mathbf{r})\dot{\chi}(\mathbf{r}) = \int \mathrm{d}^3 r \rho_b(\mathbf{r}) \int \mathrm{d}^3 r' \dot{\mathbf{A}}(\mathbf{r}')\cdot\frac{\partial\tilde{\chi}(\mathbf{r}, \mathbf{r}')}{\partial\mathbf{A}(\mathbf{r}')} = \int \mathrm{d}^3 r \dot{\mathbf{A}}(\mathbf{r})\cdot\int \mathrm{d}^3 r' \frac{\partial\tilde{\chi}(\mathbf{r}', \mathbf{r})}{\partial\mathbf{A}(\mathbf{r})}\rho_b(\mathbf{r}')$$
$$= \int \mathrm{d}^3 r \dot{\mathbf{A}}(\mathbf{r})\cdot\mathbf{P}(\mathbf{r}), \tag{58}$$

where we have defined;

$$\mathbf{P}(\mathbf{r}) \equiv \int \mathrm{d}^3 r' \frac{\partial\tilde{\chi}(\mathbf{r}', \mathbf{r})}{\partial\mathbf{A}(\mathbf{r})}\rho_b(\mathbf{r}'). \tag{59}$$

By application of this gauge transformation, the Lagrangian has changed its form so the momenta conjugate to $\mathbf{q}$ and $\mathbf{A}$ will correspondingly change theirs;

$$\mathbf{p}' = \frac{\partial L'}{\partial\dot{\mathbf{q}}} = m\dot{\mathbf{q}} - e\mathbf{A}(\mathbf{q}) + e\nabla\chi(\mathbf{q}) = \mathbf{p}(\mathbf{q}) + e\nabla\chi(\mathbf{q}), \tag{60}$$

$$\boldsymbol{\Pi}'(\mathbf{r}) = \frac{\partial\mathscr{L}'}{\partial\dot{\mathbf{A}}} = \varepsilon_0[\dot{\mathbf{A}}(\mathbf{r}) + \nabla\phi(\mathbf{r})] - \mathbf{P}(\mathbf{r}) = \boldsymbol{\Pi}(\mathbf{r}) - \mathbf{P}(\mathbf{r}). \tag{61}$$

[1] Here $\delta_\perp$ is the *transverse delta function*, defined in detail in Eq. (67) later on.

Our derivation of the Hamiltonian (53) was done in an arbitrary gauge, so still remains true in the new gauge we have transformed to here. However, the velocities $\dot{\mathbf{q}}$ and $\dot{\mathbf{A}}$ take on different forms when expressed in terms of the new canonical momenta, giving

$$H = \frac{1}{2m}\left[\mathbf{p}'(\mathbf{q}) - e\nabla\chi(\mathbf{q}) + e\mathbf{A}(\mathbf{q})\right]^2 + \frac{1}{2}\int \mathrm{d}^3r \left\{\frac{1}{\varepsilon_0}\left[\mathbf{\Pi}'(\mathbf{r}) + \mathbf{P}(\mathbf{r})\right]^2 + \frac{1}{\mu_0}\mathbf{B}(\mathbf{r})^2\right\} \tag{62}$$

as the Hamiltonian of a system of charged particles coupled to the electromagnetic field in an arbitrary gauge for $\mathbf{A}$, with all quantities except $\mathbf{B}$ being gauge-dependent. To write this in a new gauge, one would simply declare the various fields and particular momenta to be in a particular gauge, generated by a certain χ, with the values of the Poisson brackets remaining the same if the fields are expressed in the new gauge. The particular form of χ will be determined by the choice of gauge, of which we will discuss two examples: Coulomb gauge and multipolar gauge.

2.5. Coulomb gauge

The textbook way to introduce Coulomb gauge is via a constraint on the vector potential, but here we will begin by specifying the gauge generating function χ and ultimately show that this reproduces the familiar transversality condition on $\mathbf{A}$. This will serve as a mathematically simpler introduction to the corresponding calculation for multipolar gauge in the next section.

Consider the following generator [6]

$$\chi_{\mathrm{C}}(\mathbf{r}) = \frac{1}{4\pi}\int \mathrm{d}r'\mathbf{A}(\mathbf{r}')\cdot\nabla'\frac{1}{|\mathbf{r}-\mathbf{r}'|} \equiv \int \mathrm{d}r'\tilde{\chi}_{\mathrm{C}}(\mathbf{r},\mathbf{r}'), \tag{63}$$

and its gradient;

$$\nabla_i\chi_{\mathrm{C}}(\mathbf{r}) = \frac{1}{4\pi}\int \mathrm{d}r' A_j(\mathbf{r}')\nabla_i\nabla_j'\frac{1}{|\mathbf{r}-\mathbf{r}'|} = -\frac{1}{4\pi}\int \mathrm{d}r' A_j(\mathbf{r}')\nabla_i'\nabla_j'\frac{1}{|\mathbf{r}-\mathbf{r}'|}, \tag{64}$$

where we have used an identity to switch the variable onto which the derivative has been applied. A vector field $\mathbf{V}$ is longitudinal if it satisfies $\nabla\times\mathbf{V} = \mathbf{0}$ at all points in space. For any scalar field φ, the vector calculus identity $\nabla\times(\nabla\varphi) = 0$ holds, so the quantity $\nabla\chi_{\mathrm{C}}(\mathbf{r})$ in Eq. (64) must be longitudinal, which we denote by the symbol $\|$. We can therefore use it to define the longitudinal delta function $\boldsymbol{\delta}_{\|}$ with components $\delta_{\|,ij}$,

$$\boldsymbol{\delta}_{\|}(\mathbf{r}-\mathbf{r}') = -\frac{1}{4\pi}\nabla\otimes\nabla\frac{1}{|\mathbf{r}-\mathbf{r}'|} \tag{65}$$

$[(\mathbf{a}\otimes\mathbf{b})_{ij} = a_ib_j]$ which 'picks out' the longitudinal part of a field, as in:

$$\int \mathrm{d}^3r'\boldsymbol{\delta}_{\|}(\mathbf{r}-\mathbf{r}')\cdot\mathbf{X}(\mathbf{r}') = \mathbf{X}_{\|}(\mathbf{r}). \tag{66}$$

Invoking the Helmholtz theorem, this naturally leads to the definition of an analogous quantity that picks out the transverse part of a field, given by subtracting (65) from the 'total' delta function:

$$\boldsymbol{\delta}_{\perp}(\mathbf{r}-\mathbf{r}') = \boldsymbol{\delta}(\mathbf{r}-\mathbf{r}') - \boldsymbol{\delta}_{\|}(\mathbf{r}-\mathbf{r}') = \boldsymbol{\delta}(\mathbf{r}-\mathbf{r}') + \frac{1}{4\pi}\nabla\otimes\nabla\frac{1}{|\mathbf{r}-\mathbf{r}'|}. \tag{67}$$

Using the longitudinal delta function, we find

$$\nabla\chi_{\mathrm{C}}(\mathbf{r}) = \int \mathrm{d}^3r'\boldsymbol{\delta}_{\|}(\mathbf{r}-\mathbf{r}')\cdot\mathbf{A}(\mathbf{r}') = \mathbf{A}_{\|}(\mathbf{r}), \tag{68}$$

showing that the chosen generator is the one whose gradient [which is the quantity that appears in the Hamiltonian (62)] depends only on the transverse part of $\mathbf{A}$. If we now write out the three-vector part of gauge transformation in terms of longitudinal and transverse fields

$$\mathbf{A}_{\mathrm{C}}(\mathbf{r}) = \mathbf{A}_{\perp}(\mathbf{r}) + \mathbf{A}_{\|}(\mathbf{r}) - \nabla\chi_{\mathrm{C}}(\mathbf{r}). \tag{69}$$

the final two terms cancel so we are left with;

$$\mathbf{A}_{\mathrm{C}}(\mathbf{r}) = \mathbf{A}_{\perp}(\mathbf{r}). \tag{70}$$

This is entirely transverse, so $\mathbf{A}_{\mathrm{C}}$ satisfies the definition of a transverse field;

$$\nabla\cdot\mathbf{A}_{\mathrm{C}}(\mathbf{r}) = 0, \tag{71}$$

as expected.

Choosing a gauge generator also fixes $\mathbf{P}_{\mathrm{C}}$, which we can see from (59);

$$\mathbf{P}_{\mathrm{C}}(\mathbf{r}) = \frac{1}{4\pi}\int \mathrm{d}r'\frac{\partial\left[\mathbf{A}(\mathbf{r})\cdot\nabla\frac{1}{|\mathbf{r}-\mathbf{r}'|}\right]}{\partial\mathbf{A}(\mathbf{r})}\rho_b(\mathbf{r}') = \nabla\frac{1}{4\pi}\int \mathrm{d}r'\frac{1}{|\mathbf{r}-\mathbf{r}'|}\rho_b(\mathbf{r}'). \tag{72}$$

Taking the divergence of this gives;

$$\nabla \cdot \mathbf{P}_{\mathrm{C}}(\mathbf{r}) = \nabla \cdot \nabla \frac{1}{4\pi} \int \mathrm{d}r' \frac{\rho_b(\mathbf{r}')}{|\mathbf{r} - \mathbf{r}'|} = -\int \mathrm{d}r' \rho_b(\mathbf{r}')\delta(\mathbf{r} - \mathbf{r}') = -\rho_b(\mathbf{r}, t). \tag{73}$$

One of Maxwell's equations that follows from the Lagrangian is [c.f. Eq. (36)]

$$\varepsilon_0 \nabla \cdot \mathbf{E} = \rho_b, \tag{74}$$

so $\nabla \cdot \mathbf{P}_{\mathrm{C}} = -\varepsilon_0 \nabla \cdot \mathbf{E}$. Since $\mathbf{P}_{\mathrm{C}}(\mathbf{r})$ is the gradient of a scalar, the curl of $\mathbf{P}_{\mathrm{C}}(\mathbf{r})$ must be zero, meaning it is a longitudinal quantity. Therefore we can identify;

$$\mathbf{P}_{\mathrm{C}}(\mathbf{r}) = -\mathbf{E}^{\parallel}(\mathbf{r}), \tag{75}$$

where possible constant additions are excluded by the assumption that all fields vanish at spatial infinity. This is then combined with Eq. (61) to show that the momentum conjugate to $\mathbf{A}$ is;

$$\boldsymbol{\Pi}_{\mathrm{C}}(\mathbf{r}) = \frac{\partial \mathscr{L}}{\partial \dot{\mathbf{A}}} = \dot{\mathbf{A}} + \nabla\phi - \mathbf{E}_{\parallel} = -\mathbf{E} + \mathbf{E}_{\parallel} = -\mathbf{E}_{\perp}, \tag{76}$$

so is therefore a transverse vector field. The Coulomb gauge Hamiltonian is immediately obtained from Eq. (62) simply by specifying that all gauge-dependent quantities are now in Coulomb gauge, denoted by a subscript C.

$$H_{\mathrm{C}} = \frac{1}{2m}(\mathbf{p}_{\mathrm{C}} - e\nabla\chi_{\mathrm{C}} + e\mathbf{A}_{\mathrm{C}})^2 + \frac{1}{2}\int \mathrm{d}r \left\{ \frac{1}{\varepsilon_0}[\boldsymbol{\Pi}_{\mathrm{C}} + \mathbf{P}_{\mathrm{C}}]^2 + \frac{1}{\mu_0}\mathbf{B}^2 \right\}. \tag{77}$$

Then, substituting in (68)

$$H_{\mathrm{C}} = \frac{1}{2m}(\mathbf{p}_{\mathrm{C}} + e\mathbf{A}_{\perp})^2 + \frac{1}{2}\int \mathrm{d}r \left\{ \frac{1}{\varepsilon_0}\left[\boldsymbol{\Pi}_{\mathrm{C}}^2 + \mathbf{P}_{\mathrm{C}}^2\right] + \frac{1}{\mu_0}\mathbf{B}^2 \right\}, \tag{78}$$

where the expansion of the square bracket in the integrand follows because $\boldsymbol{\Pi}(\mathbf{r})$ is transverse and $\mathbf{P}_{\mathrm{C}}(\mathbf{r})$ is longitudinal. Using Eqs. (75) and (76) gives finally;

$$H_{\mathrm{C}} = \frac{1}{2m}(\mathbf{p}_{\mathrm{C}} + e\mathbf{A}_{\perp})^2 + \frac{1}{2}\int \mathrm{d}r \left[\frac{1}{\varepsilon_0}\mathbf{E}^2 + \frac{1}{\mu_0}\mathbf{B}^2 \right] \tag{79}$$

as the Hamiltonian in Coulomb gauge.

2.6. Multipolar gauge

2.6.1. Basic expressions

Following [6], we now consider the following alternative gauge generating function

$$\chi_{\mathrm{M}}(\mathbf{r}) = -\int \mathrm{d}^3 r' \int_0^1 \mathrm{d}\lambda\, \mathbf{A}(\mathbf{r}') \cdot \mathbf{r}\delta(\mathbf{r}' - \lambda\mathbf{r}). \tag{80}$$

This choice of gauge generator is harder to physically motivate than the corresponding one in Coulomb gauge, but it will become clear that this is a choice which causes the polarisation field to be that of a straight line of singular dipole moment density from the fixed origin $\mathbf{r}'$ to the position $\mathbf{r}$ of a charge. In order to show this we will follow the same recipe as in the Coulomb gauge calculation in the previous section, namely finding the gradient of the gauge generating function and an expression for the polarisation field, then using these in the arbitrary gauge Hamiltonian (62). We therefore begin by calculating

$$\nabla\chi_{\mathrm{M}}(\mathbf{r}) = -\int \mathrm{d}^3 r' \int_0^1 \mathrm{d}\lambda\, \nabla\left[\mathbf{A}(\mathbf{r}') \cdot \mathbf{r}\delta(\mathbf{r}' - \lambda\mathbf{r})\right]. \tag{81}$$

In Appendix this is shown to be equal to;

$$\nabla\chi_{\mathrm{M}}(\mathbf{r}) = \mathbf{A}(\mathbf{r}) + \frac{1}{e}\int \mathrm{d}^3 r'\, \boldsymbol{\theta}(\mathbf{r}', \mathbf{r}) \times \mathbf{B}(\mathbf{r}'). \tag{82}$$

where

$$\boldsymbol{\theta}(\mathbf{r}', \mathbf{r}) \equiv -e\int_0^1 \mathrm{d}\lambda\, \lambda\mathbf{r}\delta(\mathbf{r}' - \lambda\mathbf{r}) \tag{83}$$

We will also need the polarisation field given by Eq. (59). As noted in [6], it is convenient for this part of the calculation to write the charge density as $\rho_b(\mathbf{r}, \mathbf{q})$, emphasising its dependence on the electron coordinate as well as the observation

position. Since the polarisation $\mathbf{P}_\mathrm{M}$ depends on $\rho_b(\mathbf{r},\mathbf{q})$ we also emphasise its dependence on $\mathbf{q}$, writing:

$$\begin{aligned}\mathbf{P}_\mathrm{M}(\mathbf{r},\mathbf{q}) \equiv \int \mathrm{d}^3r' \frac{\partial \tilde{\chi}_\mathrm{M}(\mathbf{r}',\mathbf{r})}{\partial \mathbf{A}(\mathbf{r})}\rho_b(\mathbf{r}',\mathbf{q}) &= \int \mathrm{d}^3r' \frac{\partial \tilde{\chi}_\mathrm{M}(\mathbf{r}',\mathbf{r})}{\partial \mathbf{A}(\mathbf{r})}\left[-e\delta(\mathbf{r}'-\mathbf{q})+e\delta(\mathbf{r}')\right] \\ &= -e\frac{\partial \tilde{\chi}_\mathrm{M}(\mathbf{q},\mathbf{r})}{\partial \mathbf{A}(\mathbf{r})} + e\frac{\partial \tilde{\chi}_\mathrm{M}(\mathbf{0},\mathbf{r})}{\partial \mathbf{A}(\mathbf{r})}. \end{aligned} \tag{84}$$

The solution to this differential equation is;

$$-e\left[\tilde{\chi}_\mathrm{M}(\mathbf{q},\mathbf{r}) - \tilde{\chi}_\mathrm{M}(\mathbf{0},\mathbf{r})\right] = \mathbf{A}(\mathbf{r})\cdot\mathbf{P}_\mathrm{M}(\mathbf{r},\mathbf{q}). \tag{85}$$

We can see from (84) that $\mathbf{P}_\mathrm{M}(\mathbf{r},\mathbf{0}) = 0$, so to satisfy Eq. (84) we can choose $\tilde{\chi}_\mathrm{M}(\mathbf{0},\mathbf{r}) = 0$, giving;

$$\tilde{\chi}_\mathrm{M}(\mathbf{q},\mathbf{r}) = -\frac{1}{e}\mathbf{A}(\mathbf{r})\cdot\mathbf{P}_\mathrm{M}(\mathbf{r},\mathbf{q}) = \int_0^1 \mathrm{d}\lambda\, \mathbf{A}(\mathbf{r})\cdot\mathbf{q}\delta(\mathbf{r}-\lambda\mathbf{q}), \tag{86}$$

where the second equality follows from the definition (80) of the gauge generator. This also allows us to identify;

$$\mathbf{P}_\mathrm{M}(\mathbf{r},\mathbf{q}) = -e\int_0^1 \mathrm{d}\lambda\, \mathbf{q}\delta(\mathbf{r}-\lambda\mathbf{q}) \tag{87}$$

as the polarisation field in the multipolar gauge, which fits with the interpretation of this gauge given at the start of this section.

2.6.2. Hamiltonian

The multipolar gauge Hamiltonian is immediately obtained from Eq. (62) simply by specifying that all gauge-dependent quantities are now in multipolar gauge, denoted by a subscript M.

$$H_\mathrm{M} = \frac{1}{2m}\left[\mathbf{p}_\mathrm{M}(\mathbf{q}) - e\nabla\chi_\mathrm{M}(\mathbf{q}) + e\mathbf{A}_\mathrm{M}(\mathbf{q})\right]^2 + \frac{1}{2}\int \mathrm{d}^3r\left\{\frac{1}{\varepsilon_0}\left[\mathbf{\Pi}_\mathrm{M}(\mathbf{r}) + \mathbf{P}_\mathrm{M}(\mathbf{r},\mathbf{q})\right]^2 + \frac{1}{\mu_0}\mathbf{B}(\mathbf{r})^2\right\}. \tag{88}$$

Of course, the actual utility of this comes from using the forms of the gradient of the gauge generator and the polarisation field derived in the previous subsection. Using Eq. (82)

$$\begin{aligned}H_\mathrm{M} = \frac{1}{2m}&\left(\mathbf{p}_\mathrm{M}(\mathbf{q}) - \int \mathrm{d}^3r'\,\boldsymbol{\theta}(\mathbf{r}',\mathbf{q})\times\mathbf{B}(\mathbf{r}')\right)^2 \\ &+ \frac{1}{2}\int \mathrm{d}^3r\left\{\frac{1}{\varepsilon_0}\left[\mathbf{\Pi}_\mathrm{M}(\mathbf{r}) + \mathbf{P}_\mathrm{M}(\mathbf{r},\mathbf{q})\right]^2 + \frac{1}{\mu_0}\mathbf{B}(\mathbf{r})^2\right\}.\end{aligned} \tag{89}$$

Using the cyclic property of the triple product $\mathbf{a}\cdot(\mathbf{b}\times\mathbf{c})$ we can expand the cross term outside the integral;

$$\begin{aligned}&\mathbf{p}_\mathrm{M}(\mathbf{q})\cdot\left[\boldsymbol{\theta}(\mathbf{r}',\mathbf{q})\times\mathbf{B}(\mathbf{r}')\right] + \left[\boldsymbol{\theta}(\mathbf{r}',\mathbf{q})\times\mathbf{B}(\mathbf{r}')\right]\cdot\mathbf{p}_\mathrm{M}(\mathbf{q}) \\ &\qquad = \mathbf{B}(\mathbf{r}')\cdot\left[\mathbf{p}_\mathrm{M}(\mathbf{q})\times\boldsymbol{\theta}(\mathbf{r}',\mathbf{q})\right] + \left[\mathbf{p}_\mathrm{M}(\mathbf{q})\times\boldsymbol{\theta}(\mathbf{r}',\mathbf{q})\right]\cdot\mathbf{B}(\mathbf{r}') \\ &\qquad = \mathbf{B}(\mathbf{r}')\cdot\left[\boldsymbol{\theta}(\mathbf{r}',\mathbf{q})\times\mathbf{p}_\mathrm{M}(\mathbf{q}) - \mathbf{p}_\mathrm{M}(\mathbf{q})\times\boldsymbol{\theta}(\mathbf{r}',\mathbf{q})\right].\end{aligned} \tag{90}$$

If we define;

$$\mathscr{M}(\mathbf{r}',\mathbf{q}) = \frac{1}{2m}[\boldsymbol{\theta}(\mathbf{r}',\mathbf{q})\times\mathbf{p}_\mathrm{M}(\mathbf{q}) - \mathbf{p}_\mathrm{M}(\mathbf{q})\times\boldsymbol{\theta}(\mathbf{r}',\mathbf{q})], \tag{91}$$

then the first term of Eq. (89) can be multiplied out to give;

$$\frac{\mathbf{p}_\mathrm{M}^2}{2m} - \int \mathrm{d}^3r'\mathbf{B}(\mathbf{r}')\cdot\mathscr{M}(\mathbf{r}',\mathbf{q}) + \frac{1}{2m}\left(\int \mathrm{d}^3r'\,\boldsymbol{\theta}(\mathbf{r}',\mathbf{q})\times\mathbf{B}(\mathbf{r}')\right)^2. \tag{92}$$

Combining this with the second term of (89);

$$\begin{aligned}H_\mathrm{M} = \frac{\mathbf{p}_\mathrm{M}^2}{2m} + \frac{1}{2m}&\left(\int \mathrm{d}^3r'\,\boldsymbol{\theta}(\mathbf{r}',\mathbf{q})\times\mathbf{B}(\mathbf{r}')\right)^2 - \int \mathrm{d}^3r'\mathbf{B}(\mathbf{r}')\cdot\mathscr{M}(\mathbf{r}',\mathbf{q}) \\ &+ \frac{1}{2}\int \mathrm{d}^3r\left\{\frac{1}{\varepsilon_0}\left[\mathbf{\Pi}_\mathrm{M}(\mathbf{r}) + \mathbf{P}_\mathrm{M}(\mathbf{r},\mathbf{q})\right]^2 + \frac{1}{\mu_0}\mathbf{B}(\mathbf{r})^2\right\}\end{aligned} \tag{93}$$

and again multiplying out, we get the full expression of the multipolar gauge Hamiltonian

$$H_{\mathrm{M}} = \frac{\mathbf{p}_{\mathrm{M}}^2}{2m} + \frac{1}{2m}\left(\int \mathrm{d}^3 r\, \boldsymbol{\theta}(\mathbf{r},\mathbf{q}) \times \mathbf{B}(\mathbf{r})\right)^2 + \frac{1}{2}\int \mathrm{d}^3 r \left\{ \frac{1}{\varepsilon_0}\boldsymbol{\Pi}_{\mathrm{M}}(\mathbf{r})^2 + \frac{1}{\varepsilon_0}\mathbf{P}_{\mathrm{M}}^2(\mathbf{r},\mathbf{q}) + \frac{2}{\varepsilon_0}\boldsymbol{\Pi}_{\mathrm{M}}(\mathbf{r})\cdot\mathbf{P}_{\mathrm{M}}(\mathbf{r},\mathbf{q}) - 2\mathbf{B}(\mathbf{r})\cdot\boldsymbol{\mathscr{M}}(\mathbf{r},\mathbf{q}) + \frac{1}{\mu_0}\mathbf{B}(\mathbf{r})^2 \right\}. \tag{94}$$

in agreement with [6].

2.6.3. Long wavelength approximation

The most useful form of the multipolar Hamiltonian (94) comes from applying a long wavelength approximation, which allows systematic approximation in terms of the multipole moments of a charge distribution. This expansion is physically useful as in most situations the wavelength of incident light is much larger than any characteristic size associated with the atom.

The long wavelength approximation begins from a small $\mathbf{q}$ expansion of the delta function appearing in the statement (87) of $\mathbf{P}_{\mathrm{M}}$;

$$\begin{aligned}\mathbf{P}_{\mathrm{M}}(\mathbf{r},\mathbf{q}) &= -e\int_0^1 \mathrm{d}\lambda\, \mathbf{q}\delta(\mathbf{r}-\lambda\mathbf{q}) = -e\int_0^1 \mathrm{d}\lambda\, \mathbf{q}\left[\delta(\mathbf{r}) - \lambda(\mathbf{q}\cdot\nabla)\delta(\mathbf{r}) + \cdots\right] \\ &= -e\mathbf{q}\delta(\mathbf{r}) + \frac{e}{2}\mathbf{q}(\mathbf{q}\cdot\nabla)\delta(\mathbf{r}) + \cdots,\end{aligned} \tag{95}$$

and similarly in the auxiliary function θ defined in Eq. (83), where we also expand up to first order in λ

$$\theta(\mathbf{r}',\mathbf{q}) = -e\int_0^1 \mathrm{d}\lambda\, \lambda\mathbf{q}\delta(\mathbf{r}'-\lambda\mathbf{q}) = -\frac{e}{2}\mathbf{q}\delta(\mathbf{r}') + \cdots, \tag{96}$$

which in turn also gives us the magnetisation defined in Eq. (91)

$$\boldsymbol{\mathscr{M}}(\mathbf{r}',\mathbf{q}) = -\frac{e}{4m}[\mathbf{q}\times\mathbf{p}_{\mathrm{M}} - \mathbf{p}_{\mathrm{M}}\times\mathbf{q}]\delta(\mathbf{r}') + \cdots. \tag{97}$$

Using the general conjugate momenta defined via Eqs. (48) and (61), we have;

$$\boldsymbol{\Pi}_{\mathrm{M}} = -\varepsilon_0\mathbf{E} - \mathbf{P}_{\mathrm{M}} \equiv -\mathbf{D}, \tag{98}$$

where we have introduced the usual definition of the electric displacement field $\mathbf{D}$.

These can be used in the multipolar Hamiltonian (94), beginning with the electric polarisation coupling term;

$$\begin{aligned}\frac{1}{\varepsilon_0}\int \mathrm{d}^3 r \boldsymbol{\Pi}_{\mathrm{M}}\cdot\mathbf{P}_{\mathrm{M}}(\mathbf{r},\mathbf{q}) &= \frac{e}{\varepsilon_0}\int \mathrm{d}^3 r \mathbf{D}\cdot\mathbf{q}\delta(\mathbf{r}) - \frac{e}{2\varepsilon_0}\int \mathrm{d}^3 r (\mathbf{q}\cdot\mathbf{D})(\mathbf{q}\cdot\nabla)\delta(\mathbf{r}) + \cdots \\ &= \frac{e}{\varepsilon_0}\mathbf{D}(0)\cdot\mathbf{q} - \frac{e}{2\varepsilon_0}(\mathbf{q}\cdot\nabla)(\mathbf{q}\cdot\mathbf{D}(\mathbf{r}))|_{\mathbf{r}=0} + \cdots,\end{aligned} \tag{99}$$

then the two magnetic coupling terms;

$$\frac{1}{2m}\left(\int \mathrm{d}^3 r\, \theta(\mathbf{r},\mathbf{q})\times\mathbf{B}(\mathbf{r})\right)^2 = -\frac{e^2}{8m}\left(\int \mathrm{d}^3 r\, \mathbf{q}\delta(\mathbf{r})\times\mathbf{B}(\mathbf{r})\right)^2 = -\frac{e^2}{8m}[\mathbf{q}\times\mathbf{B}(\mathbf{0})]^2, \tag{100}$$

and

$$-\int \mathrm{d}^3 r \mathbf{B}(\mathbf{r})\cdot\boldsymbol{\mathscr{M}}(\mathbf{r},\mathbf{q}) = -\frac{e}{4m}\mathbf{B}(\mathbf{0})\cdot[\mathbf{q}\times\mathbf{p}_{\mathrm{M}}(\mathbf{q}) - \mathbf{p}_{\mathrm{M}}(\mathbf{q})\times\mathbf{q}] = -\mathbf{B}(\mathbf{0})\cdot\mathbf{m}, \tag{101}$$

where

$$\mathbf{m} \equiv \frac{e}{4m}[\mathbf{q}\times\mathbf{p}_{\mathrm{M}}(\mathbf{q}) - \mathbf{p}_{\mathrm{M}}(\mathbf{q})\times\mathbf{q}]. \tag{102}$$

The integrand of the term of (94) proportional to $\mathbf{P}_{\mathrm{M}}^2$ depends on the square of delta functions (and their derivatives) evaluated at $\mathbf{r}$, so the result contains various delta functions evaluated at the origin. These correspond to infinite self-energies which, while being an interesting area of physics in their own right (see, e.g. [7]), have no effect on the quantities we will calculate here so will be absorbed into a renormalisation term V_{renorm} in the Hamiltonian. This gives the multipolar gauge Hamiltonian up to second order in the long wavelength limit [denoted by the superscript (2)]

$$\begin{aligned}H_{\mathrm{M}}^{(2)} = \frac{\mathbf{p}_{\mathrm{M}}^2}{2m} - \frac{e^2}{8m}[\mathbf{q}\times\mathbf{B}(\mathbf{0})]^2 - \mathbf{B}(\mathbf{0})\cdot\mathbf{m} + \frac{e}{\varepsilon_0}\mathbf{D}(\mathbf{0})\cdot\mathbf{q} - \frac{e}{2\varepsilon_0}(\mathbf{q}\cdot\nabla)(\mathbf{q}\cdot\mathbf{D}(\mathbf{r}))|_{\mathbf{r}=0} \\ + V_{\mathrm{renorm}} + \frac{1}{2}\int \mathrm{d}^3 r\left(\frac{1}{\varepsilon_0}\mathbf{D}^2 + \frac{1}{\mu_0}\mathbf{B}^2\right).\end{aligned} \tag{103}$$

Defining the dipole moment $\mathbf{d} = -e\mathbf{q}$, we finally have;

$$H_{\mathrm{M}} = \frac{\mathbf{p}_{\mathrm{M}}^2}{2m} + \frac{1}{2}\int \mathrm{d}^3 r \left(\frac{1}{\varepsilon_0}\mathbf{D}^2 + \frac{1}{\mu_0}\mathbf{B}^2\right) + V_{\mathrm{renorm}} + H^{(2)}_{\mathrm{M,int}}, \tag{104}$$

with an interaction Hamiltonian of

$$H^{(2)}_{\mathrm{M,int}} = -\frac{1}{\varepsilon_0}\mathbf{d}\cdot\mathbf{D}(\mathbf{0}) - \mathbf{m}\cdot\mathbf{B}(\mathbf{0}) - \frac{e^2}{8m}\left[\mathbf{q}\times\mathbf{B}(\mathbf{0})\right]^2 . \tag{105}$$

There is an important subtlety to the interpretation of the first term. The electric displacement $\mathbf{D}$ is defined by the electric field and the polarisation field via Eq. (98), and the polarisation field is in turn defined via Eq. (87) in terms of the positions and charges of the particles that constitute a given atom. Therefore, the quantity $\mathbf{D}$ as written in Eq. (105) *includes* the influence of the atomic charge distribution. This fine distinction arises from the fact that there are many 'displacement fields' $\mathbf{D}$, depending on which charges are designated as 'free' or 'bound'. In this case, $\mathbf{D}$ is actually the displacement field which includes the field of the specific atom, but not the atoms which constitute the medium as may be more familiar. The electric displacement field corresponding to the latter will be defined in Section 3. As such, the field $\mathbf{D}$ discussed here is commonly denoted as $\mathbf{E}$, as in the absence of the specific atom, the field is identical to the electric field inside the medium.

Later we will restrict to the term in (105) of leading order in $\mathbf{q}$, known as the dipole approximation and motivated by the fact that the atomic or molecular extent is usually much smaller than the wavelength of incident light. Recalling the definition (102) of $\mathbf{m}$, the we are left with the final dipole-approximated interaction Hamiltonian in the multipolar gauge for an electric atom;

$$H^{(1)}_{\mathrm{M,int}} = -\mathbf{d}\cdot\mathbf{E}(\mathbf{r}_{\mathrm{A}}). \tag{106}$$

where we have also redefined the origin as being the position $\mathbf{r}_{\mathrm{A}}$ of the atom. This electric dipole Hamiltonian is used across atomic, molecular and optical physics, and will be explicitly used as the basis for calculations in Section 4.

3. Macroscopic media

3.1. Classical electrodynamics in the presence of macroscopic media

We now have everything we need to describe non-relativistic atoms weakly interacting with electromagnetic fields, as described by the Lagrangians at the end of Section 2. Since atoms consist of collections of charged (and neutral) particles, the consequences of the electromagnetic field interacting with an atomic medium can in principle be found by solving equations of motion for each atom and field variable. The problem, of course, is that atoms in general have many electrons, and macroscopic objects consist of an overwhelming number of atoms. Even the classical electron dynamics within a single given atom will ordinarily be too complex to solve, so asking for a solution of the semiclassical coupled field–matter dynamics for the approximately 10^{23} atoms making up an everyday sized object is a hopeless task.

We therefore need to abstract one level away from individual atoms, instead treating their collective properties inside a medium as something akin to a fluid which is in some sense bound to the host medium. We already know from Eqs. (5) and (6) that the four-current obeys a continuity equation

$$\partial_\mu J^\mu = 0. \tag{107}$$

Converting this into its scalar and three-vector parts and making the usual identification of J_0 as ρc gives the continuity equation

$$\dot{\rho} + \nabla\cdot\mathbf{J} = 0, \tag{108}$$

where, again, we suppress position and time arguments until they are needed. The charge density within the material may be split into a bound part ρ_b (stemming from polarisation of a dielectric material by an external field) and a free part ρ_f, each of which must obey its own independent continuity equation. As shown in Eq. (73), the bound charge density can be identified as minus the divergence of a polarisation field $\mathbf{P}$,

$$\rho_b = -\nabla\cdot\mathbf{P}. \tag{109}$$

This means the total charge density ρ may be written as;

$$\rho = \rho_b + \rho_f = -\nabla\cdot\mathbf{P} + \rho_f, \tag{110}$$

so that Gauss's law (36) becomes;

$$\varepsilon_0\nabla\cdot\mathbf{E} = -\nabla\cdot\mathbf{P} + \rho_f. \tag{111}$$

Similarly to Eq. (98), we can use the definition of the electric displacement $\mathbf{D} = \varepsilon_0\mathbf{E} + \mathbf{P}$, transforming this into;

$$\nabla\cdot\mathbf{D} = \rho_f. \tag{112}$$

Using Eq. (109) the continuity equation for bound charge ($\dot{\rho}_b + \nabla \cdot \mathbf{J}_b = 0$) can be rewritten as

$$\nabla \cdot (\mathbf{J}_b - \dot{\mathbf{P}}) = 0. \tag{113}$$

Since the curl of a divergence always vanishes, this implies that $\mathbf{J}_b - \dot{\mathbf{P}}$ can be written as the curl of another quantity, which we will identify as the magnetisation $\mathbf{M}$;

$$\nabla \times \mathbf{M} = \mathbf{J}_b - \dot{\mathbf{P}}. \tag{114}$$

The total charge density $\mathbf{J} = \mathbf{J}_b + \mathbf{J}_f$ is therefore;

$$\mathbf{J} = \mathbf{J}_f + \nabla \times \mathbf{M} + \dot{\mathbf{P}} \tag{115}$$

meaning Ampere's law (39) becomes;

$$\nabla \times \mathbf{B} = \mu_0 \mathbf{J}_f + \mu_0 \nabla \times \mathbf{M} + \mu_0 \dot{\mathbf{P}} + \varepsilon_0 \mu_0 \dot{\mathbf{E}}, \tag{116}$$

or

$$\nabla \times \mathbf{H} - \dot{\mathbf{D}} = \mu_0 \mathbf{J}_f, \tag{117}$$

where $\mathbf{H} = \frac{1}{\mu_0}\mathbf{B} - \mathbf{M}$.

We now make an assumption that can only be justified on a physical basis: the polarisation field of a medium responds *linearly* to an external electromagnetic field. This is a very good approximation in most situations, the exception being when an interrogating field modifies the properties of the material itself. This can happen if the field is sufficiently strong, but can also happen at low intensities (see, e.g. [8]). This review will be concerned only with linear optics, with non-linear optics being its own rich field of study (see, e.g., [9]).

The most general way to write the response of a time-dependent quantity $x(t)$ that depends linearly on $y(t)$ is;

$$x(t) = \int_{-\infty}^{\infty} \mathrm{d}\tau \, \chi(\tau) y(t - \tau) \tag{118}$$

where $\chi(t)$ is known as the response function. This is seen to relate the value of x at a particular time t to the value of y at a *different* time $t - \tau$, identifying τ as a delay time. By integrating over all τ, the behaviour of y at all times is taken into account. The function $\chi(t)$ simply relates the response of x to y, so will in general be peaked around $\tau = 0$. Causality requires that $\chi(\tau < 0) = 0$ (negative delay would correspond to reacting to signals from the future).

Generalising this to a position and time-dependent vector field, the linear response of the polarisation field is thereby described by

$$\mathbf{P}(\mathbf{r}, t) = \varepsilon_0 \int_{-\infty}^{\infty} \mathrm{d}\tau \int \mathrm{d}^3 r' \boldsymbol{\chi}(\mathbf{r}, \mathbf{r}', \tau) \cdot \mathbf{E}(\mathbf{r}', t - \tau), \tag{119}$$

where the response function is now matrix-valued in its most general form, and a factor of ε_0 has been extracted as a matter of convention. The causality requirement becomes;

$$\boldsymbol{\chi}(\mathbf{r}, \mathbf{r}', \tau) = \mathbf{0} \qquad \text{for} \qquad |\mathbf{r} - \mathbf{r}'| > c\tau. \tag{120}$$

The Fourier transform of $\mathbf{P}(\mathbf{r}, t)$ is

$$\mathbf{P}(\mathbf{r}, \omega) = \varepsilon_0 \int \mathrm{d}^3 r' \boldsymbol{\chi}(\mathbf{r}, \mathbf{r}', \omega) \cdot \mathbf{E}(\mathbf{r}', \omega), \tag{121}$$

which becomes simpler if the response is taken to be local [$\boldsymbol{\chi}(\mathbf{r}, \mathbf{r}', \omega) \to \delta(\mathbf{r} - \mathbf{r}')\boldsymbol{\chi}(\mathbf{r}, \omega)$] and isotropic [$\boldsymbol{\chi}(\mathbf{r}, \omega) \to \mathbb{I}\chi(\mathbf{r}, \omega)$ where $\mathbb{I}$ is the identity matrix];

$$\mathbf{P}(\mathbf{r}, \omega) = \varepsilon_0 \chi(\mathbf{r}, \omega) \mathbf{E}(\mathbf{r}, \omega), \tag{122}$$

giving

$$\mathbf{D}(\mathbf{r}, \omega) = \varepsilon_0 \left[1 + \chi(\mathbf{r}, \omega)\right] \mathbf{E}(\mathbf{r}, \omega) = \varepsilon_0 \varepsilon(\mathbf{r}, \omega) \mathbf{E}(\mathbf{r}, \omega), \tag{123}$$

where the position- and frequency-dependent relative permittivity $\varepsilon(\mathbf{r}, \omega)$ has been defined. Similarly, the linear response of the magnetisation field can be described by

$$\mathbf{M}(\mathbf{r}, t) = \frac{1}{\mu_0} \int_{-\infty}^{\infty} \mathrm{d}\tau \int \mathrm{d}^3 r' \boldsymbol{\zeta}(\mathbf{r}, \mathbf{r}', \tau) \cdot \mathbf{B}(\mathbf{r}', t - \tau), \tag{124}$$

where the response function $\boldsymbol{\zeta}$ obeys the same causality constraints as its electric counterpart $\boldsymbol{\chi}$. Again specialising to a local and isotropic response, this reduces to

$$\mathbf{M}(\mathbf{r}, \omega) = \frac{\zeta(\mathbf{r}, \omega)}{\mu_0} \mathbf{B}(\mathbf{r}, \omega), \tag{125}$$

so that in turn

$$\mathbf{H}(\mathbf{r},\omega)=\frac{1}{\mu_0}\left[1-\zeta(\mathbf{r},\omega)\right]\mathbf{B}(\mathbf{r},\omega)=\frac{1}{\mu_0\mu(\mathbf{r},\omega)}\mathbf{B}(\mathbf{r},\omega), \tag{126}$$

where the position- and frequency-dependent relative permeability $\mu(\mathbf{r},\omega)$ has been defined. Eqs. (123) and (126) are together known as the constitutive relations for electrodynamics in media. They allow a description which is closely analogous to free space[2] electrodynamics, with modified **E** and **B**. To see this it is useful to convert Ampere's law (39) to the frequency domain:

$$\nabla\times\mathbf{H}(\mathbf{r},\omega)+i\omega\mathbf{D}(\mathbf{r},\omega)=\mu_0\mathbf{J}_f(\mathbf{r},\omega), \tag{127}$$

then use the constitutive relations (123) and (126), and the definition (33) of the magnetic field to convert this to

$$\nabla\times\frac{1}{\mu_0\mu(\mathbf{r},\omega)}\nabla\times\mathbf{A}(\mathbf{r},\omega)+i\omega\varepsilon_0\varepsilon(\mathbf{r},\omega)\mathbf{E}(\mathbf{r},\omega)=\mu_0\mathbf{J}_f(\mathbf{r},\omega). \tag{128}$$

Taking time derivative (in frequency space) of the whole equation and using the curl of the definition (33) of the electric field $[\nabla\times\dot{\mathbf{A}}=-\nabla\times(\mathbf{E}+\nabla\phi)=-\nabla\times\mathbf{E}]$ gives finally:

$$\nabla\times\frac{1}{\mu_0\mu(\mathbf{r},\omega)}\nabla\times\mathbf{E}(\mathbf{r},\omega)-\omega^2\varepsilon_0\varepsilon(\mathbf{r},\omega)\mathbf{E}(\mathbf{r},\omega)=i\omega\mu_0\mathbf{J}_f(\mathbf{r},\omega). \tag{129}$$

This is essentially a wave equation, which is most conveniently solved via Green's function methods (see, e.g., [10]). Defining the Green's tensor[3] $\mathbb{G}(\mathbf{r},\mathbf{r}',\omega)$ as the solution to;

$$\nabla\times\frac{1}{\mu(\mathbf{r},\omega)}\nabla\times\mathbb{G}(\mathbf{r},\mathbf{r}',\omega)-\omega^2\varepsilon_0\mu_0\varepsilon(\mathbf{r},\omega)\mathbb{G}(\mathbf{r},\mathbf{r}',\omega)=\boldsymbol{\delta}(\mathbf{r}-\mathbf{r}') \tag{130}$$

where $\boldsymbol{\delta}(\mathbf{r}-\mathbf{r}')=\mathbb{I}\delta(\mathbf{r}-\mathbf{r}')$, it is straightforward to show that the electric field obeys;

$$\mathbf{E}(\mathbf{r},t)=\frac{\mu_0}{2\pi}\int_0^\infty \mathrm{d}\omega\int d^3\mathbf{r}'[i\omega\mathbb{G}(\mathbf{r},\mathbf{r}',\omega)\cdot\mathbf{J}(\mathbf{r}',\omega)+c.c.] \tag{131}$$

where we have transformed the field back into the time domain.

3.2. Approaches to quantisation

Now that a theory of classical electromagnetism in macroscopic media has been obtained, an obvious next step is to transition to a quantum theory. This is surprisingly difficult, chiefly due to the need to include absorption in any realistic model of a material. Absorption causes energy to be lost by the electromagnetic field, stopping it from having an acceptable Hamiltonian, which in turn precludes the identification of canonically conjugate position and momenta and their respective Poisson brackets. Canonical quantisation is based on promotion of Poisson brackets of the classical theory to the commutators of the quantum theory, so without Poisson brackets the canonical quantisation procedure cannot be followed.

We will focus the discussion on three distinct approaches to avoiding or solving this issue[4]

1. Ignoring absorption and using normal modes[5] similar to in free-space quantum electrodynamics. This type of approach is also limited in which types of dispersion it can include,[6] but can be a very useful approximation for objects whose frequency-domain response is sufficiently flat at the relevant frequencies.
2. Taking the theory of classical electrodynamics in absorptive media and using it to perform a phenomenological quantisation, enforcing consistency with the fluctuation–dissipation theorem (an approach referred to here as macroscopic QED or MQED).
3. Microscopically including absorption via harmonic oscillator baths (referred to here as Huttner–Barnett QED or HBQED), such that the whole system *is* energy-conserving and a Hamiltonian formalism can be used.

---

2 Here and throughout we will use 'free space' to refer to infinite, unbounded vacuum. The reason for not referring to this case simply as 'vacuum' is that a certain point can be locally in vacuum but still be affected by the presence of an inhomogeneous environment (near a surface, for example) — this distinction will be important later.

3 Note that the quantity $\mathbb{G}$ is variously referred to as the Green's function (e.g. [11]), Green's dyadic (e.g. [12], dyad being a name for a rank 2 tensor, similar to vector for a rank 1 tensor), Green's tensor (e.g. [13]), Green's bi-tensor (e.g. [14]), dyadic Green's function (e.g. [15]) and dyadic Green's tensor (e.g. [16]). Whichever name is preferred, fundamentally the object $\mathbb{G}$ is simply a 3×3 matrix of functions relating the components of a (vector) current source to an observed electric field vector. This quantity will be referred to as the Green's tensor or dyadic Green's tensor in this review.

4 While we have focused on these three, we also mention that absorption laser theory can be accounted for by constant flux states [17], and that non-Hermitian photonics [18,19] has found success in modelling systems with both balanced and imbalanced loss and gain.

5 In this article we refer to normal modes as those which form an orthogonal and complete set of solutions to the Helmholtz equation.

6 It is possible to carry out normal-mode quantisation in the presence of an inhomogeneous dispersive medium modelled as an undamped plasma [20,21], but the techniques used there break down for any more complicated response.

Quite some mileage can be obtained using the first approach in homogeneous dielectric media [22] and highly-reflecting cavities (see, e.g., approaches used in laser theory [23,24]) A normal-mode quantisation of the modes near an imperfectly reflecting dielectric half space given by Carniglia and Mandel as long ago as 1971 [25]. These normal modes were put to great use in the subsequent few decades, being used to find, for example, static dipole moments [26], polarisabilities [27], correlation functions [28], radiation patterns [29], radiation from moving dielectrics [30]. Even after the advent of the more sophisticated quantisation schemes discussed below, the normal mode approach still finds value in being simple, physically transparent and understandable, so finds modern applications as a simplifying agent in calculations of Casimir–Polder forces near layers [31], out of equilibrium [32] and with external fields [33], as well as self energies of elementary particles [34,35], Cherenkov friction [36] and the anomalous magnetic moment of the electron [37,38]. All of these calculations ignore the unavoidable presence of dissipation in any realistic medium.

MQED was originally proposed as a solution to the dissipation problem by Welsch and co-workers [39,40] and has been used with great success in a huge variety of settings [41–43]. Its foundations are essentially phenomenological — a fluctuating noise polarisation field is postulated (loosely representing the fact that quantised electromagnetic fields fluctuate), then a number of consistency conditions are used to in order to pin down the correct form of the corresponding electromagnetic field operators. The advantage of this approach is that all details (material, geometry, etc.) of the medium are abstracted away into the macroscopic response of the medium described by a Green's tensor which need not be specified until the very end of the calculation. A notable disadvantage, in common with the Lifshitz approach [44,45], is that there is no Hamiltonian for the theory (at least not in its original form) so it cannot be strictly considered canonically quantised (as mentioned above, there is no opportunity to identify Poisson brackets and promote these to commutators). The HBQED method takes a more microscopic approach — various baths of harmonic oscillators representing a medium are coupled to the free electromagnetic field, and the resulting Hamiltonian diagonalised to find the corresponding hybrid field–matter (polaritonic) fields. The disadvantage of this in its original formulation, however, is that there is no general prescription for how to deal with different geometries. In principle the whole theory must be rebuilt each time a new situation is required as was done for the dielectric half-space in [46] (with two earlier Refs. [47,48] having similar results stemming from any method that begins with the phenomenological MQED approach instead of a rigorous quantisation provided by HBQED). The HBQED method has some commonalities with the system–bath methods used in the theory of open quantum systems [49] or in random laser theory [50–52].

More recently, the formulations of MQED and HBQED were shown to be equivalent to each other in a remarkable paper by Philbin [14]. The approach taken there gives the best of both worlds — the observables of the theory in any inhomogeneous background can be expressed in terms of the macroscopically useful and flexible notion of the Green's tensor, while it also rests on firm theoretical foundations. The calculation is somewhat involved, in the next few sections we simply give an outline of the steps required, the full algebraic details can be found in Ref. [14].

3.3. Canonical formulation of classical electrodynamics in the presence of macroscopic media

Following Ref. [14], the starting point of the quantum theory of electromagnetism in media is a Lagrangian density

$$\mathscr{L}_c = \mathscr{L}_{\text{em}} + \mathscr{L}_{\text{X}} + \mathscr{L}_{\text{Y}} + \mathscr{L}_{\text{int}}, \tag{132}$$

which will be shown to be that which reproduces the equations of classical electrodynamics in media presented in Section 3.1. The first term of (132) corresponds to the free electromagnetic field, given in Eq. (41) as:

$$\mathscr{L}_{\text{em}} = \frac{1}{2\mu_0}\left(\frac{1}{c^2}\mathbf{E}\cdot\mathbf{E} - \mathbf{B}\cdot\mathbf{B}\right). \tag{133}$$

Again we recall that here and throughout the symbols $\mathbf{E}$ and $\mathbf{B}$ are just shorthands for their representations (33) in terms of $\mathbf{A}$ and ϕ, which we repeat here

$$\mathbf{E} = -\dot{\mathbf{A}} - \nabla\phi \qquad\qquad \mathbf{B} = \nabla\times\mathbf{A}. \tag{134}$$

The second term in the Lagrangian (132) is that of a bath of reservoir oscillators $\mathbf{X}$, which will represent electric excitations, expressed in frequency space as;

$$\mathscr{L}_{\text{X}} = \frac{1}{2}\int_0^\infty \mathrm{d}\omega(\dot{\mathbf{X}}_\omega\cdot\dot{\mathbf{X}}_\omega - \omega^2\mathbf{X}_\omega\cdot\mathbf{X}_\omega). \tag{135}$$

The third term is that for another identical bath $\mathbf{Y}$, which will represent magnetic excitations.

$$\mathscr{L}_{\text{Y}} = \frac{1}{2}\int_0^\infty \mathrm{d}\omega(\dot{\mathbf{Y}}_\omega\cdot\dot{\mathbf{Y}}_\omega - \omega^2\mathbf{Y}_\omega\cdot\mathbf{Y}_\omega) \tag{136}$$

The final term in (132) represents the coupling between the electric field $\mathbf{E}$ and its bath $\mathbf{X}$, and the magnetic field $\mathbf{B}$ and its bath $\mathbf{Y}$:

$$\mathscr{L}_{\text{int}} = \int_0^\infty \mathrm{d}\omega\,(\alpha\mathbf{X}_\omega\cdot\mathbf{E} + \beta\mathbf{Y}_\omega\cdot\mathbf{B}), \tag{137}$$

where the coupling strengths are given by

$$\alpha = \sqrt{\frac{2\varepsilon_0}{\pi}\omega \mathrm{Im}\varepsilon(\mathbf{r},\omega)} \qquad \text{and} \qquad \beta = \sqrt{-\frac{2}{\mu_0\pi}\omega \mathrm{Im}\left(\frac{1}{\mu(\mathbf{r},\omega)}\right)}, \tag{138}$$

with $\varepsilon(\mathbf{r},\omega)$ and $\mu(\mathbf{r},\omega)$ being the permittivity and permeability introduced in Eqs. (123) and (126). Even though only the imaginary part of these couplings appears in the Lagrangian, the real parts follow from the Kramers–Kronig relations (see, e.g., Chapter 7 of Ref. [53]), which ultimately express the fundamental notion of causality.

Variation of the Lagrangian (132) with respect to the dynamical fields ϕ and $\mathbf{A}$ gives;

$$\varepsilon_0 \nabla\cdot\mathbf{E} + \int_0^\infty \mathrm{d}\omega \nabla\cdot[\alpha(\mathbf{r},\omega)\mathbf{X}_\omega] = 0, \tag{139}$$

$$-\frac{1}{\mu_0}\nabla\times\mathbf{B} + \varepsilon_0\dot{\mathbf{E}} + \int_0^\infty \mathrm{d}\omega\{\alpha(\mathbf{r},\omega)\dot{\mathbf{X}}_\omega + \nabla\times[\beta(\mathbf{r},\omega)\mathbf{Y}_\omega]\} = 0. \tag{140}$$

These are already reminiscent of Maxwell's inhomogeneous Eqs. (36) and (39), suggesting that the quantities given by frequency integrals in Eqs. (139) and (140) will ultimately be identified as the charge and current densities. Varying the Lagrangian (132) with respect to the bath variables $\mathbf{X}$ and $\mathbf{Y}$ gives two more equations that relate $\mathbf{X}$ to $\mathbf{E}$ and $\mathbf{Y}$ to $\mathbf{B}$;

$$-\ddot{\mathbf{X}}_\omega - \omega^2\mathbf{X}_\omega + \alpha(\mathbf{r},\omega)\mathbf{E} = 0 \qquad -\ddot{\mathbf{Y}}_\omega - \omega^2\mathbf{Y}_\omega + \beta(\mathbf{r},\omega)\mathbf{B} = 0 \tag{141}$$

Since we seek equations describing the dynamics of the electromagnetic fields $\mathbf{E}$ and $\mathbf{B}$, the task therefore to use the above equations to express $\mathbf{X}$ and $\mathbf{Y}$ in terms of $\mathbf{E}$ and $\mathbf{B}$, and then substitute these into the Maxwell-reminiscent Eqs. (139) and (140). The results are [14];

$$\nabla\cdot\mathbf{D} = \rho_f \qquad \nabla\times\mathbf{H} - \dot{\mathbf{D}} = \mathbf{J}_f, \tag{142}$$

where

$$\mathbf{D}(\mathbf{r},t) = \frac{\varepsilon_0}{2\pi}\int_0^\infty \mathrm{d}\omega[\varepsilon(\mathbf{r},\omega)\mathbf{E}(\mathbf{r},\omega)e^{-i\omega t} + \text{c.c.}], \tag{143}$$

$$\mathbf{H}(\mathbf{r},t) = \frac{1}{2\pi\mu_0}\int_0^\infty \mathrm{d}\omega\left[\frac{1}{\mu(\mathbf{r},\omega)}\mathbf{B}(\mathbf{r},\omega)e^{-i\omega t} + \text{c.c.}\right], \tag{144}$$

and the free charge and current densities are

$$\rho_f(\mathbf{r},t) = -\frac{1}{2\pi}\nabla\cdot\int_0^\infty \mathrm{d}\omega[\alpha(\mathbf{r},\omega)\mathbf{Z}_\omega(\mathbf{r})e^{-i\omega t} + \text{c.c.}], \tag{145}$$

$$\begin{aligned}\mathbf{J}_f(\mathbf{r},t) = &-\frac{1}{2\pi}\frac{\partial}{\partial t}\int_0^\infty \mathrm{d}\omega[\alpha(\mathbf{r},\omega)\mathbf{Z}_\omega(\mathbf{r})e^{-i\omega t} + \text{c.c.}] \\ &+ \frac{1}{2\pi}\nabla\times\int_0^\infty \mathrm{d}\omega[\beta(\mathbf{r},\omega)\mathbf{W}_\omega(\mathbf{r})_\omega e^{-i\omega t} + \text{c.c.}],\end{aligned} \tag{146}$$

where $\mathbf{Z}_\omega$ is the solution of the homogeneous version of the equation of motion for $\mathbf{X}_\omega$ shown in Eq. (141) (i.e. that with $\mathbf{E} = \mathbf{0}$). Eqs. (134) and (142) are the four Maxwell equations in media, showing that the Lagrangian (132) is an acceptable one for (classical) macroscopic electrodynamics in media.

3.4. Quantum electrodynamics in the presence of macroscopic media

Now that we have a Lagrangian formulation of classical electrodynamics in media, a quantisation can be readily performed by identifying the momenta conjugate to ϕ, $\mathbf{A}$, $\mathbf{X}$ and $\mathbf{Y}$;

$$\Pi_\phi = \frac{\partial\mathscr{L}_c}{\partial(\partial_t\phi)} = 0 \qquad \boldsymbol{\Pi}_A = \frac{\partial\mathscr{L}_c}{\partial(\partial_t\mathbf{A})} = -\varepsilon_0\mathbf{E} - \int_0^\infty \mathrm{d}\omega\alpha(\mathbf{r},\omega)\mathbf{X}_\omega \tag{147}$$

$$\boldsymbol{\Pi}_{X_\omega} = \frac{\partial\mathscr{L}_c}{\partial(\partial_t\mathbf{X}_\omega)} = \partial_t\mathbf{X}_\omega \qquad \boldsymbol{\Pi}_{Y_\omega} = \frac{\partial\mathscr{L}_c}{\partial(\partial_t\mathbf{Y}_\omega)} = \partial_t\mathbf{Y}_\omega \tag{148}$$

As in free-space QED, the momentum conjugate to the scalar potential ϕ vanishes, and there are redundant degrees of freedom which can be eliminated by a gauge choice. The gauge employed here is Coulomb gauge $\nabla\cdot\mathbf{A} = 0$, which also leads to a constraint on the momentum conjugate to $\mathbf{A}$. Quantisation of constrained systems proceeds via promotion of Dirac brackets to commutators, rather than promotion of Poisson brackets as in the unconstrained theory. In particular, the quantum canonical operators should be defined by the following equal-time commutation relations

$$[\hat{\mathbf{A}}(\mathbf{r},t), \hat{\boldsymbol{\Pi}}_A(\mathbf{r}',t)] = i\hbar\delta^\perp(\mathbf{r}-\mathbf{r}') \tag{149}$$

$$[\hat{\mathbf{X}}_\omega(\mathbf{r},t), \hat{\boldsymbol{\Pi}}_{X,\omega'}(\mathbf{r}',t)] = i\hbar\boldsymbol{\delta}(\mathbf{r}-\mathbf{r}')\delta(\omega-\omega') \tag{150}$$

$$[\hat{\mathbf{Y}}_\omega(\mathbf{r},t),\hat{\boldsymbol{\Pi}}_{Y,\omega'}(\mathbf{r}',t)]=i\hbar\boldsymbol{\delta}(\mathbf{r}-\mathbf{r}')\delta(\omega-\omega') \tag{151}$$

with the transverse delta function defined in (67), and all other commutators being zero. Performing a Legendre transformation to obtain the Hamiltonian operator

$$\begin{aligned}\hat{H}=\int d^3r\Bigg\{&\frac{1}{\varepsilon_0}\hat{\boldsymbol{\Pi}}_A\cdot\left[\frac{1}{2}\hat{\boldsymbol{\Pi}}_A+\int_0^\infty \mathrm{d}\omega\alpha(\mathbf{r},\omega)\hat{\mathbf{X}}_\omega\right]+\frac{1}{2\mu_0}(\nabla\times\hat{\mathbf{A}})^2\\&+\frac{1}{2}\int_0^\infty \mathrm{d}\omega\left[\hat{\boldsymbol{\Pi}}_{X_\omega}^2+\hat{\boldsymbol{\Pi}}_{Y_\omega}^2+\omega^2(\hat{\mathbf{X}}_\omega^2+\hat{\mathbf{Y}}_\omega^2)\right]+\frac{1}{2\varepsilon_0}\left[\int_0^\infty \mathrm{d}\omega\alpha(\mathbf{r},\omega)\hat{\mathbf{X}}_\omega\right]^2\\&-\int_0^\infty \mathrm{d}\omega\beta(\mathbf{r},\omega)\hat{\mathbf{Y}}_\omega\cdot(\nabla\times\hat{\mathbf{A}})\Bigg\},\end{aligned} \tag{152}$$

one can then verify using the above commutators that the Heisenberg equations of motion produce four equations which are identical in form to Eqs. (140) and (141), but with $\mathbf{A}$, $\mathbf{X}$ and $\mathbf{Y}$ promoted to operators $\hat{\mathbf{A}}$, $\hat{\mathbf{X}}$ and $\hat{\mathbf{Y}}$.

Given the Hamiltonian (152), one in principle has all the ingredients necessary for a description of quantised electric fields in media. However, the Hamiltonian can be written in a much more useful form by diagonalising it in terms of bosonic creation and annihilation operators $\hat{\mathbf{f}}_\lambda^\dagger(\mathbf{r},\omega)$ and $\hat{\mathbf{f}}_\lambda(\mathbf{r},\omega)$ for the eigenmodes of the (combined field–matter) system. The Hamiltonian is quadratic in the canonical variables, so we aim to show that Hamiltonian can be written in the following form

$$\hat{H}=\sum_{\lambda=e,m}\int d^3\mathbf{r}\int_0^\infty \mathrm{d}\omega\hbar\omega\hat{\mathbf{f}}_\lambda^\dagger(\mathbf{r},\omega)\cdot\hat{\mathbf{f}}_\lambda(\mathbf{r},\omega) \tag{153}$$

with

$$\left[\hat{\mathbf{f}}_\lambda(\mathbf{r},\omega),\hat{\mathbf{f}}_{\lambda'}^\dagger(\mathbf{r}',\omega')\right]=\delta_{\lambda\lambda'}\delta(\omega-\omega')\boldsymbol{\delta}(\mathbf{r}-\mathbf{r}') \tag{154}$$

and all other commutators being zero, and $\lambda=e,m$ representing the electric and magnetic responses of the system. The six fields ($\hat{\mathbf{A}}$, $\hat{\mathbf{X}}_\omega(\mathbf{r},t)$ and $\hat{\mathbf{Y}}_\omega(\mathbf{r},t)$, together with their corresponding canonical momenta) appearing in the Hamiltonian (152) are assumed to be expressible as linear combinations of the operators $\hat{\mathbf{f}}$ and $\hat{\mathbf{f}}^\dagger$, meaning that the task reduces to finding the correct expansion coefficients[7] such that the diagonal form (153) of the Hamiltonian is produced. A lengthy procedure[8] follows in order to find the explicit form of the coefficients, which we will not repeat here. Instead, we will summarise the steps taken in the clear and explicit process detailed in Section 4 of Ref. [14], namely:

1. The fields are taken to be expressible as a linear combination of the diagonalised operators $\hat{\mathbf{f}}_\lambda$, e.g. $\hat{\mathbf{A}}(\mathbf{r})=\sum_\lambda\int d^3\mathbf{r}'\int_0^\infty \mathrm{d}\omega\mathbf{s}_\lambda(\mathbf{r},\mathbf{r}',\omega)\cdot\hat{\mathbf{f}}_\lambda(\mathbf{r}',\omega)$ and similarly for the other fields and conjugate momenta. This expansion must be invertible and consistency implies that $\hat{\mathbf{f}}_\lambda$ can be written as a linear combination of the coefficients and their corresponding fields and conjugate momenta.
2. The desired Hamiltonian (153) and commutation relations (154) imply that we can use $\hbar\omega\hat{\mathbf{f}}_\lambda=[\hat{\mathbf{f}}_\lambda,\hat{H}]$ (expanded in terms of the fields and conjugate momenta) to find an expression for the coefficients. These take the form of a coupled set of differential equations, which resemble Maxwell's equations together with the equations of motion for the baths $\hat{\mathbf{X}}$ and $\hat{\mathbf{Y}}$
3. The solution of these differential equations, normalised by demanding consistency with the commutation relation (154) when expanded in terms of the fields, completes the procedure. In the case of the photon field, the coefficients are given in terms of the Green's tensor [see Eq. (130)].

The result of this procedure is that the operator corresponding to the electric field (131) is;

$$\hat{\mathbf{E}}(\mathbf{r},t)=\frac{\mu_0}{2\pi}\int_0^\infty \mathrm{d}\omega\int d^3\mathbf{r}'[i\omega\mathbb{G}(\mathbf{r},\mathbf{r}',\omega)\cdot\hat{\mathbf{J}}(\mathbf{r}',\omega)e^{-i\omega t}+c.c.], \tag{155}$$

where

$$\hat{\mathbf{J}}(\mathbf{r},\omega)=-2\pi i\omega\sqrt{\frac{\hbar\varepsilon_0}{\pi}\mathrm{Im}\varepsilon(\mathbf{r},\omega)}\hat{\mathbf{f}}_e(\mathbf{r},\omega)+2\pi\nabla\times\left[\sqrt{-\frac{\hbar}{\mu_0\pi}\mathrm{Im}\left(\frac{1}{\mu(\mathbf{r},\omega)}\right)}\hat{\mathbf{f}}_m(\mathbf{r},\omega)\right], \tag{156}$$

[7] A caution about notation — in Ref. [14] the diagonalising operators which we call $\hat{\mathbf{f}}$ are instead called $\hat{\mathbf{C}}$, and the expansion coefficients which we have named $\mathbf{s}$ are called $\mathbf{f}$ in Ref. [14].

[8] It is noteworthy that this follows in an identical fashion to the lossless normal mode case, except that the matter field(s) is now a bath of oscillators.

which, as promised, shows that the field can be written in terms of the diagonalising operators $\hat{\mathbf{f}}_\lambda(\mathbf{r},\omega)$ with a coefficient $\mathbb{G}_e$ or $\mathbb{G}_m$ that depends on the Green's tensor $\mathbb{G}$. It proves useful to define;

$$\mathbb{G}_e(\mathbf{r},\mathbf{r}',\omega) = i\frac{\omega^2}{c^2}\sqrt{\frac{\hbar}{\pi\varepsilon_0}\mathrm{Im}\varepsilon(\mathbf{r}',\omega)}\mathbb{G}(\mathbf{r},\mathbf{r}',\omega), \tag{157}$$

$$\mathbb{G}_m(\mathbf{r},\mathbf{r}',\omega) = i\frac{\omega}{c}\sqrt{\frac{\hbar}{\pi\varepsilon_0}\frac{\mathrm{Im}\mu(\mathbf{r}',\omega)}{|\mu(\mathbf{r}',\omega)|^2}}[\nabla'\times\mathbb{G}(\mathbf{r},\mathbf{r}',\omega)]^{\mathrm{T}}, \tag{158}$$

which obey a useful integral relation [see, e.g., Ref. [42]. Eq. (2.262)]

$$\sum_{\lambda=e,m}\int \mathrm{d}^3s\mathbb{G}_\lambda(\mathbf{r},\mathbf{s},\omega)\cdot\mathbb{G}_\lambda^{*\mathrm{T}}(\mathbf{r}',\mathbf{s},\omega) = \frac{\hbar\mu_0}{\pi}\omega^2\mathrm{Im}\mathbb{G}(\mathbf{r},\mathbf{r}',\omega). \tag{159}$$

Finally, $\mathbf{E}$ becomes;

$$\hat{\mathbf{E}}(\mathbf{r},t) = \int_0^\infty \mathrm{d}\omega\sum_{\lambda=e,m}\int d^3\mathbf{r}'\left[\mathbb{G}_\lambda(\mathbf{r},\mathbf{r}',\omega)\cdot\hat{\mathbf{f}}_\lambda(\mathbf{r}',\omega)e^{-i\omega t}+c.c.\right], \tag{160}$$

or in terms of frequency components

$$\hat{\mathbf{E}}(\mathbf{r}) = \int_0^\infty \mathrm{d}\omega\sum_{\lambda=e,m}\int d^3\mathbf{r}'\left[\mathbb{G}_\lambda(\mathbf{r},\mathbf{r}',\omega)\cdot\hat{\mathbf{f}}_\lambda(\mathbf{r}',\omega)+c.c.\right]. \tag{161}$$

This is the central equation for the 'end user' of quantum electrodynamics in the presence of media, representing the electric field in terms of a bosonic field with creation and annihilation operators $\hat{\mathbf{f}}^\dagger$ and $\hat{\mathbf{f}}$. Excitations of this field represent combined field–matter excitations, as can easily be motivated by observing that (161) depends on the permittivity and permeability via Eqs. (157) and (158). This mixed light–matter character means they are sometimes referred to as being 'polariton-like'. It will become important later to distinguish between the polaritons arising from a mixture of light with the bulk medium described as simple harmonic oscillators, and 'polaritons' arising from the coupling of *that* field to quantum emitters. To avoid this confusion we will follow a standard convention from the macroscopic QED literature, referring to the excitations created and annihilated by $\hat{\mathbf{f}}^\dagger$ and $\hat{\mathbf{f}}$ as 'photons', even though they have a matter component. This is consistent with the common practice of treating $\mathbf{D}$ and $\mathbf{H}$ like electric and magnetic fields, even though they both also have a matter component.

There is one more delicate point to discuss — in the limit of a non-absorptive medium the imaginary parts of the permittivity and permeability will vanish, so inspection of (157) and (158) implies that the field $\mathbf{E}$ in (161) should vanish in this case. This would naïvely imply, for example, that there is no vacuum field in free space, meaning no spontaneous decay, which would be in clear contradiction with both normal-mode QED and experiment. It would also appear to invalidate the relation (159) — the right hand side remains finite in the lossless limit while the left hand side seems to vanish. This question has been revisited a number of times [54–58], and there are several perspectives on an answer. Perhaps most convincingly, it was shown in [58] that if sufficient care is taken with evaluation of the limit of small absorption, then Eq. (159) does in fact hold (for unit relative permeability) in the lossless limit even though at first sight it appears not to. The crucial ingredient is that evaluation of the spatial integral reveals a factor cancelling the imaginary part of the permittivity. In a finite medium the situation is more delicate, but it was shown in [55] that (159) should be supplemented by a surface term. This surface term vanishes in the presence of a background medium with any amount of loss (even infinitesimal). This is related to earlier physical arguments [59,60] that at least a small amount of absorption should always be retained if no boundary contribution is to arise. This issue is usually of no consequence in practical calculations, since one invariably ends up with combinations of Green's tensors like that shown in (159), use of which causes the offending factors of $\mathrm{Im}\varepsilon$ and $\mathrm{Im}\mu$ to drop out of the calculation.[9] This ad-hoc procedure allows the lossless limit to be taken at the end of the calculation, which is in agreement with the corresponding results if lossless QED had been used from the start (see e.g. [59,60] for discussions specifically of this, and any of the literature on atomic processes in macroscopic QED for agreements with lossless limits).

4. Selected perturbative atomic processes

In this section we will give an overview of selected perturbative atomic processes that can be modified by choice of an electromagnetic environment, with the ultimate goal of having some observables to optimise in Section 6. We begin in Section 4.1 with the spontaneous decay of an excited atom, then move on to the Casimir–Polder force in Section 4.2, followed by energy transfer in 4.3. It should be noted that even in the weak coupling regime considered here, this is by no means an exhaustive list of atomic processes, instead acting as a representative selection for introducing perturbative methods. Other phenomena that can be described in similar ways include (but are not limited to) atomic waveguide QED [61,62], photon condensation [63], Auger decay [64] and non-linear optics [65].

[9] A rigorous proof that observable quantities in unbounded space cannot suffer from this problem would be a valuable addition to the subject.

4.1. Spontaneous decay in free space

Left to its own devices, an excited atom will eventually release its energy into the electromagnetic field. This is the process famously described by Einstein's A coefficient [66], and can be understood either as radiation reaction from an oscillating dipole, or stimulated emission induced by vacuum fluctuations (or indeed any mixture between the two [67]). Here we will quantify this rate of spontaneous decay by carrying out a simple calculation (analogous to those appearing in [57,68,69]) that will lead into a first example of how light–matter interactions can be manipulated for a given purpose.

We will assume that the dominant mechanism of relaxation is an electric dipole transition, so the interaction Hamiltonian will be taken from Eq. (106) as

$$H_{\text{int}} = -\hat{\mathbf{d}} \cdot \hat{\mathbf{E}}(\mathbf{r}_{\text{A}}) \tag{162}$$

We will calculate the emission rate Γ from Fermi's Golden Rule (see, for example, Chapter 5 of [70])

$$\Gamma = \frac{2\pi}{\hbar} \sum_f |\langle f|H_{\text{int}}|i\rangle|^2 \delta(E_f - E_i), \tag{163}$$

where $|i\rangle$ is the initial state, $|f\rangle$ is the final state and $E_{i/f}$ are their respective energies. The summation should be taken to be either a summation or integral (or both), depending on the nature and normalisation of the final states which we do not know yet, in principle. We will take the initial and final states to be products of the eigenstates of the atom and photon field

$$|i\rangle = |e\rangle \otimes |0\rangle \equiv |e; 0\rangle \qquad |f\rangle = |g\rangle \otimes |\mathbf{1}_\lambda(\mathbf{r}, \omega)\rangle \equiv |g; \mathbf{1}_\lambda(\mathbf{r}, \omega)\rangle, \tag{164}$$

where $|g\rangle$ and $|e\rangle$ are the ground and excited states as indicated in Fig. 1, $|0\rangle$ is the ground state of the photon field, and finally $|\mathbf{1}_\lambda(\mathbf{r}, \omega)\rangle \equiv \hat{\mathbf{f}}^\dagger_\lambda(\mathbf{r}, \omega)|0\rangle$ is a one-photon state. Note that $|f\rangle$ is now strictly a vector of kets, so the appropriate statement of Fermi's golden rule is[10]

$$\Gamma = \frac{2\pi}{\hbar} \int \mathrm{d}^3 r'' \int \mathrm{d}\omega' \sum_{\lambda'} \langle e; 0|H_{\text{int}}|g; \mathbf{1}_\lambda(\mathbf{r}'', \omega')\rangle \cdot \langle g; \mathbf{1}_\lambda(\mathbf{r}'', \omega')|H_{\text{int}}|e; 0\rangle \delta(E_f - E_i) \tag{165}$$

The electric field is given by (161), repeated in expanded form here for clarity;

$$\hat{\mathbf{E}}(\mathbf{r}, t) = \int_0^\infty \mathrm{d}\omega \sum_{\lambda=e,m} \int \mathrm{d}^3 r' \left[\mathbb{G}_\lambda(\mathbf{r}, \mathbf{r}', \omega) \cdot \hat{\mathbf{f}}_\lambda(\mathbf{r}', \omega) e^{-i\omega t} + \mathbb{G}^*_\lambda(\mathbf{r}, \mathbf{r}', \omega) \cdot \hat{\mathbf{f}}^\dagger_\lambda(\mathbf{r}', \omega) e^{i\omega t} \right] \tag{166}$$

Then we can calculate each factor in the rate (165) in turn;

$$\begin{aligned} \langle g; \mathbf{1}_\lambda(\mathbf{r}'', \omega')|H_{\text{int}}|e; 0\rangle = \langle g; \mathbf{1}_{\lambda'}(\mathbf{r}'', \omega')| \int_0^\infty \mathrm{d}\omega \sum_{\lambda=e,m} \int \mathrm{d}^3 r' \Big[\mathbb{G}_\lambda(\mathbf{r}, \mathbf{r}', \omega) \cdot \hat{\mathbf{f}}_\lambda(\mathbf{r}', \omega) e^{-i\omega t} \\ + \mathbb{G}^*_\lambda(\mathbf{r}, \mathbf{r}', \omega) \cdot \hat{\mathbf{f}}^\dagger_\lambda(\mathbf{r}', \omega) e^{i\omega t} \Big] |e; 0\rangle. \end{aligned} \tag{167}$$

Using the commutation relation (154), this becomes

$$\begin{aligned} \langle g; \mathbf{1}_\lambda(\mathbf{r}'', \omega')|H_{\text{int}}|e; 0\rangle &= \langle g; \mathbf{1}_{\lambda'}(\mathbf{r}'', \omega')|\hat{\mathbf{d}} \cdot \int_0^\infty \mathrm{d}\omega \sum_{\lambda=e,m} \int \mathrm{d}^3 r' \mathbb{G}^*_\lambda(\mathbf{r}, \mathbf{r}', \omega) \cdot \hat{\mathbf{f}}^\dagger_\lambda(\mathbf{r}', \omega) e^{i\omega t}|e; 0\rangle \\ &= \mathbf{d}^\downarrow \cdot \mathbb{G}^*_{\lambda'}(\mathbf{r}, \mathbf{r}'', \omega') e^{i\omega' t}, \end{aligned} \tag{168}$$

where $\mathbf{d}^\downarrow \equiv \langle g|\hat{\mathbf{d}}|e\rangle$. Similarly;

$$\langle e; 0|H_{\text{int}}|g; \mathbf{1}_\lambda(\mathbf{r}'', \omega')\rangle = \mathbf{d}^\uparrow \cdot \mathbb{G}_{\lambda'}(\mathbf{r}, \mathbf{r}'', \omega') e^{-i\omega t}, \tag{169}$$

where $\mathbf{d}^\uparrow \equiv \langle e|\hat{\mathbf{d}}|g\rangle$. Combining (168) and (169) as dictated by Eq. (165) gives

$$\langle e; 0|H_{\text{int}}|g; \mathbf{1}_\lambda(\mathbf{r}'', \omega')\rangle \cdot \langle g; \mathbf{1}_\lambda(\mathbf{r}'', \omega')|H_{\text{int}}|e; 0\rangle = [\mathbf{d}^\uparrow \cdot \mathbb{G}_{\lambda'}(\mathbf{r}, \mathbf{r}'', \omega')] \cdot [\mathbf{d}^\downarrow \cdot \mathbb{G}^*_{\lambda'}(\mathbf{r}, \mathbf{r}'', \omega')]. \tag{170}$$

This can be simplified by noting the identity that $(\mathbf{a} \cdot \mathbb{B}) \cdot (\mathbf{c} \cdot \mathbb{D}) = \mathbf{a} \cdot (\mathbb{B} \cdot \mathbb{D}^{\text{T}}) \cdot \mathbf{c}$ for vectors $\mathbf{a}$, $\mathbf{c}$ and matrices $\mathbb{B}$, $\mathbb{D}$. Applying this to the above gives;

$$\langle e; 0|H_{\text{int}}|g; \mathbf{1}_\lambda(\mathbf{r}'', \omega')\rangle \cdot \langle g; \mathbf{1}_\lambda(\mathbf{r}'', \omega')|H_{\text{int}}|e; 0\rangle = \mathbf{d}^\downarrow \cdot [\mathbb{G}_{\lambda'}(\mathbf{r}, \mathbf{r}'', \omega') \cdot \mathbb{G}^{*T}_{\lambda'}(\mathbf{r}, \mathbf{r}'', \omega')] \cdot \mathbf{d}^\uparrow \tag{171}$$

[10] A note on dimensions and normalisation — the operator $\hat{\mathbf{f}}_\lambda(\mathbf{r}, \omega)$ has a dimension of (volume × frequency)$^{-1/2}$ as can be seen from the commutation relation (154), so $|f\rangle = |g; \mathbf{1}_\lambda(\mathbf{r}, \omega)\rangle = \hat{\mathbf{f}}^\dagger_\lambda(\mathbf{r}, \omega)|g; 0\rangle$ shares this dimension. The state $|f\rangle$ appears twice in the integrand of (165) so the dimensions cancel with those of the integration measure, ensuring that the whole expression produces a rate.

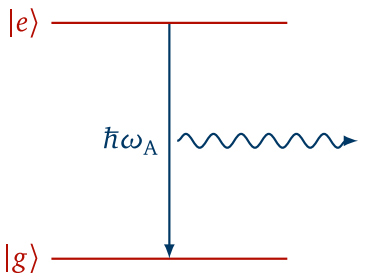

Fig. 1. Levels and energies involved in spontaneous decay.

giving for the rate (165):

$$\Gamma = \frac{2\pi}{\hbar}\int \mathrm{d}^3 r'' \int \mathrm{d}\omega' \sum_{\lambda'} \mathbf{d}^{\downarrow} \cdot [\mathbb{G}_{\lambda'}(\mathbf{r}, \mathbf{r}'', \omega') \cdot \mathbb{G}^{*T}_{\lambda'}(\mathbf{r}, \mathbf{r}'', \omega')] \cdot \mathbf{d}^{\uparrow} \delta(E_f - E_i) \tag{172}$$

Using the integral relation (159), this simplifies to

$$\Gamma = \frac{2\pi}{\hbar}\frac{\hbar\mu_0}{\pi}\int \mathrm{d}\omega' \omega'^2 \mathbf{d}^{\downarrow} \cdot \mathrm{Im}\mathbb{G}(\mathbf{r}, \mathbf{r}, \omega') \cdot \mathbf{d}^{\uparrow} \delta(E_f - E_i), \tag{173}$$

giving finally

$$\Gamma = \frac{2\omega_{\mathrm{A}}^2}{\hbar\varepsilon_0 c^2}\mathbf{d}^{\downarrow} \cdot \mathrm{Im}\mathbb{G}(\mathbf{r}, \mathbf{r}, \omega) \cdot \mathbf{d}^{\uparrow}, \tag{174}$$

where $E_f - E_i = \hbar\omega' - \hbar\omega_{\mathrm{A}}$, the scaling property of the delta function [$\delta(ax) = |a|^{-1}\delta(x)$] and $\mu_0 = 1/(\varepsilon_0 c^2)$ were used. This result relies on the non-trivial weak-coupling and timescale separation assumptions that went into deriving Fermi's Golden Rule in the first place (see, e.g., Ref. [71]), but nevertheless this elementary derivation (the simplest example of working with a **G** in perturbation theory) is in agreement with more complex calculations based on explicit atomic dynamics [72]. Note here that we have also neglected any environment-induced shifts in the atomic transition frequency (known as the Lamb shift when in free space [73], and the Casimir–Polder shift when an inhomogeneous medium is introduced as discussed in detail in Section 4.2).

The simplest case of Eq. (174) is vacuum, for which the Green's tensor is given by (see, e.g. Appendix B of [42]);

$$\mathbb{G}^{\mathrm{vac}}(\mathbf{r}, \mathbf{r}', \omega) = -\frac{c^2}{3\omega^2}\delta(\boldsymbol{\rho}) - \frac{c^2 e^{i\omega\rho/c}}{4\pi\omega^2\rho^3}\left\{\left[1 - i\frac{\omega\rho}{c} - \left(\frac{\omega\rho}{c}\right)^2\right]\mathbb{I}_3 - \left[3 - 3i\frac{\omega\rho}{c} - \left(\frac{\omega\rho}{c}\right)^2\right]\mathbf{e}_\rho \otimes \mathbf{e}_\rho\right\} \tag{175}$$

where $\boldsymbol{\rho} = \mathbf{r} - \mathbf{r}'$, $\rho = |\boldsymbol{\rho}|$ and $\mathbf{e}_\rho = \boldsymbol{\rho}/\rho$. We require the imaginary part of this at equal positions $\mathbf{r} = \mathbf{r}'$, which immediately presents a problem as it appears to diverge as $\rho \to 0$ (and indeed the real part does). Taylor-expanding the exponential, however, reveals that

$$\mathrm{Im}\mathbb{G}^{\mathrm{vac}}(\mathbf{r}, \mathbf{r}, \omega) = \frac{\omega}{6\pi c}\mathbb{I}_3, \tag{176}$$

which can be substituted into (174) to find;

$$\Gamma^{\mathrm{vac}} = \frac{|\mathbf{d}|^2\omega_{\mathrm{A}}^3}{3\pi\hbar\varepsilon_0 c^3}, \tag{177}$$

which is the well-known rate of spontaneous decay in free space. It is hopefully obvious that use of a different $\mathbb{G}$ (corresponding to a different environment) would have resulted in a different value for the rate Γ – this ability to tune a decay rate through the environment is known as the Purcell effect, introduced in a remarkably short paper in 1946 [74]. The arguments originally put forward by Purcell were not based on Eq. (174), but instead concerned modifications to the density of states available to an emitter. This is of course equivalent to the more modern approach, where the local density of states (LDOS) for an emitter at position $\mathbf{r}_{\mathrm{A}}$ with transition dipole moment aligned along the direction $\hat{\mathbf{n}}$ which can be derived from classical electrodynamics as [75–77]

$$\rho_{\mathrm{L}}(\mathbf{r}_{\mathrm{A}}) = \frac{2\omega_{\mathrm{A}}}{\pi c^2}\hat{\mathbf{n}} \cdot \mathrm{Im}\mathbb{G}(\mathbf{r}_{\mathrm{A}}, \mathbf{r}_{\mathrm{A}}, \omega_{\mathrm{A}}) \cdot \hat{\mathbf{n}}, \tag{178}$$

with a particularly clear pedagogical derivation being found in Ref. [78]. This formula assumes a fixed emitter direction so is sometimes known as the partial LDOS. If the total emitted power of a randomly oriented dipole is desired then one should sum over the three orientations, giving the 'full' LDOS

$$\rho_{\mathrm{L,full}}(\mathbf{r}_{\mathrm{A}}) = \frac{2\omega_{\mathrm{A}}}{\pi c^2}\mathrm{Tr}\left[\mathrm{Im}\mathbb{G}(\mathbf{r}_{\mathrm{A}}, \mathbf{r}_{\mathrm{A}}, \omega_{\mathrm{A}})\right]. \tag{179}$$

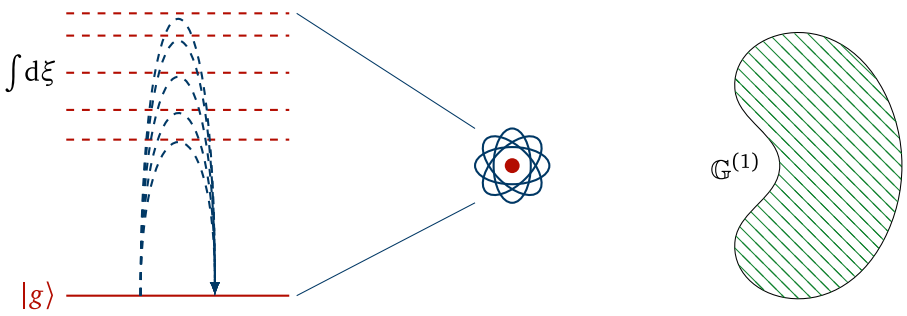

Fig. 2. Schematic illustration of the ground Casimir–Polder potential as a integral over virtual transitions to all excited states, modified by the presence of an arbitrary inhomogeneous environment with scattering Green's tensor $\mathbb{G}^{(1)}$.

The spontaneous decay rate in terms of the LDOS is [76]

$$\Gamma = \frac{\pi\omega_{\mathrm{A}}}{\hbar\varepsilon_0}|\mathbf{d}|^2\rho(\mathbf{r}_{\mathrm{A}}). \tag{180}$$

Combining this with Eq. (178) reproduces the environment-dependent decay rate (174) as expected. One can also define a similar quantity known as the 'cross' density of states

$$\rho_{\mathrm{C}}(\mathbf{r}_{\mathrm{A}}, \mathbf{r}_{\mathrm{B}}) = \frac{2\omega}{\pi c^2}\hat{\mathbf{n}}_{\mathrm{A}} \cdot \mathrm{Im}\mathbb{G}(\mathbf{r}_{\mathrm{A}}, \mathbf{r}_{\mathrm{B}}, \omega) \cdot \hat{\mathbf{n}}_{\mathrm{B}}, \tag{181}$$

which characterises the degree of coherence between two emitters A and B (see, for example, Refs. [77,79–81]), or can alternatively be understood in a classical sense as counting the contribution of the modes connecting $\mathbf{r}_{\mathrm{A}}$ and $\mathbf{r}_{\mathrm{B}}$ at a specific frequency ω [82].

Beginning with the pioneering measurement of dielectric interface modified decay time by Drexhage in [83], the modified spontaneous decay rate in an environment been experimentally observed and exploited far too many times to count as it forms the basis of the pervasive Purcell effect (see, for example, [84–87]). More recently the environment-dependent LDOS and/or CDOS have been characterised in their own right in microwave circuits [88,89] as discussed in more detail in Section 5.5. The LDOS has also been experimentally probed with electron energy loss spectroscopy [90] and fluorescence intensity measurements in the near-field [91,92].

In exactly the same way as the rate of spontaneous decay can be adjusted by choice of environment with a different $\mathbb{G}$, a wide variety of different atomic quantities and processes can be written in terms of $\mathbb{G}$ and therefore designed by its choice. In the following subsections we will very briefly outline the derivation of a selection of these and for each we will survey how the expressions have been taken advantage of in order to manipulate light–matter interactions. In all of the examples below, the basic logic is the same — an atomic process which involves emission/absorption from vacuum modes is modified when those vacuum modes become subject to the boundary conditions imposed by macroscopic objects.

4.2. Ground-state Casimir–Polder potential

The energy levels of an atom are modified slightly by the existence of the quantised vacuum field into which it can emit and re-absorb virtual photons — in free space this is known as the Lamb shift [73]. The properties of an atom are similarly modified if it is brought close to its mirror image in a conducting surface — this was known before the invention of QED as the London dispersion force. Some discrepancies with experiment in the long-range behaviour of intermolecular forces [93] caused Casimir and Polder to consider the influence of relativistic retardation on this effect [94], necessitating the full apparatus of QED and producing the effect which bears their names.[11] Interestingly, Casimir and Polder's original derivation of the potential did not invoke the idea of the vacuum field at all, instead relying on retarded correlations between fluctuating dipole moments, which incidentally turns out to be very complicated. While both points of view (source theory and vacuum fluctuations) are correct [99] (being connected by the fluctuation–dissipation theorem), Casimir and Polder remark that the simple form of their results might mean that they can be derived in an alternative and simpler way — this turned out to be the case using the vacuum field for which Casimir's famous effect [100] is one of the main observable signatures.

[11] There is some unfortunate confusion in the literature about nomenclature for Casimir–Polder and van der Waals forces. Some authors refer to any far-zone interaction between atoms or between an atom and a macroscopic body as Casimir–Polder, with the corresponding short-distance limits being called van der Waals (e.g. [95,96]). However, other authors refer to the Casimir–Polder effect as being the interaction (at any distance) between a neutral atom and a macroscopic body (e.g. [97]), and the van der Waals force as being the interaction (at any distance) between neutral atoms (e.g. [98]). Either of these is a reasonable reading of Casimir and Polder's original paper, whose contribution was a theory that works at arbitrary distances between atoms *and* between an atom and a plate, with the far-zone limit being their main novel result.

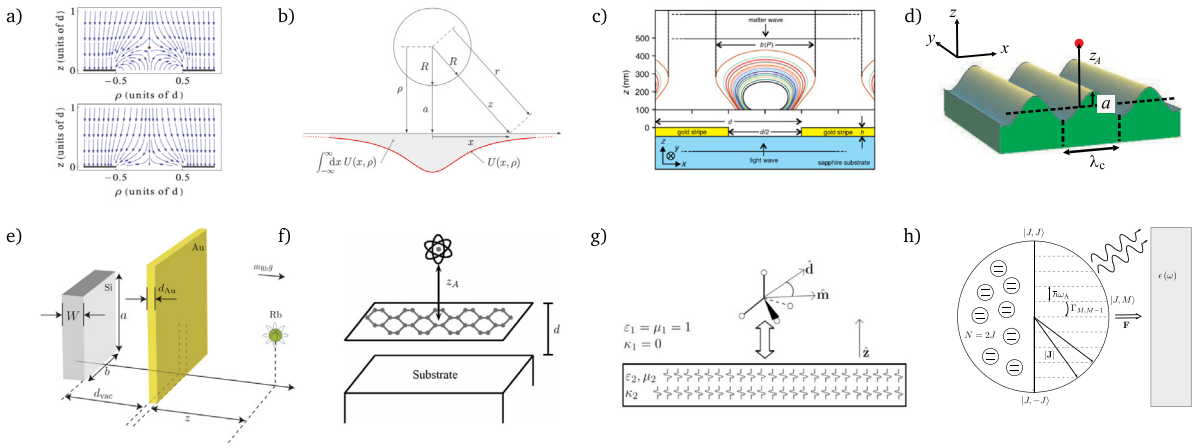

Fig. 3. Selected systems to which the theory of Casimir–Polder forces has been applied. (a) Plate with a hole of diameter d, obtained by Kelvin transformation of the (static) Green's function [114] (see also Section 5.3.2). (b) Phase accumulated at a dielectric sphere of radius R for use in matter–wave diffraction calculations [115]. (c) Potential landscape for probing Casimir–Polder interactions of a grating using a BEC [116] (d) Lateral forces with corrugated surfaces [117]. (e) Shielding of vacuum fluctuations to expose possible fifth forces [118]. (f) Shielding vacuum fluctuations a distance d above a gold substrate using graphene [119]. (g) Casimir–Polder forces between chiral objects [120], which requires a non-zero electric dipole moment **d** *and* a non-zero magnetic dipole moment **m** (h) N-body Casimir–Polder effect enhanced by collective behaviour [111].

For a ground state atom, the Casimir–Polder effect can be understood as originating in virtual transitions from the ground level to all other states (real or virtual) lying above it (see Fig. 2). The potential arising from this can be calculated from second-order time-independent perturbation theory, and for the simplest case of an electrically polarisable atom at zero temperature is given explicitly by [72];

$$U(\mathbf{r}_\mathrm{A}) = \frac{\hbar\mu_0}{2\pi}\int_0^\infty \mathrm{d}\xi\, \xi^2 \mathrm{Tr}\left[\alpha_\mathrm{A}(i\xi)\cdot\mathbb{G}^{(1)}(\mathbf{r}_\mathrm{A},\mathbf{r}_\mathrm{A},i\xi)\right], \tag{182}$$

where $\alpha_\mathrm{A}(\omega)$ is the dynamical polarisability of the atom, and the integration contour has been rotated to imaginary frequencies to tame a rapidly-oscillating integral. The force on the atom (in conservative cases, see e.g. [101]) then follows as minus the gradient of this potential. In the case of a perfectly reflecting planar surface, this equation reproduces Casimir and Polder's original results [94]. Similar formulae can be reached for atoms prepared in excited states [21,72,102–104], the essential difference being additional terms that result from resonant processes to lower-lying levels. The theory can be extended for paramagnetic [105,106] and diamagnetic [107] atoms, as well as for non-zero temperature [44,108–110] and collective effects [111,112]. Theoretical investigations based on formula (182) and its generalisations are far too numerous to list in full (for a recent comprehensive review on atom–surface interactions see [113]), selected systems to which the formula (182) can be directly applied are shown in Fig. 3.

As mentioned above, the Casimir–Polder force is closely related to the short-range London dispersion force between an atom and its image which was observed in various experiments dating back to the 1960s. Such experiments were either carried out with conducting surfaces [121,122] (see Fig. 4a) [123–126] or dielectrics [127–129]. More recently the effect of these short-range forces on matter–wave diffraction has been quantified [130–133], including most very recently with Poisson spot diffraction [134]. The longer-range Casimir–Polder force was first measured in 1993 [135] (see Fig. 4b) by measuring the deflection of sodium atoms passing through a micron-sized cavity. This was followed by measurements of Casimir–Polder forces using quantum reflection [136–139], ion trapping [140,141], Bose–Einstein condensates [142–144] (see Fig. 4c), and very recently by slow atom diffraction [145] (see Fig. 4d).

4.3. Resonant energy transfer and interatomic Coulombic decay

Resonant energy transfer is a process by which energy is transferred from an excited atom or molecule (referred to as the donor) to another atom or molecule (known as the acceptor), as schematically illustrated in Fig. 5. The process should be contrasted with the shorter-range Dexter energy transfer [146], where atomic or molecular wave function overlap is significant enough for electrons themselves to be transferred between donor and acceptor — in RET the donor and acceptor are taken to be well enough separated that all electrons stay bound to their respective nuclei.

The history of RET is long and meandering, as detailed in a recent comprehensive review by Jones and Bradshaw [147]. Briefly, RET was first observed in the 1920s under the name 'sensitised fluorescence' [148–150] when, upon illumination of a binary mixture of vapours at the resonance frequency of one of the constituents, emission was observed at that of the other, implying an interspecies transfer of energy which was first explained theoretically in Ref. [151]. The theory was

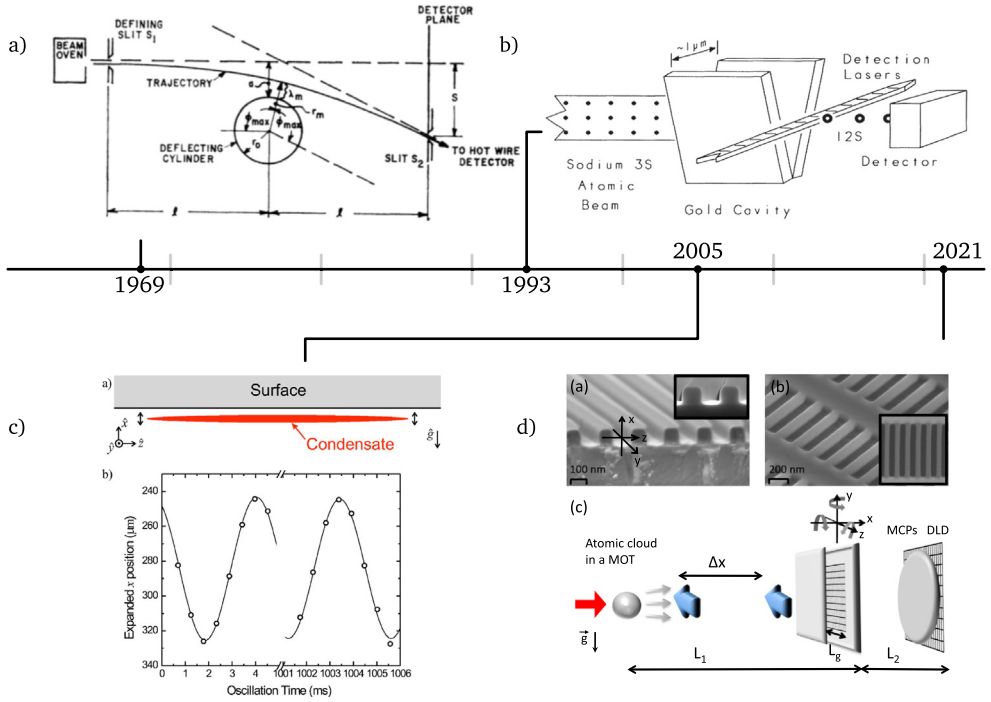

Fig. 4. Illustration of selected methods of measuring atom–surface forces. (a) Apparatus for measuring the deflection of a beam of caesium atoms by a gold cylinder (from [122]). (b) Experimental schematic of a micron-sized cavity for deflection of sodium atoms (from [135]). (c) Oscillations of a BEC trapped near a surface from (from [142]). (d) Slow atom diffraction by a grating (from [145]).

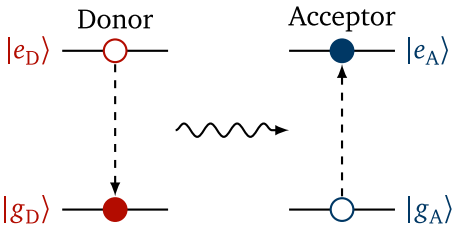

Fig. 5. Schematic illustration of resonance energy transfer by relaxation to the ground state $|g_D\rangle$ of a donor molecule initially in its excited state $|e_D\rangle$, transmitting its energy to an acceptor molecule, causing it to be excited from its ground state $|g_A\rangle$ to its excited state $|e_A\rangle$.

refined and put into the most basic (short-range) version of its modern form by Förster[12] [152,153]. Förster's theory was the first to include the effect of broadened – and hence possibly overlapping – donor emission and acceptor absorption spectra. It was also the first to exploit the close analogy between the interaction energy of oscillating dipoles and the interaction of a single transition dipole with light, and the first to quantitatively predict the characteristic dependence of the RET rate on the inverse sixth power of the separation, as experimentally verified some decades later [154]. This high sensitivity to distance is the basis of the idea of the 'spectroscopic ruler' [155] still in use as an analytical tool today in the field known as FRET microscopy (see, for example, [156–161]). Modern usage of the Förster theory in interpreting microscopy data comes with significant caveats concerning deviations from the original Förster theory [162,163], with the common theme being breakdown of a point-dipole model at short distances (discussed in the context of the closely-related interatomic Coulombic decay process in [164]).

The modern theory of resonance energy transfer at general intermolecular distances (that is, any distance larger than the orbital overlap region) is based on non-relativistic QED as described in Section 2. This incorporates the short-distance limit as originally predicted by Förster, but also predicts deviations at distances significantly larger than the characteristic wavelength of the donor transition. While the first steps towards an account of far-zone RET were taken in the 1960s [165,166], the first full statement of the theory connecting the two regimes was given in the 1980s by Power and Thirunamachandran [167] and advanced further by Andrews and co-workers [168,169] in the subsequent years. One

[12] For this reason RET sometimes bears the name Förster energy transfer or FRET, where the F is sometimes taken to denote 'fluorescence'.

of the main difficulties and points of contention in the QED theory of RET is the correct choice of contour in the complex frequency plane when integrating over wave vectors, this problem was circumvented in [170] by careful re-expression of the involved integrals to be oscillatory but convergent, finding agreement of final results with the choice of contour deemed to be most physically acceptable in prior work. More recently an approach based on vector spherical harmonics was taken [171], eliminating the need for contour integration entirely and confirming the choices made in previous works. In practice, probably the most convenient method of dealing with this issue is simply displacing the offending poles away from the real axis [172], equivalent to having started with the presence of vibronic structure which would entail using the so-called *generalised* Fermi's Golden Rule;

$$\Gamma = \frac{2\pi}{\hbar}\sum_f |\langle f|T|i\rangle|^2\delta(E_f - E_i), \tag{183}$$

with

$$T = H_{\rm int} + \lim_{\epsilon\to 0} H_{\rm int}\frac{1}{E_i - H + i\epsilon}H_{\rm int}. \tag{184}$$

and the summation representing the same notion as in Eq. (163). Considering donor and acceptor to be modelled as dipoles interacting via Hamiltonian (106), sitting in free space separated by a distance ρ, calculation of the RET rate using Fermi's Golden rule and the QED formalism of Ref. [167] leads to;

$$\Gamma_{\rm vac} = \frac{|\mathbf{d}_{\rm D}^{\uparrow}|^2|\mathbf{d}_{\rm A}^{\downarrow}|^2}{36\pi\hbar\varepsilon_0^2}\left[\frac{3}{\rho^6} + \frac{\omega_{\rm D}^2}{c^2}\frac{1}{\rho^4} + \frac{\omega_{\rm D}^4}{c^4}\frac{1}{\rho^2}\right], \tag{185}$$

where, similarly to in Section 4.1, $\mathbf{d}_{\rm D}^{\downarrow} = \langle g_{\rm D}|\hat{\mathbf{d}}_{\rm D}|e_{\rm D}\rangle$ and $\mathbf{d}_{\rm A}^{\uparrow} = \langle e_{\rm A}|\hat{\mathbf{d}}_{\rm A}|g_{\rm A}\rangle$ and $\omega_{\rm D}$ is the transition frequency of the donor. Eq. (185) exhibits the expected $1/\rho^6$ dependence of the Förster theory at short distances, but also contains additional contributions which depend on distance as $1/\rho^4$ and $1/\rho^2$. These become more important at higher frequencies, when the wave-like nature of the mediating photon becomes more relevant. As we will discuss in more detail in relation to the Green's tensor in Section 5.2.3, the short- and long-distance limits are also known as the non-retarded and retarded (or near-zone and far-zone) regimes since they are distinguished by the significance of the time delay between emission and absorption.

Once the fundamental formalism for calculating the RET rate using QED had been laid down, a profusion of extensions and generalisations began to appear. A selection of these are discussed next.

4.3.1. Higher multipole moments

Instead being described simply by their electric dipole moments $\mathbf{d}$, donor and acceptor can also be taken to have magnetic dipole moments $\mathbf{m}$ and/or electric quadrupole moments [173–176]. This is of importance when ultra-short range processes are considered, such that the donor and acceptor can no longer be considered point-like. The particular combination of electric–magnetic coupling is of importance to chiral discriminatory RET [174,175], where the relevant coupling is the optical rotatory strength $\mathrm{Im}(\mathbf{d}\cdot\mathbf{m})$. Expressions for the rate for electric multipole moments of arbitrary order have been given [177], with included special cases worked out all the way up to quadrupole–quadrupole and dipole–octupole coupling.

4.3.2. Mediating particles

Studies of the effect of mediating particles on the RET process began in Ref. [178] which concentrated on the short-range asymptotics of the transfer matrix element in the presence of a third body. Later works extended this to arbitrary distances [179], highly polar [180], charged [181] and non-absorbing [182] mediators, as well as dimensionally-constrained systems (e.g. quantum dots) replacing the molecules [183] and mediators embedded in homogeneous media [184,185]. A mediator has also been considered as an agent that can placed and oriented such that energy transfer can be switched on and off [186]. Further extension to two mediating particles (i.e. four bodies in total) has also been investigated [187], and the advances in inclusion of external environments discussed in the next section have been combined with a three-body calculation [188].

4.3.3. External environments

The first foray into the quantum theory of RET with an external environment was the microscopically derived approach of Ref. [189], where many-body QED was used in order to derive the modified rate of dipole–dipole energy transfer in a homogeneous (non-vacuum) medium. In the earlier Ref. [190], the classical rate of energy transfer was evaluated for molecules adsorbed at or near surfaces, with a similar calculation for microspheres carried out in Ref. [191]. Normal-mode QED was used to calculate the rate in aerosol particles [192], dielectric nanospheres [193], a highly-reflecting cavity [194,195] and near a dielectric surface [196]. The normal-mode basis of those works meant they could not include absorption (see Section 3.2) and became cumbersome for complex geometries — this difficulty was overcome

in Ref. [197] where macroscopic QED was used to find general expressions for the two-body transfer rate in arbitrarily-shaped dispersing and absorbing media. For donor and acceptor with dipole operators $\hat{\mathbf{d}}_\mathrm{A}$ and $\hat{\mathbf{d}}_\mathrm{D}$ and positions $\mathbf{r}_\mathrm{A}$ and $\mathbf{r}_\mathrm{D}$ undergoing the process shown in Fig. 5, it reads in the same notation as Eq. (185) as;

$$\Gamma = \frac{2\pi\mu_0^2\omega_\mathrm{D}^4}{\hbar}|\mathbf{d}_\mathrm{A}^\uparrow \cdot \mathbb{G}(\mathbf{r}_\mathrm{A}, \mathbf{r}_\mathrm{D}, \omega_\mathrm{D}) \cdot \mathbf{d}_\mathrm{D}^\downarrow|^2. \tag{186}$$

Using $\mathbf{d}_{\mathrm{D/A}}^\uparrow = \mathbf{d}_{\mathrm{D/A}}^{\downarrow *}$, and carrying out isotropic averaging via [see, e.g., Ref. [198]. Eq. (16)];

$$\mathbf{d}_\mathrm{D}^\downarrow \otimes \mathbf{d}_\mathrm{D}^\uparrow \to \frac{1}{3}\mathbf{d}_\mathrm{D}^\uparrow\mathbf{d}_\mathrm{D}^\downarrow\mathbb{I} = \frac{1}{3}|\mathbf{d}_\mathrm{D}^\downarrow|^2\mathbb{I} \qquad \mathbf{d}_\mathrm{A}^\uparrow \otimes \mathbf{d}_\mathrm{A}^\downarrow \to \frac{1}{3}\mathbf{d}_\mathrm{A}^\downarrow\mathbf{d}_\mathrm{A}^\uparrow\mathbb{I} = \frac{1}{3}|\mathbf{d}_\mathrm{A}^\uparrow|^2\mathbb{I} \tag{187}$$

we have[13];

$$\Gamma_\mathrm{iso} = \frac{2\pi\mu_0^2\omega_\mathrm{D}^4|\mathbf{d}_\mathrm{D}^\uparrow|^2|\mathbf{d}_\mathrm{A}^\downarrow|^2}{9\hbar}\mathrm{Tr}\left[\mathbb{G}(\mathbf{r}_\mathrm{A}, \mathbf{r}_\mathrm{D}, \omega_\mathrm{D}) \cdot \mathbb{G}^*(\mathbf{r}_\mathrm{D}, \mathbf{r}_\mathrm{A}, \omega_\mathrm{D})\right] \tag{188}$$

where Lorentz reciprocity $\mathbb{G}(\mathbf{r}, \mathbf{r}', \omega) = \mathbb{G}^\mathrm{T}(\mathbf{r}', \mathbf{r}, \omega)$ has been used. Substituting in the vacuum Green's tensor from Eq. (175) and simplifying, one finds exactly the free space rate Eq. (185).

As discussed in more detail in Section 5.5, Refs. [89,199] and report close agreement between the predictions of Eq. (186) and experiments on microwave cavities. The expression (186) has been used to theoretically investigate enhancement of the rate in dielectric layers and near microspheres [197], as well as in nanocavities [200], near wires, wedges and channels [201], and in the evanescent fields of non-local media [202]. Similarly, the general phenomenon of environment-dependent RET has been observed to exist in a wide variety of contexts ranging from the plasmon-assisted processes reported in [203,204], to experiments on energy transfer within aerosol particles [205], microcavities [206], hyperbolic metamaterials [207] and quantum well complexes [208], between quantum dot monolayers [209] as well as near a movable photonic nanoantenna [210] and nanoparticles positioned using DNA origami [211,212].

A process closely related to RET is interatomic Coulombic decay (ICD), which gained recognition as a novel process in 1997 [213] though qualitatively similar processes had been described earlier.[14] As shown in Fig. 6, the essential difference from RET is that the acceptor atom or molecule is no longer excited to a higher state, instead being ejected entirely and causing the acceptor to become ionised. Combined with a preparation step, this can cause a 'Coulomb explosion' which is one of the characteristic signatures of ICD. With hindsight, ICD is known to have been observed in neon dimers [216] and silicon fluoride [217], though not explicitly identified as a separate energy transfer process. Later, ICD was specifically searched for and observed in neon clusters [218], and has been observed in a wide variety of dimers and clusters since then, including in water [219,220]. It has also been shown that the ionisation of the acceptor atom produces a low-energy free electron [221], which are known to be damaging to DNA [222]. This, coupled with the recently-confirmed presence of interatomic decay in liquid water [223] means that the ICD process is a key mechanism in radiation biology [221,224]. ICD is most efficient at very short distances (of the order of the atomic radii), where orbital overlap is significant so electronic correlations can play a role [225]. At larger distances the main mechanism of energy transfer is a (virtual) photon, so at these distances the phenomenology of ICD can be expected to be very similar to that of RET. This is indeed the case [225,226] (see Fig. 7a), with the essential difference in the theory being that the dipole moment of the acceptor is converted to a photoionisation cross section. At distances beyond orbital overlap, the characteristic rate dependence on the inverse sixth power of the distance is recovered [see Fig. 7a]. In Ref. [226] is showing that all the theoretical machinery developed for RET (influence of retardation, dielectric environments etc.) can be transferred over to the case of the long-distance behaviour of ICD, using for example the surface-enhancement and local-field corrections. Mirroring the development of RET, three body effects have recently been investigated in parallel using both the QED model and ab initio quantum chemistry [227,228]. The 'single-body' version of ICD (Auger decay) has also been investigated in the framework of macroscopic QED [64]

When comparing and contrasting RET and ICD, one needs to be careful with terminology. In the RET community the donor and acceptor are almost universally considered to be distant enough that orbital overlap is not relevant, so there the 'short distance' regime is synonymous with the electrostatic or non-retarded regime where the first term of (185) dominates (this is discussed further in the context of the Green's tensor in Section 5.2.3). Similarly, for RET the long-distance regime is synonymous with the far-zone or retarded regime. In ICD, however, 'short' distances refer to those with orbital overlap (sometimes referred to as ultra-short in literature discussing ICD and RET, e.g. [147]), while 'long' distances are those in which a non-retarded virtual photon model suffices. Distances where retardation matter are almost never considered in ICD because most ICD-active systems are separated by distances within or just outside the orbital overlap region, so there is no standard long-distance terminology although 'ultra-long' would probably be appropriate. This nomenclature, alongside an illustrative rate plot for a RET/ICD-like process is shown in Fig. 8.

[13] For vectors $\mathbf{a}$ and $\mathbf{b}$ and matrix $\mathbb{M}$ one has $|\mathbf{a}\cdot\mathbb{M}\cdot\mathbf{b}|^2 = a_i M_{ij} b_j a_k M_{kl}^* b_l = (\mathbf{a}\otimes\mathbf{a}^*)_{ik} M_{ij} M_{kl}^* (\mathbf{b}\otimes\mathbf{b}^*)_{jl}$ Carrying out isotropic averaging over $\mathbf{a}$ and $\mathbf{b}$ this becomes $(1/9)|\mathbf{a}|^2|\mathbf{b}|^2\delta_{ik}M_{ij}M_{kl}^*\delta_{jl} = (1/9)|\mathbf{a}|^2|\mathbf{b}|^2 M_{ij}M_{ij}^* = (1/9)|\mathbf{a}|^2|\mathbf{b}|^2\mathrm{Tr}(\mathbb{M}\cdot\mathbb{M}^{*\mathrm{T}})$.

[14] For example Penning ionisation [214] is essentially the same process but expressed in the language of collisions as discussed in [215].

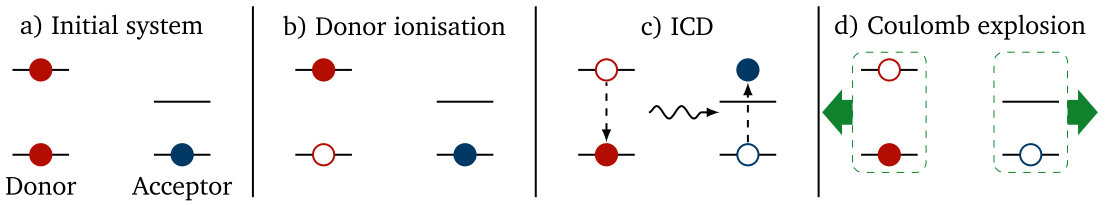

Fig. 6. Schematic illustration of an interatomic relaxation process resulting in Coulomb explosion. (a) A neutral donor and neutral acceptor are prepared. (b) The donor is ionised in an inner vacancy by an external agent (e.g. a laser). (c) The ICD process ejects an electron from the acceptor using the excess energy from relaxation of the donor. As discussed in the main text, this is the step that can be described along the same lines as RET. (d) Both donor and acceptor are now ionised (only the outer levels are shown here) so experience strong Coulomb repulsion.

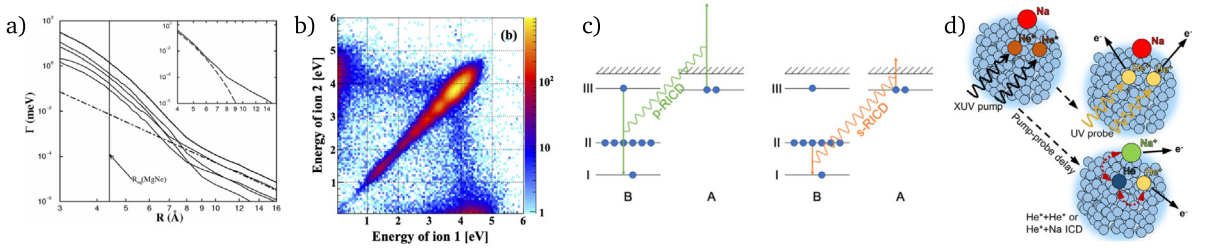

Fig. 7. Representative examples of results, systems and theoretical underpinnings of ICD (a) Theoretical demonstration of the deviations from the virtual photon model at short distances (from [225]). The straight dot-dashed line shows the predictions of the virtual photon model, with the other lines representing the results of ab initio quantum chemistry calculations. (b) Distinctive diagonal experimental signature of Coulomb explosion in coincidence detection of the ionic partners (from [229]) (c) Illustration of two sub-types of ICD, p-RICD (participator resonant ICD) and s-RICD (spectator resonant ICD) (from [230]) — these are only a tiny subset of the very many ICD-related processes gaining attention cite ICEC (d) Schematic of ICD in sodium-doped helium nanodroplets (from [231]) — this is one of the systems in which environment-modified ICD as described by macroscopic QED is clearly of relevance.

Distance	Typically < 10Å	$\rho \ll \lambda_D$	$\rho \approx \lambda_D$	$\rho \gg \lambda_D$
Physical meaning	Orbital overlap	Non-retarded/ near-zone	Hybrid behaviour	Retarded/ far-zone
RET perspective	Ultra-short	Short	Intermediate	Long
ICD perspective	Standard (no name)	Long / virtual photon regime	Ultra-long (not studied)	

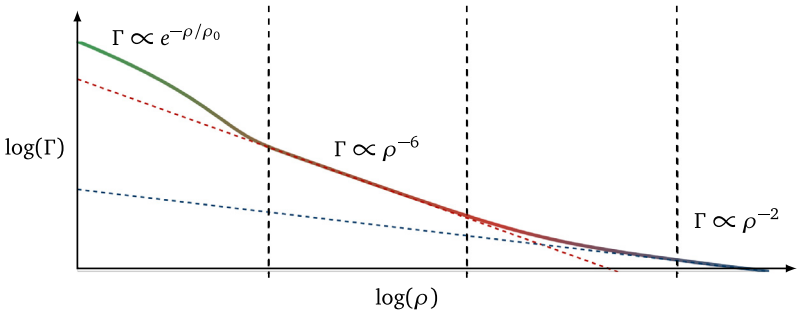

Fig. 8. Summary of distance perspectives taken in the RET and ICD communities, and an illustration of how the position dependence of the rate varies with distance ρ. The distance ρ_0 is the characteristic length for the exponential decay region where orbital overlap is important (see, e.g. Ref. [215] and Fig. 7a), and depends on the specific donor/acceptor combination at hand.

5. The Green's tensor

In the previous section, only the simplest Green's tensor was discussed — that describing unbounded empty space. In this section we will discuss the generalisation to inhomogeneous environments, and discuss one particular inhomogeneous Green's tensor (that for a dielectric half-space) in detail. We will also discuss selected methods for approximating Green's tensors analytically and outline methods for calculating them fully numerically.

5.1. Green's tensors for inhomogeneous environments

There are a variety of existing works containing exhaustive presentations of the derivation of Green's tensors in bulk (homogeneous but non-vacuum) media and in the presence of planes, cylinders, spheres and layered versions thereof. Textbooks include Refs. [15,42,43,232,233] with representative references for layered planar media being [234–237], with [238–240] for cylindrical and spherical media, respectively. Here we will introduce the general principles needed for writing down Green's tensors for inhomogeneous environments, and then discuss one example in detail.

The defining Eq. (130) is linear $\mathbb{G}$, so it will always be possible (and eventually useful) to decompose it into two parts which we will call $\mathbb{G}^{(0)}$ and $\mathbb{G}^{(1)}$:

$$\mathbb{G}(\mathbf{r}, \mathbf{r}', \omega) = \mathbb{G}^{(0)}(\mathbf{r}, \mathbf{r}', \omega) + \mathbb{G}^{(1)}(\mathbf{r}, \mathbf{r}', \omega). \tag{189}$$

This decomposition is evidently not unique — the only constraint is that $\mathbb{G}(\mathbf{r}, \mathbf{r}', \omega)$ should solve the defining Eq. (130) with a given set of boundary conditions. Assuming for a moment that the source and observation points are both in the same medium, we choose to identify the term $\mathbb{G}^{(0)}(\mathbf{r}, \mathbf{r}', \omega)$ with the (fictitious) situation that the medium is considered to be unbounded and homogeneous. This means that $\mathbb{G}^{(1)}(\mathbf{r}, \mathbf{r}', \omega)$ must make up the remainder of the whole process described by $\mathbb{G}$, so therefore must represent any effect of boundaries between different media. If the source and observation points are in different media, then $\mathbb{G}^{(0)}(\mathbf{r}, \mathbf{r}', \omega)$ is defined as simply zero as there is no other meaningful way to define it.[15] We are thus left with:

$$\mathbb{G}(\mathbf{r}, \mathbf{r}', \omega) = \begin{cases} \mathbb{G}^{(0)}(\mathbf{r}, \mathbf{r}', \omega) + \mathbb{G}^{(1)}(\mathbf{r}, \mathbf{r}', \omega) & \text{if } \mathbf{r} \text{ and } \mathbf{r}' \text{are both in the same medium,} \\ \mathbb{G}^{(1)}(\mathbf{r}, \mathbf{r}', \omega) & \text{otherwise.} \end{cases} \tag{190}$$

In the common case of a medium described by a frequency dependent local, scalar[16] permittivity $\varepsilon(\omega)$ and permittivity $\mu(\omega)$, the bulk Green's tensor $\mathbb{G}^{(0)}(\mathbf{r}, \mathbf{r}', \omega)$ is given by (see, e.g. Appendix B of [42]);

$$\mathbb{G}^{(0)}(\mathbf{r}, \mathbf{r}', \omega) = -\frac{\mu(\omega)}{3k^2}\delta(\boldsymbol{\rho}) - \frac{\mu(\omega)e^{ik\rho}}{4\pi k^2 \rho^3}\left\{\left[1 - ik\rho - (k\rho)^2\right]\mathbb{I}_3 - \left[3 - 3ik\rho - (k\rho)^2\right]\mathbf{e}_\rho \otimes \mathbf{e}_\rho\right\} \tag{191}$$

with $k = \sqrt{\varepsilon(\omega)\mu(\omega)}\frac{\omega}{c}$ and the remaining notation the same as in Eq. (175). In the limit $\epsilon(\omega) \to 1$, $\mu(\omega) \to 1$ the bulk Green's tensor (191) reduces to the vacuum Green's tensor (175) as expected.

Bulk media is essentially the only situation where the Green's tensor can be given as an elementary algebraic formula at all distances. Considering layered planar geometries, for example, the Green's tensor is most usefully expression in the spectral domain, which introduces an integral over wave vector $\mathbf{k}$. One integral over the component of the $\mathbf{k}$ vector perpendicular to the interface (normally called $k_\perp$ or k_z) can be done analytically via contour methods without knowledge of the specific Green's tensor (see, e.g. [232]. Chapter 7). The specifics of the remaining integral over the parallel wave vector $\mathbf{k}_\parallel = (k_x, k_y)$

$$\mathbb{G}(\mathbf{r}, \mathbf{r}', \omega) = \int \mathrm{d}^2 k_\parallel \mathbb{G}(\mathbf{r}, \mathbf{r}', \omega; k_\parallel) \tag{192}$$

depend on the problem at hand, and ultimately mean that the actual evaluation of the Green's tensor for a given frequency cannot always proceed analytically (not to mention any complications from an additional frequency integral required for some observables). The $k_\parallel$ integral entails quite some technical overhead [13], so it is often worth considering the physical parameters of the problem to see if approximations can be made that allow the integration to be circumvented. Since this review is geared towards design of complex geometries for which $\mathbb{G}$ cannot be expressed analytically, we will only discuss this for one case (a dielectric half-space) in order to illustrate the general principles involved, leaving any more complex geometries to fully numerical treatments.

5.2. The half-space Green's tensor and its approximations

Consider a dielectric half-space of permittivity $\varepsilon(\omega)$ and permeability $\mu(\omega) = 1$ filling the region $z < 0$, with vacuum in the region $z > 0$ as shown in Fig. 9. The source and observation points $\mathbf{r}'$ and $\mathbf{r}$ will be taken as being in the vacuum region. This particular arrangement is an important special case as (ordinarily) for an atomic radiative process taking place in vacuum near an object, both source and observation points will be located at the atom [see, e.g., the spontaneous decay rate (174) or Casimir–Polder potential (182)]. The half-space is also important because for sufficiently small distances any complex geometry can be approximated locally as a half-space — indeed a version of this for parallel plates is the basis of the widely-used proximity-force approximation (PFA) for the Casimir force [241].

[15] For example, trying to generalise the definition for when source and observation points and in the same medium, one runs into the problem of which medium's properties should be chosen as those for the (fictitious) unbounded and homogeneous one.

[16] This excludes non-local, non-reciprocal, and anisotropic media. These have permittivities and permeabilities which matrix-valued (non-reciprocal case), require the use of auxiliary parameters besides ε and μ (anisotropic) or have defining equations which involved additional spatial convolutions (non-local media).

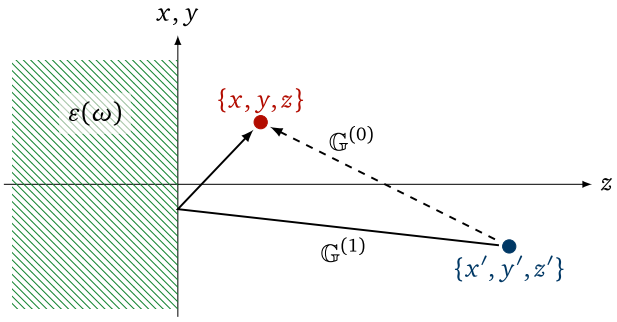

Fig. 9. Half space of permittivity $\varepsilon(\omega)$ (and unit permeability) filling the region $z < 0$, with $z > 0$ being vacuum. The solid line indicates the type of contribution the scattering Green's tensor $\mathbb{G}^{(1)}$ makes, while the dashed one indicates the contribution of the homogeneous Green's tensor $\mathbb{G}^{(0)}$, which in this case will be that for vacuum.

The half-space Green's tensor we will work with is (see, for example, Appendix B of [42]);

$$\mathbb{G}^{(1)}(\mathbf{r},\mathbf{r}',\omega) = \frac{i}{8\pi^2}\int d^2k_\parallel \frac{1}{k_z} e^{i\mathbf{k}_\parallel\cdot(\mathbf{r}-\mathbf{r}')+ik_z(z+z')} \sum_{\sigma=s,p} r_\sigma(\omega,k_\parallel)\mathbf{e}_{\sigma+}\otimes\mathbf{e}_{\sigma-}, \tag{193}$$

where

$$r_s(\omega,k_\parallel) = \frac{k_z - k_z^d}{k_z + k_z^d}, \qquad r_p(\omega,k_\parallel) = \frac{\varepsilon(\omega)k_z - k_z^d}{\varepsilon(\omega)k_z + k_z^d} \tag{194}$$

and

$$\begin{aligned} k_z &= \sqrt{\omega^2/c^2 - k_\parallel^2} \equiv \sqrt{k_0^2 - k_\parallel^2},\\ k_z^d &= \sqrt{\varepsilon(\omega)\omega^2/c^2 - k_\parallel^2} = \sqrt{\varepsilon(ck_0)k_0^2 - k_\parallel^2},\\ \mathbf{e}_{s\pm} &= \mathbf{e}_{k_\parallel}\times\mathbf{e}_z,\\ \mathbf{e}_{p\pm} &= \frac{1}{k}(k_\parallel\mathbf{e}_z \mp k_z\mathbf{e}_{k_\parallel}), \end{aligned} \tag{195}$$

with $\mathbf{e}_{k_\parallel} = \frac{1}{k_\parallel}(k_x, k_y, 0)$ and $\mathbf{e}_z = (0,0,1)$. It should be emphasised that k_z and k_z^d appearing in Eq. (193) are simply shorthands — the independent variables are $k_\parallel$ and $\omega = ck_0$. Using the definitions (194) and (195) in the Green's tensor (193), one finds;

$$\mathbb{G}^{(1)}(\mathbf{r},\mathbf{r}',\omega) = \frac{i}{8\pi^2 k_0^2}\int_{-\infty}^{\infty} dk_x \int_{-\infty}^{\infty} dk_y \frac{e^{i(k_xX+k_yY+Z\sqrt{k_0^2-k_x^2-k_y^2})}}{\sqrt{k_0^2-k_x^2-k_y^2}} g(k_x,k_y) \tag{196}$$

where $X = x - x'$, $Y = y - y'$, $Z = z + z'$ and;

$$g(k_x,k_y) = \begin{pmatrix} \frac{k_0^2\left(k_y^2 r_s - k_x^2 r_p\right) + k_x^2 r_p\left(k_x^2+k_y^2\right)}{\left(k_x^2+k_y^2\right)^2} & \frac{k_x k_y\left(r_p\left(k_x^2+k_y^2\right) - k_0^2(r_p+r_s)\right)}{\left(k_x^2+k_y^2\right)^2} & -\frac{k_x r_p\sqrt{-k_x^2-k_y^2+k_0^2}}{k_x^2+k_y^2}\\ \frac{k_x k_y\left(r_p\left(k_x^2+k_y^2\right) - k_0^2(r_p+r_s)\right)}{\left(k_x^2+k_y^2\right)^2} & \frac{k_0^2\left(k_x^2 r_s - k_y^2 r_p\right) + k_y^2 r_p\left(k_x^2+k_y^2\right)}{\left(k_x^2+k_y^2\right)^2} & -\frac{k_y r_p\sqrt{-k_x^2-k_y^2+k_0^2}}{k_x^2+k_y^2}\\ \frac{k_x r_p\sqrt{-k_x^2-k_y^2+k_0^2}}{k_x^2+k_y^2} & \frac{k_y r_p\sqrt{-k_x^2-k_y^2+k_0^2}}{k_x^2+k_y^2} & r_p \end{pmatrix} \tag{197}$$

No assumptions have been made about the reflection coefficients r_s and r_p so far, they still depend on ω, k_x and k_y in an unknown way.

The first simplification that can be made is to assume that the material has no spatial dispersion — the permittivity can only depend on the frequency rather than the wave vector. This means that the reflection coefficients only depend on total transverse wave vector $k_\parallel$, rather than on its individual components k_x and k_y. This means we can transform into cylindrical polar coordinates $k_x = k_\parallel\cos\theta$ and $k_y = k_\parallel\sin\theta$, analytically carry out the angular integral and therefore be left with a single integral, which is much more amenable to numerical analysis than the double integral from which it came. For simplicity we choose $y' = y$ ($Y = 0$) — any coordinate system can be rotated such that this is true so there is no loss of generality here. Combined with the angular integration, this causes the Green's tensor components G_{xy}, G_{yx}, G_{zy}

and G_{yz} to vanish, leaving only five of the nine components,

$$\mathbb{G}^{(1)}(x,z,x',z',\omega) = \frac{i}{4\pi k_0^2}\int_0^\infty dk_\parallel \frac{k_\parallel^3 e^{iZ\sqrt{k_0^2-k_\parallel^2}}}{\sqrt{k_0^2-k_\parallel^2}} \begin{pmatrix} g_{xx} & 0 & g_{xz} \\ 0 & g_{yy} & 0 \\ g_{zx} & 0 & g_{zz} \end{pmatrix} \tag{198}$$

with (dimensionless) matrix elements

$$\begin{aligned} g_{xx} &= \frac{1}{k_\parallel^3 X}\left(k_0^2\left(r_p+r_s\right)-k_\parallel^2 r_p\right)J_1\left(Xk_p\right)+\frac{1}{k_\parallel^2}\left(k_\parallel^2-k_0^2\right)r_p J_0\left(k_\parallel X\right), \\ g_{yy} &= \frac{1}{|X|k_\parallel^3}\left(k_\parallel^2 r_p-k_0^2\left(r_p+r_s\right)\right)J_1\left(|X|k_\parallel\right)+\frac{k_0^2 r_s}{k_\parallel^2}J_0\left(Xk_\parallel\right), \\ g_{xz} &= \frac{i}{k_\parallel}\sqrt{k_0^2-k_\parallel^2}\,r_p J_1\left(Xk_\parallel\right) = -g_{zx} \\ g_{zz} &= r_p J_0\left(Xk_\parallel\right), \end{aligned} \tag{199}$$

where J_n is the nth Bessel function of the first kind (similar expressions but in cylindrical polar coordinates appear for example in the appendix of [13])

5.2.1. A user's guide to the half-space Green's tensor

Eq. (198) is a very general and useful form of the Green's tensor, so we will devote some attention to how to actually work with it in a real calculation. It is usually a good idea to transform the integrand into a scale-invariant form by introducing dimensionless variables defined by some arbitrary length scale a.

$$k_0 \to \bar{k}_0/a \qquad k_\parallel \to \bar{k}_\parallel/a \qquad Z \to \bar{Z}a \qquad X \to \bar{X}a \tag{200}$$

Then one has;

$$\mathbb{G}^{(1)}(x,z,x',z',\omega) = \frac{i}{4\pi a\bar{k}_0^2}\int_0^\infty d\bar{k}_\parallel \frac{\bar{k}_\parallel^3 e^{i\bar{Z}\sqrt{\bar{k}_0^2-\bar{k}_\parallel^2}}}{\sqrt{\bar{k}_0^2-\bar{k}_\parallel^2}} \begin{pmatrix} g_{xx} & 0 & g_{xz} \\ 0 & g_{yy} & 0 \\ g_{zx} & 0 & g_{zz} \end{pmatrix} \tag{201}$$

where the dimensionless coefficients g_{ij}, of course, remain dimensionless and given by

$$\begin{aligned} g_{xx} &= \frac{1}{\bar{k}_\parallel^3\bar{X}}\left(\bar{k}_0^2\left(r_p+r_s\right)-\bar{k}_\parallel^2 r_p\right)J_1(\bar{k}_\parallel\bar{X})+\frac{1}{\bar{k}_\parallel^2}\left(\bar{k}_\parallel^2-\bar{k}_0^2\right)r_p J_0(\bar{k}_\parallel\bar{X}) \\ g_{yy} &= \frac{1}{|\bar{X}|\bar{k}_\parallel^3}\left(\bar{k}_\parallel^2 r_p-\bar{k}_0^2\left(r_p+r_s\right)\right)J_1\left(|\bar{X}|\bar{k}_\parallel\right)+\frac{\bar{k}_0^2 r_s}{\bar{k}_\parallel^2}J_0\left(\bar{X}\bar{k}_\parallel\right) \\ g_{xz} &= \frac{i}{\bar{k}_\parallel}\sqrt{\bar{k}_0^2-\bar{k}_\parallel^2}\,r_p J_1\left(\bar{X}\bar{k}_\parallel\right) = -g_{zx} \\ g_{zz} &= r_p J_0\left(\bar{X}\bar{k}_\parallel\right) \end{aligned} \tag{202}$$

with the reflection coefficients also written in terms of the dimensionless variables;

$$r_s(\bar{k}_0,\bar{k}_\parallel) = \frac{\sqrt{\bar{k}_0^2-\bar{k}_\parallel^2}-\sqrt{\varepsilon(\omega)\bar{k}_0^2-\bar{k}_\parallel^2}}{\sqrt{\bar{k}_0^2-\bar{k}_\parallel^2}+\sqrt{\varepsilon(\omega)\bar{k}_0^2-\bar{k}_\parallel^2}} \tag{203}$$

$$r_p(\bar{k}_0,\bar{k}_\parallel) = \frac{\varepsilon(\omega)\sqrt{\bar{k}_0^2-\bar{k}_\parallel^2}-\sqrt{\varepsilon(\omega)\bar{k}_0^2-\bar{k}_\parallel^2}}{\varepsilon(\omega)\sqrt{\bar{k}_0^2-\bar{k}_\parallel^2}+\sqrt{\varepsilon(\omega)\bar{k}_0^2-\bar{k}_\parallel^2}} \tag{204}$$

While formidable looking, (201) is now ready for numerical integration. The only dimensions are carried by the factor a, so for numerical examples we multiply through by this and report the dimensionless number $a\mathbb{G}^{(1)}(x,z,x',z',\omega)$. Care should be taken in the co-linear limit $X \to 0$, which, while well-defined if taken properly, will cause a division by zero error if expression (201) is used naively — it is usually advisable to either avoid this point or split this off into a special case (see next section).

The main difficulty in evaluation of (201) is the presence of a factor $\sqrt{\bar{k}_0^2-\bar{k}_\parallel^2}$ in the integrand, which introduces branch cuts where the sign of its imaginary part changes. Recalling the discussion at the end of Section 3 and in appreciation of causality, we are proceeding under the prescription that the vacuum wavenumber k_0 has a small positive imaginary part. This leads us to consider (201) to be a contour integral in the complex $\bar{k}_\parallel$ plane, and seek to deform the contour to

one that avoids the branch cuts entirely. In order to deform the contour it must be completed in the upper half plane — we will do this by extending the range of the integral to be over the whole real $\bar{k}_\parallel$ axis and subsequently showing that a large semicircle in the upper half-plane does not contribute by Jordan's lemma.

Firstly we note that (201) is a sum of terms of the form;

$$\int_0^\infty \mathrm{d}x\mathscr{O}(x)J_n(x) \qquad \text{with } n \text{ even, and} \qquad \int_0^\infty \mathrm{d}x\mathscr{E}(x)J_n(x) \qquad \text{with } n \text{ odd,} \tag{205}$$

where $\mathscr{E}(x)$ and $\mathscr{O}(x)$ are arbitrary even or odd functions, respectively. We make use of the following identity relating Bessel and Hankel functions of the first kind $H_n^{(1)}(x)$ [see, e.g., Ref. [242]. Eqs. (10.4.4) and (10.11.5)];

$$J_n(x) = \frac{1}{2}\left[H_n^{(1)}(x) - e^{in\pi}H_n^{(1)}(-x)\right] \tag{206}$$

Using this in both cases of (205) separately, changing variables $x \to -x$ in the term proportional to $H_n^{(1)}(-x)$, and finally taking advantage of the parities of $\mathscr{E}(x)$ and $\mathscr{O}(x)$, one finds;

$$\begin{aligned}
\int_0^\infty \mathrm{d}x\mathscr{O}(x)J_n(x) &= \frac{1}{2}\int_{-\infty}^\infty \mathrm{d}x\mathscr{O}(x)H_n^{(1)}(x) \qquad \text{with } n \text{ even, and} \\
\int_0^\infty \mathrm{d}x\mathscr{E}(x)J_n(x) &= \frac{1}{2}\int_{-\infty}^\infty \mathrm{d}x\mathscr{E}(x)H_n^{(1)}(x) \qquad \text{with } n \text{ odd.}
\end{aligned} \tag{207}$$

These relations mean that the Green's tensor (201) can be equivalently represented by replacing each Bessel function J_n with a Hankel function (of the first kind) $H_n^{(1)}$, extending the lower limit of the integration to $-\infty$, and dividing by 2. For complex x, the Hankel functions $H_n^{(1)}(x)$ decay to zero exponentially in the upper half-plane (see Ref. [242]. Eq. 10.17.5), so the form of (201) in terms of Hankel functions allows us to carry out the required deformations of the integration contour.

In order to avoid the branch cut when deforming the contour we want to maintain $\mathrm{Im}\sqrt{\bar{k}_0^2 - \bar{k}_\parallel^2} > 0$, so the critical values are those where it is real, i.e. where $\mathrm{Re}\sqrt{\bar{k}_0^2 - \bar{k}_\parallel^2} = 0$;

$$\begin{aligned}
\sqrt{\bar{k}_0^2 - \bar{k}_\parallel^2} &= \left\{[\mathrm{Re}(\bar{k}_0) + i\mathrm{Im}(\bar{k}_0)]^2 - [\mathrm{Re}(\bar{k}_0) + i\mathrm{Im}(\bar{k}_0)]^2\right\}^{1/2} \\
&= \left\{\mathrm{Re}(\bar{k}_0)^2 + 2i\mathrm{Re}(\bar{k}_0)\mathrm{Im}(\bar{k}_0) - \mathrm{Im}(\bar{k}_0)^2 - \mathrm{Re}(\bar{k}_\parallel)^2 - 2i\mathrm{Re}(\bar{k}_\parallel)\mathrm{Im}(\bar{k}_0) + \mathrm{Im}(\bar{k}_\parallel)^2\right\}^{1/2}
\end{aligned} \tag{208}$$

which is real if;

$$\mathrm{Re}(\bar{k}_\parallel)\mathrm{Im}(\bar{k}_\parallel) = \mathrm{Re}(\bar{k}_0)\mathrm{Im}(\bar{k}_0) \qquad \text{and} \qquad \mathrm{Re}(\bar{k}_\parallel)^2 - \mathrm{Im}(\bar{k}_\parallel)^2 \leq \mathrm{Re}(\bar{k}_0)^2 - \mathrm{Im}(\bar{k}_0)^2. \tag{209}$$

The first of these defines curves, while the second defines a region. Where the curves and region overlap, the branch cuts exist and the contour should not be deformed through them. This can be used as a guiding principle in construction of a contour — a problem which is well-studied in the literature (see, e.g. [232]). A permissible choice of contour is the Sommerfeld path shown in Fig. 10, though some authors use other paths for numerical convenience [13]. We will parameterise the Sommerfeld contour by defining a complex number η with $\mathrm{Re}(\eta) > 0$ and $\mathrm{Im}(\eta) > 0$, then the Sommerfeld contour runs from a point $\{-\infty, \mathrm{Im}(\eta)\}$ to η, then down to η^*, then along to $\{+\infty, -\mathrm{Im}(\eta)\}$ as shown in Fig. 10 for a particular choice $\eta = \eta_0$. That figure also shows that Sommerfeld contour avoids the branch cuts, as long as the displacement from the axis is not too large, or, equivalently, the imaginary part of k_0 is not too small. Taking the example physical parameters as $\bar{X} = 1, \bar{Z} = 1, \bar{k}_0 = 1 + 0.5i$ and $\varepsilon(\omega) = 2 + 2i$ and the integration path as being defined by $\eta = 0.1 + 0.1i \equiv \eta_0$ (which is a permissible combination of parameters as shown in Fig. 10a), we carry out integral (201),[17] using the `NIntegrate` routine in MATHEMATICA [243] finding

$$a\mathbb{G}^{(1)}(\bar{X} = 1, \bar{Z} = 1, \bar{k}_0 = 1 + 0.5i) = \begin{pmatrix} -0.0088 - 0.0016i & 0. & -0.0223 - 0.0053i \\ 0. & 0.0153 - 0.0037i & 0. \\ 0.0223 + 0.0053i & 0. & -0.0014 + 0.0112i \end{pmatrix} \tag{210}$$

We can also see explicitly which contours would not have been appropriate by varying the value of η in the complex plane. A representation of this is shown in Fig. 11, where the absolute value of the trace of the Green's tensor with these parameters is evaluated for various η and compared with the corresponding result for the acceptable contour that led to the corresponding result for (210) ($|0.0051 + 0.0059i| = 0.0078$). There it is seen there are some contours which cross the branch cut but evaluate to the correct result anyway, this is because they cross a square-root branch cut twice and thereby find their way back to the correct Riemann sheet (see, for example, Chapter 6 of [244]). Contours which only cross the branch cut once result in incorrect values for the integral, quickly diverging away from the correct answer.

[17] The contour is implemented in practice simply by splitting up the integration range and changing variables so that the integration variable runs over real numbers only, parameterising the path along that section. For example the vertical section of the Sommerfeld contour corresponds to an integral from $\bar{k}_\parallel = \eta_0$ to η_0^*, so an appropriate variable change to a new variable p is $\bar{k}_\parallel \to 0.1 + ip$, with the p integral running from $+0.1$ to -0.1.

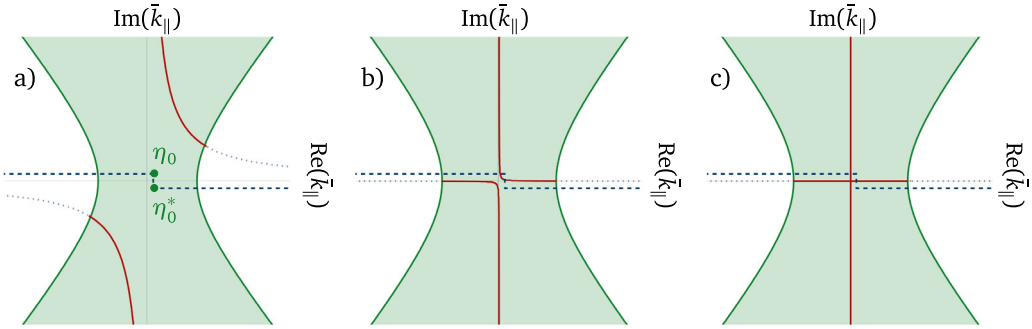

Fig. 10. Schematic illustration of the complex $\bar{k}_\parallel$ plane with the curves and regions defined by Eqs. (209), for decreasing values of $\mathrm{Im}(\bar{k}_0)$, with $\eta = 0.1 + 0.1i \equiv \eta_0$ in all cases. Where the solid curves and shaded region overlap, the branch cuts exist and the contour should not be deformed through them. (a) $\mathrm{Im}(\bar{k}_0) = 0.5$, representing an acceptable combination of parameters and contour (b) $\mathrm{Im}(\bar{k}_0) = 0.002$, demonstrating that there are non-zero values of $\mathrm{Im}(\bar{k}_0)$ for which the branch cut is crossed (c) $\mathrm{Im}(\bar{k}_0) = 0$, which will necessarily cause the integration path to cross the branch cuts.

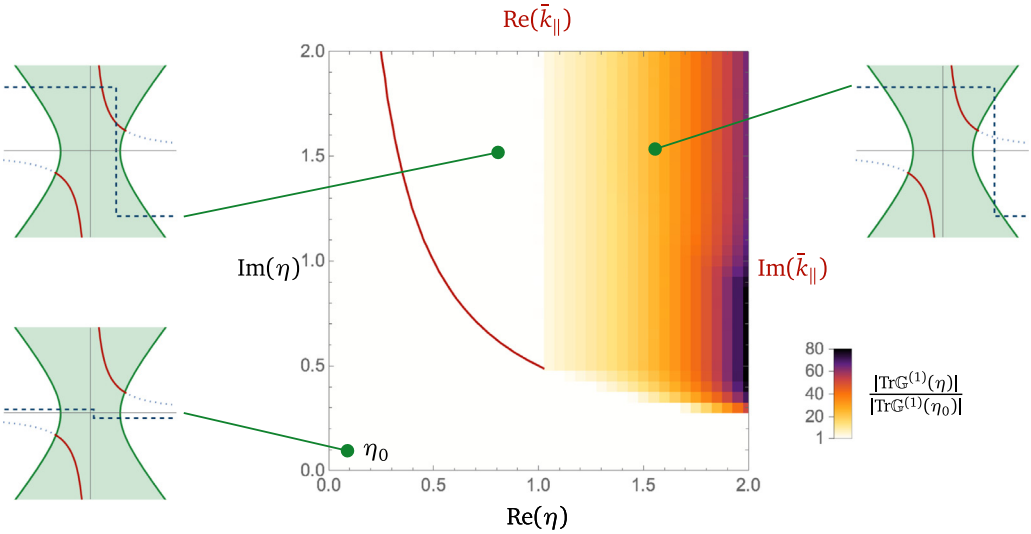

Fig. 11. Evaluation of the absolute value of the trace of the half-space Green's tensor with the same parameters that led to Eq. (210), with various choices of integration path normalised to the result for the path shown in Fig. 10a.

The above was all done in dimensionless units for convenience, but we can easily convert back to SI units. If we take our arbitrary length scale a to be, say, 1 μm, then we have found for example that

$$\mathrm{Re}\mathbb{G}^{(1)}_{zz}(x, z, x', z', \omega) = -0.0088\ \mu\mathrm{m}^{-1} \tag{211}$$

at $z + z' = 0.1$ μm, $x - x' = 1$ μm, $\omega = ck_0 = c\bar{k}_0/a = 299.8 \times (1 + 0.5i)$ THz.

Finally, in the limit where $x' \to x$, the Green's tensor becomes diagonal.

$$\mathbb{G}^{(1)}(z, z', \omega) = \frac{i}{4\pi k_0^2}\int_0^\infty \mathrm{d}k_\parallel \frac{k_\parallel^3 e^{iZ\sqrt{k_0^2 - k_\parallel^2}}}{\sqrt{k_0^2 - k_\parallel^2}} \mathrm{diag}\left\{\frac{k_0^2(r_s - r_p) + k_\parallel^2 r_p}{2k_\parallel^2}, \frac{k_0^2(r_s - r_p) + k_\parallel^2 r_p}{2k_\parallel^2}, r_p\right\}, \tag{212}$$

which is a suitable starting point for the perfect reflector and short/long distance limits discussed in the next two subsections.

5.2.2. Perfect reflector

Integral (212) can be carried out at general distances if r_s and r_p are taken as constants. A physically-motivated choice for those constants is given by 'perfect reflector' approximation defined by $\varepsilon \to \infty$, in which case $r_s \to -1$ and $r_p \to 1$,

giving:

$$\mathbb{G}^{(1)}_{\mathrm{PM}}(z,z',\omega)=\frac{i}{4\pi k_0^2}\int_0^\infty \mathrm{d}k_\parallel \frac{k_\parallel^3 e^{iZ\sqrt{k_0^2-k_\parallel^2}}}{\sqrt{k_0^2-k_\parallel^2}}\mathrm{diag}\left\{\frac{k_\parallel^2-2k_0^2}{2k_\parallel^2},\frac{k_\parallel^2-2k_0^2}{2k_\parallel^2},1\right\} \tag{213}$$

These integrals can be carried out analytically, with result;

$$\mathbb{G}^{(1)}_{\mathrm{PM}}(z,z',\omega)=\frac{1}{Z}\frac{e^{\frac{i\omega Z}{c}}}{4\pi}\left(\frac{\omega Z}{c}\right)^2\mathrm{diag}\left\{1-i\frac{\omega Z}{c}-\left(\frac{\omega Z}{c}\right)^2,1-i\frac{\omega Z}{c}-\left(\frac{\omega Z}{c}\right)^2,\frac{1}{2}\left(1-\frac{i\omega Z}{c}\right)\right\} \tag{214}$$

5.2.3. Short- and long-distance limits

The Green's tensor (212) only contains one separation distance so can be more easily approximated for small and large distances without assuming a specific form of the permittivity. The short distance (also called non-retarded, near-zone or electrostatic) limit is defined by $Zk_0 \ll 1$. This implies that k_0 should be small, which in turn can be equivalently expressed as the main contribution to (212) is when $k_\parallel \gg k_0 = \omega/c$. The long distance (retarded, far-zone, radiation-zone) limit is similarly defined by the opposite limit $Zk_0 \gg 1$, under which circumstances (212) becomes highly oscillatory. In that case the main contribution to (212) is from the stationary phase point where the following is satisfied;

$$\frac{\mathrm{d}}{\mathrm{d}k_\parallel}Z\sqrt{k_0^2-k_\parallel^2}=-\frac{Zk_\parallel}{\sqrt{k_0^2-k_\parallel^2}}=0 \tag{215}$$

solved by $k_\parallel = 0$, meaning we take the condition as $k_\parallel \ll k_0 = \omega/c$. Before evaluating (212) directly, we can use these conditions on $k_\parallel$ to work out simplified expressions for the non-retarded (NR) and retarded (R) reflection coefficients[18]

$$r_s(\omega,k_\parallel)=\frac{\sqrt{\omega^2/c^2-k_\parallel^2}-\sqrt{\varepsilon(\omega)\omega^2/c^2-k_\parallel^2}}{\sqrt{\omega^2/c^2-k_\parallel^2}+\sqrt{\varepsilon(\omega)\omega^2/c^2-k_\parallel^2}}\approx\begin{cases}0 & \text{for } k_\parallel\gg\omega/c \quad (\mathrm{NR})\\ \frac{1-\sqrt{\varepsilon}}{1+\sqrt{\varepsilon}} & \text{for } k_\parallel\ll\omega/c \quad (\mathrm{R})\end{cases} \tag{216}$$

$$r_p(\omega,k_\parallel)=\frac{\varepsilon(\omega)\sqrt{\omega^2/c^2-k_\parallel^2}-\sqrt{\varepsilon(\omega)\omega^2/c^2-k_\parallel^2}}{\varepsilon(\omega)\sqrt{\omega^2/c^2-k_\parallel^2}+\sqrt{\varepsilon(\omega)\omega^2/c^2-k_\parallel^2}}\approx\begin{cases}\frac{\varepsilon-1}{\varepsilon+1} & \text{for } k_\parallel\gg\omega/c \quad (\mathrm{NR})\\ -\frac{1-\sqrt{\varepsilon}}{1+\sqrt{\varepsilon}} & \text{for } k_\parallel\ll\omega/c \quad (\mathrm{R})\end{cases} \tag{217}$$

The non-retarded versions of these can then be substituted back into to small k_0 limit of (212)

$$\mathbb{G}^{(1)}_{\mathrm{NR}}(z,z',\omega)=\frac{1}{8\pi k_0^2}\int_0^\infty dk_\parallel k_\parallel^2 e^{-(z+z')k_\parallel}\frac{\varepsilon-1}{\varepsilon+1}\begin{pmatrix}1&0&0\\0&1&0\\0&0&2\end{pmatrix} \tag{218}$$

and the integral carried out to find

$$\mathbb{G}^{(1)}_{\mathrm{NR}}(z,z',\omega)=\frac{1}{4\pi k_0^2(z+z')^3}\frac{\varepsilon-1}{\varepsilon+1}\begin{pmatrix}1&0&0\\0&1&0\\0&0&2\end{pmatrix} \tag{219}$$

Similarly substituting the retarded versions into the large k_0 limit of (212) and evaluating the integral, one finds;

$$\mathbb{G}^{(1)}_{\mathrm{R}}(z,z',\omega)=\frac{e^{-i(z+z')\omega/c}}{4\pi(z+z')^3}\frac{1-\sqrt{\varepsilon}}{1+\sqrt{\varepsilon}}\begin{pmatrix}1&0&0\\0&1&0\\0&0&0\end{pmatrix} \tag{220}$$

A summary of long- and short-distance behaviours is shown in Fig. 12.

We can use the same stationary phase approach to verify, for example, Snell's law[19] is contained within the relevant Green's tensor. We need a slightly different expression to Eq. (193) because for a refraction problem the source and observation points should be on opposite sides of the interface. The full expression for $z > 0$ (permittivity ε_1) and $z' < 0$ (permittivity ε_2) with unit relative permeability everywhere can be found for example in Appendix B of [42], here we

[18] Note that strictly the reflection coefficients do not depend on distance z so cannot have distinct 'short' and 'long' distance limits. A certain 'distance limit' of a reflection coefficient should be understood as 'the reflection coefficient evaluated at a transverse wavenumber that dominates the integrand the reflection coefficient appears in when the relevant distance limit is taken in that integrand', with the less-than-rigorous shorthand statement being preferred for obvious reasons.

[19] As discussed in detail in Ref. [245], this law of refraction was known long before Snell's 1621 statement. The law was first written down in partial form by Ptolemy in the second century, before being completed by Ibn Sahl in the tenth century, and later by Thomas Harriot in around 1600. It was also arrived at independently just after Snell by Descartes in 1637 and also by Fermat as an application of his principle of least action [246].

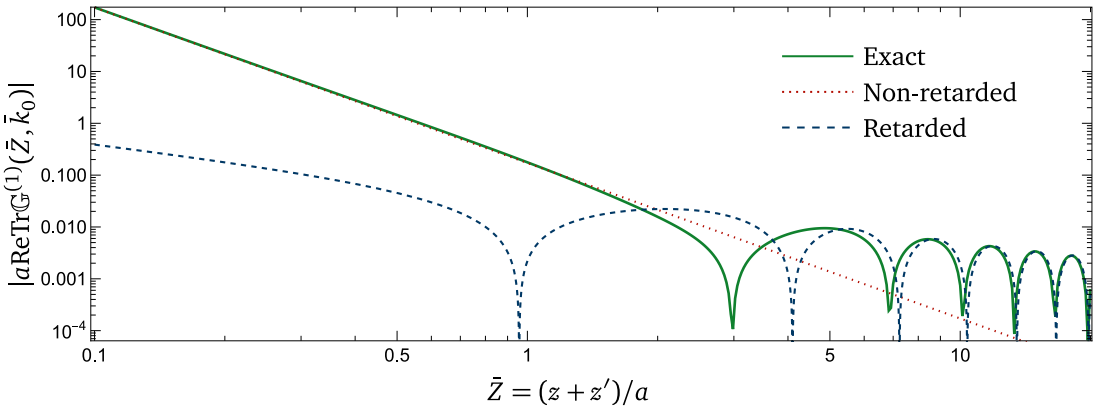

Fig. 12. Non-retarded and retarded approximations to the absolute value of the trace of the half-space scattering Green's tensor at length scale a with coincident lateral coordinates [solid line, given by (212) converted into the dimensionless quantities defined in (200)], with $\varepsilon = 2 + 2i$, $\bar{k}_0 = 1 + i\delta$ with $\delta \to 0$, compared to the non-retarded [dotted line, given by (219), similarly converted] and retarded [dashed line, given by (220)] approximations. Agreement is best far away from the critical point $\bar{Z} = \frac{c}{\omega} = \frac{1}{\bar{k}_0} = 1$, as expected.

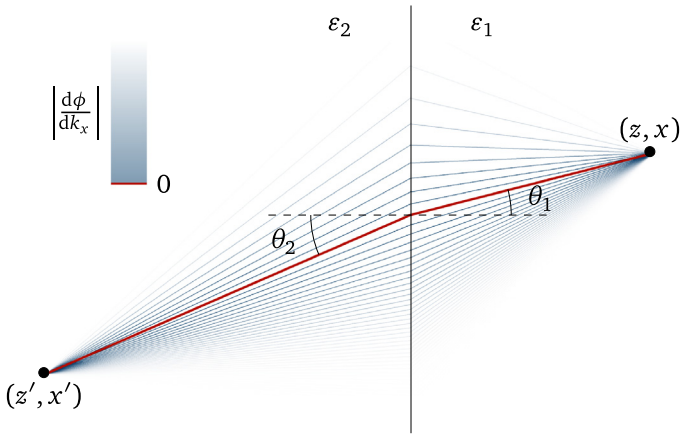

Fig. 13. Example trajectories defined by k_x, k_{z1} and k_{z2}, with the colour scale representing the absolute value of the phase derivative (222) for that trajectory. The trajectory highlighted in red is the one which satisfies Snell's law, which is the one with the smallest phase derivative.

only report the part important for the stationary phase approximation, which is the oscillating exponential factor in the $\mathbf{k}_\parallel$ integrand;

$$e^{i\mathbf{k}_\parallel\cdot(\mathbf{r}-\mathbf{r}')+ik_{z1}z-ik_{z2}z'} = e^{ik_x(x-x')+ik_{z1}z-ik_{z2}z'} \equiv e^{i\phi} \tag{221}$$

where $k_{zi} = \sqrt{\varepsilon_i\omega^2 - k_\parallel^2}$ and we have assumed without loss of generality that $y = y'$. Differentiating the exponent with respect to k_x and setting the result to zero in order to find the points of stationary phase in the k_x integral, we have;

$$\frac{\mathrm{d}\phi}{\mathrm{d}k_x} = x - x' + \frac{k_x}{k_{z1}}z - \frac{k_x}{k_{z2}}z' = 0 \tag{222}$$

The values of this phase gradient for various values of k_x and fixed frequency ω (and the resulting k_{z1} and k_{z2}) are shown in Fig. 13 with $\varepsilon_1 > \varepsilon_2$. The k_x for which the phase gradient vanishes has been highlighted in red, and indeed this is the one that satisfies Snell's law of refraction $\sqrt{\varepsilon_1}\sin\theta_1 = \sqrt{\varepsilon_2}\sin\theta_2$. This means the biggest contribution to the $k_\parallel$ integral in the far-field Green's tensor is from that trajectory.

5.3. Approximations for more general geometries

Having discussed the methods by which the half-space Green's tensor can be approximated by making assumptions about the materials and distances involved, we now turn to approximation methods which can take into account more complex geometries.

5.3.1. Born series

If the situation at hand can be meaningfully decomposed into an analytically solvable 'background' region, plus a perturbation on top of that, then the Green's tensor can be approximated by the techniques of the Born series [247], which is closely related to the later Dyson series [248] and the Lippmann–Schwinger equation [249].

Before deriving the Born series for the Green's tensor, we will first look at an analogy provided by the following Schrödinger-like equation

$$(\nabla^2 + k^2)\psi(\mathbf{r}) = V(\mathbf{r})\psi(\mathbf{r}). \tag{223}$$

The general solution of this is the sum of the solution $\psi_0(\mathbf{r})$ to the associated homogeneous equation

$$(\nabla^2 + k^2)\psi_0(\mathbf{r}) = 0, \tag{224}$$

(assumed to be known), and of a particular solution, which we will write as

$$\psi_{\mathrm{P}}(\mathbf{r}) = \int \mathrm{d}^3 r' g(\mathbf{r} - \mathbf{r}')V(\mathbf{r}')\psi(\mathbf{r}'), \tag{225}$$

where a Green's function $g(\mathbf{r} - \mathbf{r}')$ has been defined as the solution to;

$$(\nabla^2 + k^2)g(\mathbf{r} - \mathbf{r}') = \delta(\mathbf{r} - \mathbf{r}'). \tag{226}$$

The whole solution to Eq. (223) can then be written as;

$$\psi(\mathbf{r}) = \psi_0(\mathbf{r}) + \int \mathrm{d}^3 r' g(\mathbf{r} - \mathbf{r}')V(\mathbf{r}')\psi(\mathbf{r}'). \tag{227}$$

Essentially nothing has happened so far — all that we have done is converted an equation from differential form (223) to integral form (227). The advantage of the integral form, however, is that it can be solved iteratively by substitution of $\psi(\mathbf{r})$ into the integrand in the final term;

$$\psi(\mathbf{r}) = \psi_0(\mathbf{r}) + \int \mathrm{d}^3 r' g(\mathbf{r} - \mathbf{r}')V(\mathbf{r}')\psi_0(\mathbf{r}') + \int \mathrm{d}^3 r' \int \mathrm{d}^3 r'' g(\mathbf{r} - \mathbf{r}')V(\mathbf{r}')g(\mathbf{r}' - \mathbf{r}'')V(\mathbf{r}'')\psi(\mathbf{r}'') \tag{228}$$

If linear order in V is considered sufficient, then we can truncate to;

$$\psi(\mathbf{r}) \approx \psi_0(\mathbf{r}) + \int d^3 r' g(\mathbf{r} - \mathbf{r}')V(\mathbf{r}')\psi_0(\mathbf{r}') \tag{229}$$

where the right hand side now depends only on the solution $\psi_0(\mathbf{r})$ to the homogeneous equation, which is assumed to be known. Therefore, if we know the Green's tensor $g(\mathbf{r} - \mathbf{r}')$ we have enough information to evaluate the whole solution $\psi(\mathbf{r})$ to linear order in V. The process can of course be repeated [beginning by substituting (227) into the final term of (228)] to find $\psi(\mathbf{r})$ to arbitrary order in V.

We can use the same method to perturbatively solve for the Green's tensor defined as the solution to the differential equation (130). Following [250] and assuming a non-magnetic environment ($\mu(\omega) = 1$ everywhere), we begin by writing the permittivity as;

$$\varepsilon(\mathbf{r}, \omega) = \bar{\varepsilon}(\mathbf{r}, \omega) + \delta\varepsilon(\mathbf{r}, \omega), \tag{230}$$

where $\varepsilon(\mathbf{r}, \omega)$ is the permittivity of the whole environment for which the Green's tensor is to be found, $\bar{\varepsilon}(\mathbf{r}, \omega)$ is the background permittivity for which the Green's tensor $\bar{\mathbb{G}}(\mathbf{r}, \mathbf{r}', \omega)$ is analytically known, and $\delta\varepsilon(\mathbf{r}, \omega)$ is a small[20] perturbation on top of that as shown in Fig. 14. By definition we can then assume that the solution $\bar{\mathbb{G}}(\mathbf{r}, \mathbf{r}', \omega)$ to the following equation is known;

$$\nabla \times \nabla \times \bar{\mathbb{G}}(\mathbf{r}, \mathbf{r}', \omega) - \frac{\omega^2}{c^2}\bar{\varepsilon}(\mathbf{r}, \omega)\bar{\mathbb{G}}(\mathbf{r}, \mathbf{r}', \omega) = \boldsymbol{\delta}(\mathbf{r} - \mathbf{r}') \tag{231}$$

and the solution to the following equation is sought;

$$\nabla \times \nabla \times \mathbb{G}(\mathbf{r}, \mathbf{r}', \omega) - \frac{\omega^2}{c^2}\varepsilon(\mathbf{r}, \omega)\mathbb{G}(\mathbf{r}, \mathbf{r}', \omega) = \boldsymbol{\delta}(\mathbf{r} - \mathbf{r}'). \tag{232}$$

Subtracting (231) from (232) we have

$$\nabla \times \nabla \times \left[\mathbb{G}(\mathbf{r}, \mathbf{r}', \omega) - \bar{\mathbb{G}}(\mathbf{r}, \mathbf{r}', \omega)\right] - \frac{\omega^2}{c^2}\left[\varepsilon(\mathbf{r}, \omega)\mathbb{G}(\mathbf{r}, \mathbf{r}', \omega) - \bar{\varepsilon}(\mathbf{r}, \omega)\bar{\mathbb{G}}(\mathbf{r}, \mathbf{r}', \omega)\right] = 0. \tag{233}$$

[20] The exact conditions for convergence of this series are complex — it is often assumed that the use of a small permittivity contrast $\delta\varepsilon(\mathbf{r}, \omega) \ll 1$ (the 'dilute' approximation if the background is vacuum) is sufficient, but of course an arbitrarily large object will induce significant scattering, regardless of the weakness of its dielectric response. For detailed discussions of this and related questions, see for example Refs. [251–254].

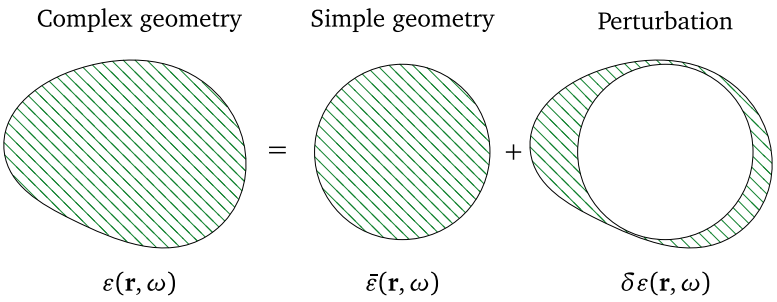

Fig. 14. Basic idea behind the Born series.

Defining $\delta\mathbb{G}(\mathbf{r},\mathbf{r}',\omega)=\mathbb{G}(\mathbf{r},\mathbf{r}',\omega)-\bar{\mathbb{G}}(\mathbf{r},\mathbf{r}',\omega)$, we can eliminate $\mathbb{G}(\mathbf{r},\mathbf{r}',\omega)$ and $\varepsilon(\mathbf{r},\omega)$ in favour of $\delta\mathbb{G}(\mathbf{r},\mathbf{r}',\omega)$, $\bar{\mathbb{G}}(\mathbf{r},\mathbf{r}',\omega)$, $\delta\varepsilon(\mathbf{r},\omega)$ and $\bar{\varepsilon}(\mathbf{r},\omega)$;

$$\nabla\times\nabla\times\delta\mathbb{G}(\mathbf{r},\mathbf{r}',\omega)-\frac{\omega^2}{c^2}\bar{\varepsilon}(\mathbf{r},\omega)\delta\mathbb{G}(\mathbf{r},\mathbf{r}',\omega)=\omega^2\delta\varepsilon(\mathbf{r},\omega)\left[\bar{\mathbb{G}}(\mathbf{r},\mathbf{r}',\omega)+\delta\mathbb{G}(\mathbf{r},\mathbf{r}',\omega)\right] \tag{234}$$

This is now an inhomogenous differential equation for $\delta\mathbb{G}(\mathbf{r},\mathbf{r}',\omega)$ analogous to Eq. (223), with the permittivity contrast $\delta\varepsilon(\mathbf{r},\omega)$ playing the role of the scattering potential V. The Green's function for this differential equation (which is itself a differential equation for a Green's function) satisfies;

$$\nabla\times\nabla\times\mathbb{H}(\mathbf{r},\mathbf{r}',\omega)-\frac{\omega^2}{c^2}\bar{\varepsilon}(\mathbf{r},\omega)\mathbb{H}(\mathbf{r},\mathbf{r}',\omega)=\delta(\mathbf{r}-\mathbf{r}') \tag{235}$$

which is the analogous relation to Eq. (226). Comparing this with Eq. (231) shows that we may take $\mathbb{H}=\bar{\mathbb{G}}$. Thus the solution to differential equation (234) is;

$$\delta\mathbb{G}(\mathbf{r},\mathbf{r}',\omega)=\frac{\omega^2}{c^2}\int \mathrm{d}^3s\bar{\mathbb{G}}(\mathbf{r},\mathbf{s},\omega)\delta\varepsilon(\mathbf{s},\omega)\cdot\left[\bar{\mathbb{G}}(\mathbf{s},\mathbf{r}',\omega)+\delta\mathbb{G}(\mathbf{s},\mathbf{r}',\omega)\right] \tag{236}$$

giving finally

$$\mathbb{G}(\mathbf{r},\mathbf{r}',\omega)=\bar{\mathbb{G}}(\mathbf{r},\mathbf{r}',\omega)+\frac{\omega^2}{c^2}\int \mathrm{d}^3s\bar{\mathbb{G}}(\mathbf{r},\mathbf{s},\omega)\delta\varepsilon(\mathbf{s},\omega)\cdot\mathbb{G}(\mathbf{s},\mathbf{r}',\omega) \tag{237}$$

which is analogous to Eq. (227) in that no approximations have yet been made but the equation is implicit, containing the desired solution $\mathbb{G}(\mathbf{r},\mathbf{r}',\omega)$ on both sides. The way around this is, as before, to undertake repeated re-substitution;

$$\begin{aligned}\mathbb{G}(\mathbf{r},\mathbf{r}',\omega)=\bar{\mathbb{G}}(\mathbf{r},\mathbf{r}',\omega)&+\frac{\omega^2}{c^2}\int \mathrm{d}^3s_1\bar{\mathbb{G}}(\mathbf{r},\mathbf{s}_1,\omega)\delta\varepsilon(\mathbf{s}_1,\omega)\cdot\bar{\mathbb{G}}(\mathbf{s}_1,\mathbf{r}',\omega)\\&+\frac{\omega^4}{c^4}\int \mathrm{d}^3s_1\int \mathrm{d}^3s_2\bar{\mathbb{G}}(\mathbf{r},\mathbf{s}_2,\omega)\delta\varepsilon(\mathbf{s}_2,\omega)\cdot\bar{\mathbb{G}}(\mathbf{s}_2,\mathbf{s}_1,\omega)\delta\varepsilon(\mathbf{s}_1,\omega)\cdot\bar{\mathbb{G}}(\mathbf{s}_1,\mathbf{r}',\omega)+\cdots\end{aligned} \tag{238}$$

or to arbitrary order

$$\mathbb{G}(\mathbf{r},\mathbf{r}',\omega)=\bar{\mathbb{G}}(\mathbf{r},\mathbf{r}',\omega)+\sum_{k=1}^{\infty}\left(\frac{\omega}{c}\right)^{2k}\left[\prod_{j=1}^{k}\int \mathrm{d}^3s_j\delta\varepsilon(\mathbf{s}_j,\omega)\right]\bar{\mathbb{G}}(\mathbf{r},\mathbf{s}_1,\omega)\cdot\bar{\mathbb{G}}(\mathbf{s}_1,\mathbf{s}_2,\omega)\cdots\bar{\mathbb{G}}(\mathbf{s}_k,\mathbf{r}',\omega) \tag{239}$$

An important special case is when the background environment is free space, so that $\bar{\mathbb{G}}(\mathbf{r},\mathbf{r}',\omega)$ is given by $\mathbb{G}^{\mathrm{vac}}(\mathbf{r},\mathbf{r}',\omega)$ via (175) and $\bar{\varepsilon}(\mathbf{r},\omega)=1$. The dielectric contrast in this case is given by $\delta\varepsilon(\mathbf{r},\omega)=\varepsilon(\mathbf{r},\omega)-1$. This can be converted into a polarisability $\alpha(\mathbf{r})$ using the dilute limit of the Clausius–Mosotti law [53];

$$\delta\varepsilon(\mathbf{r},\omega)=\varepsilon(\mathbf{r},\omega)-1=\frac{n(\mathbf{r})\alpha(\mathbf{r})}{\varepsilon_0}=\mu_0c^2n(\mathbf{r})\alpha(\mathbf{r}) \tag{240}$$

where $n(\mathbf{r})$ is the number density of atoms having polarisability α. Then, for example, Eq. (238) becomes;

$$\begin{aligned}\mathbb{G}(\mathbf{r},\mathbf{r}',\omega)=\mathbb{G}^{\mathrm{vac}}(\mathbf{r},\mathbf{r}',\omega)&+\mu_0\omega^2\int \mathrm{d}^3s_1\mathbb{G}^{\mathrm{vac}}(\mathbf{r},\mathbf{s}_1,\omega)n(\mathbf{s}_1)\alpha(\mathbf{s}_1,\omega)\cdot\mathbb{G}^{\mathrm{vac}}(\mathbf{s}_1,\mathbf{r}',\omega)\\&+\mu_0^2\omega^4\int \mathrm{d}^3s_1\int \mathrm{d}^3s_2\mathbb{G}^{\mathrm{vac}}(\mathbf{r},\mathbf{s}_2,\omega)n(\mathbf{s}_2)\alpha(\mathbf{s}_2,\omega)\cdot\mathbb{G}^{\mathrm{vac}}(\mathbf{s}_2,\mathbf{s}_1,\omega)n(\mathbf{s}_1)\alpha(\mathbf{s}_1,\omega)\cdot\mathbb{G}^{\mathrm{vac}}(\mathbf{s}_1,\mathbf{r}',\omega)+\cdots\end{aligned} \tag{241}$$

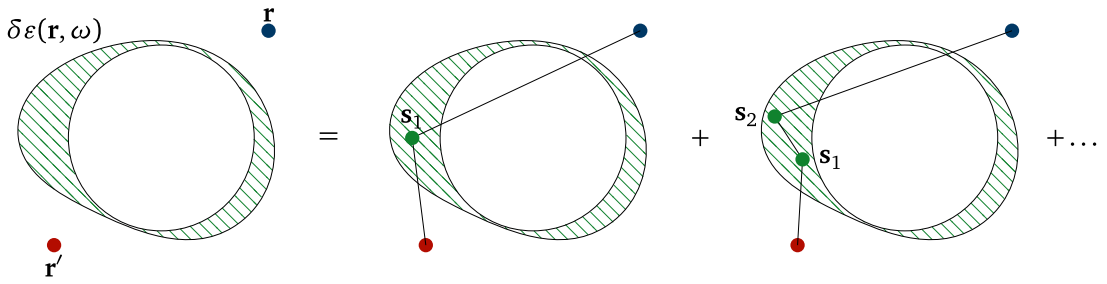

Fig. 15. Multiple scattering interpretation of Born series.

If the dielectric constant is assumed to be piecewise constant, then

$$\mathbb{G}(\mathbf{r},\mathbf{r}',\omega) = \mathbb{G}^{\text{vac}}(\mathbf{r},\mathbf{r}',\omega) + \mu_0\omega^2 n\alpha(\omega)\int_V \mathrm{d}^3 s_1 \mathbb{G}^{\text{vac}}(\mathbf{r},\mathbf{s}_1,\omega)\cdot\mathbb{G}^{\text{vac}}(\mathbf{s}_1,\mathbf{r}',\omega) + \mu_0^2\omega^4 n^2\alpha^2(\omega)\int_V \mathrm{d}^3 s_1 \int_V \mathrm{d}^3 s_2 \mathbb{G}^{\text{vac}}(\mathbf{r},\mathbf{s}_2,\omega)\cdot\mathbb{G}^{\text{vac}}(\mathbf{s}_2,\mathbf{s}_1,\omega)\cdot\mathbb{G}^{\text{vac}}(\mathbf{s}_1,\mathbf{r}',\omega) + \cdots \tag{242}$$

where V represents the volume of the object(s) placed in the vacuum environment.

The Born series has a useful physical interpretation based on multiple scattering, as shown in Fig. 15. It approximates the full Green's tensor (which takes into account all possible scatterings) as a sum of terms containing a one scattering event, then two scattering events and so on. For a sufficiently dilute medium, the probability of multiple scattering will be so low that the series converges quickly, meaning only one or two orders need to be taken into account (comparing contributions from successive terms can give an indication of the convergence of the series, and a rigorous condition is provided in [255]). The scattering interpretation also provides some physical insight, for example in calculation of the Casimir force between two macroscopic objects using the Born series, only terms which have (at least) one scattering event in one object and (at least) one scattering event in the other object contribute [256], necessitating the use of a Born series of at least second order in the permittivity contrast. This is to be expected as scattering from one object to the other is the only way for them to 'know' of each other's presence, and is therefore the only mechanism that can result in a non-zero Casimir force.

The Born series has provided fundamental understanding of local-field corrections for atoms embedded in macroscopic media [257,258], the microscopic origins of dispersion forces [259], and the form of the stress tensor in colloidal media [260]. On top of this, it has provided practical calculations of the interactions between atoms and non-trivially structured surfaces [116,261–264], as well as similar calculations for Casimir forces [256] which have complemented various dielectric-contrast perturbation theories [265–267]. The Born series also forms a crucial part of the inverse design techniques derived in [268] and detailed in Section 6 and, in a more general sense, is the basis of numerical calculations via the volume integral method discussed in Section 5.4.2.

5.3.2. Transformations in the electrostatic limit

The final method of analytic approximation we will discuss in this review is based on the ideas of transformation optics (see, e.g., [269] for a recent review), in which complicated optical problems can be solved by relating the real problem at hand to a fictional one. In our context, this will mean beginning with a simple geometry, applying a coordinate transformation that transforms the simple geometry to a more complicated one while preserving the Green's tensor and thereby generating solutions for the complex geometry that we desire. One well-known method for this is the Kelvin transform [270], which preserves the form of solutions of the Poisson equation (which is the low-frequency limit of (130), which is a form of the Helmholtz equation). To work with the Kelvin transform it is therefore useful to understand how to convert between the general form of the Green's tensor and its low frequency limit.

The defining Eq. (130) for the Green's tensor specialised to a non-magnetic medium is;

$$\nabla\times\nabla\times\mathbb{G}(\mathbf{r},\mathbf{r}',\omega) - \frac{\omega^2}{c^2}\varepsilon(\mathbf{r},\omega)\mathbb{G}(\mathbf{r},\mathbf{r}',\omega) = \boldsymbol{\delta}(\mathbf{r}-\mathbf{r}') \tag{243}$$

Following [271], we take the divergence of both sides

$$-\frac{\omega^2}{c^2}\nabla\cdot\left[\varepsilon(\mathbf{r},\omega)\mathbb{G}(\mathbf{r},\mathbf{r}',\omega)\right] = \nabla\cdot\boldsymbol{\delta}(\mathbf{r}-\mathbf{r}') \tag{244}$$

and then define as an intermediate result the static limit $\mathbb{G}^{\text{stat}}(\mathbf{r},\mathbf{r}')$ of the Green's tensor via

$$\lim_{\omega\to 0}\frac{\omega^2}{c^2}\mathbb{G}(\mathbf{r},\mathbf{r}',\omega) = \mathbb{G}^{\text{stat}}(\mathbf{r},\mathbf{r}') \tag{245}$$

under which conditions Eq. (244) becomes;

$$-\nabla\cdot\left[\varepsilon(\mathbf{r},\omega)\mathbb{G}^{\text{stat}}(\mathbf{r},\mathbf{r}')\right]=\nabla\delta(\mathbf{r}-\mathbf{r}') \tag{246}$$

where we also used $[\nabla\cdot\boldsymbol{\delta}(\mathbf{r}-\mathbf{r}')]_j=[\nabla\cdot\mathbb{I}\delta(\mathbf{r}-\mathbf{r}')]_j=\partial_i\delta_{ij}\delta(\mathbf{r}-\mathbf{r}')=\partial_j\delta(\mathbf{r}-\mathbf{r}')=[\nabla\delta(\mathbf{r}-\mathbf{r}')]_j$.

The scalar Green's function G of electrostatics is defined via the Poisson equation as;

$$-\nabla\cdot[\varepsilon(\mathbf{r})\nabla G(\mathbf{r},\mathbf{r}')]=\delta(\mathbf{r}-\mathbf{r}') \tag{247}$$

Taking the gradient of both sides with respect to $\mathbf{r}'$ and switching to index notation we have

$$-\partial_i'\partial_j\varepsilon(\mathbf{r})\partial_j G(\mathbf{r},\mathbf{r}')=\partial_i'\delta(\mathbf{r}-\mathbf{r}')=\partial_j\varepsilon(\mathbf{r})G^{\text{stat}}_{ji}(\mathbf{r},\mathbf{r}') \tag{248}$$

where in the second equality we used (246) and $\nabla\delta(\mathbf{r}-\mathbf{r}')=-\nabla'\delta(\mathbf{r}-\mathbf{r}')$. Comparing the leftmost and rightmost expressions in Eq. (248), and taking advantage of the boundary condition that the Green's tensor should vanish at spatial infinity, we can identify $\partial_i'\partial_j G(\mathbf{r},\mathbf{r}')=G^{\text{stat}}_{ji}(\mathbf{r},\mathbf{r}')$. Switching back to vector notation and using Eq. (245) we now have the relations between the full Green's tensor $\mathbb{G}$, its static limit $\mathbb{G}^{\text{stat}}$ and the scalar Green's function G;

$$\nabla\nabla' G(\mathbf{r},\mathbf{r}')=-\mathbb{G}^{\text{stat}}(\mathbf{r},\mathbf{r}')=\lim_{\omega\to 0}\frac{\omega^2}{c^2}\mathbb{G}(\mathbf{r},\mathbf{r}',\omega) \tag{249}$$

The atomic processes considered in Section 4 were written in terms of $\mathbb{G}$, so we can write down general expressions for their low-frequency limits using the above prescription. For example, the Casimir–Polder potential given by Eq. (182) depends linearly on $\mathbb{G}$, so can be expected to depend linearly on $\nabla\nabla' G(\mathbf{r},\mathbf{r}')$ in the static limit, as is borne out in Ref. [114].

Having found the low-frequency (electrostatic) limit, we are now ready to discuss the Kelvin transform itself, which non-linear coordinate transformation in space corresponding to reflection through a sphere of radius S, and is defined as;

$$\mathbf{T}(\mathbf{r})=\frac{S^2}{|\mathbf{r}-\mathbf{s}|^2}(\mathbf{r}-\mathbf{s})+\mathbf{s} \tag{250}$$

This transform is useful here because the transformed Green's function $G(\mathbf{T}(\mathbf{r}),\mathbf{T}(\mathbf{r}'))$, with an appropriate pre-factor, also satisfies (247), as in;

$$-\nabla^2\left[\frac{S^2}{|\mathbf{r}-\mathbf{s}||\mathbf{r}'-\mathbf{s}|}G(\mathbf{T}(\mathbf{r}),\mathbf{T}(\mathbf{r}'))\right]=\delta(\mathbf{r}-\mathbf{r}'), \tag{251}$$

so that the transformation

$$G(\mathbf{r},\mathbf{r}')\to\frac{S^2}{|\mathbf{r}-\mathbf{s}||\mathbf{r}'-\mathbf{s}|}G(\mathbf{T}(\mathbf{r}),\mathbf{T}(\mathbf{r}'))\equiv G'(\mathbf{r},\mathbf{r}'), \tag{252}$$

produces an exact new solution $G'(\mathbf{r},\mathbf{r}')$ of the transformed geometry from a known one $G(\mathbf{r},\mathbf{r}')$. Depending on the initial geometry and the choice of parameters $\mathbf{s}$ and S in the transformation (250), a variety of geometries can be generated and their (electrostatic) Green's functions $G'(\mathbf{r},\mathbf{r}')$ produced. One example of this is shown in Fig. 16 where a half-plane is transformed into a plate with a hole as is done in [114], where the resultant Green's function is used to evaluate the Casimir–Polder force on an atom near such a structure. Further applications have included the interaction of a neutral atom with a sphere and a 'boss-hat' (a hemisphere on a plane) [272], a conductor-patched dielectric and conducting spherical bowl [273], and a toroid [274]. Evaluations of other physical effects using the same ideas include the use of perfectly reflecting surfaces as starting point for numerical modelling of heat transfer [275], quantification of electric field noise [276], Coulomb interactions [271] superconductor-mediated magnetic dipole–dipole interactions [277], as well as van der Waals forces [278].

5.3.3. Quasinormal modes

Atomic processes in regular, highly reflecting cavities can often be understood as coming from one or several resonances — these can be described by quasi-normal modes [279–283] which have complex eigenvalues and outgoing boundary conditions (rather than vanishing at infinity, as is the case with normal modes). Despite not being true modes of the system (unless the lossy nature of the mode is shifted instead into an imaginary part of the permittivity [284]), they form a locally bi-orthogonal and complete set. In certain cases they can be shown to be orthogonal inside a resonator [285,286] but not necessarily outside [284,287,288] and can be the basis of perturbation theory [289]. Quasi-normal modes work by analogy to normal modes, but are applicable to systems with absorption where normal modes cannot be defined. Even after restriction to just a few of the important modes of the cavity, close agreement is found with full numerical simulations of, for example, nanosize photonic and plasmonic resonators [290,291] and coupled gain–loss resonators [288,292].

The quasi-normal expansion can be applied by taking advantage of the spectral decomposition of the dyadic Green's function [293,294]

$$\mathbb{G}(\mathbf{r},\mathbf{r}',\omega)\sim\sum_\alpha\frac{\mathbf{E}_\alpha(\mathbf{r})\otimes\mathbf{E}_\alpha(\mathbf{r}')}{2\omega(\omega_\alpha-\omega)} \tag{253}$$

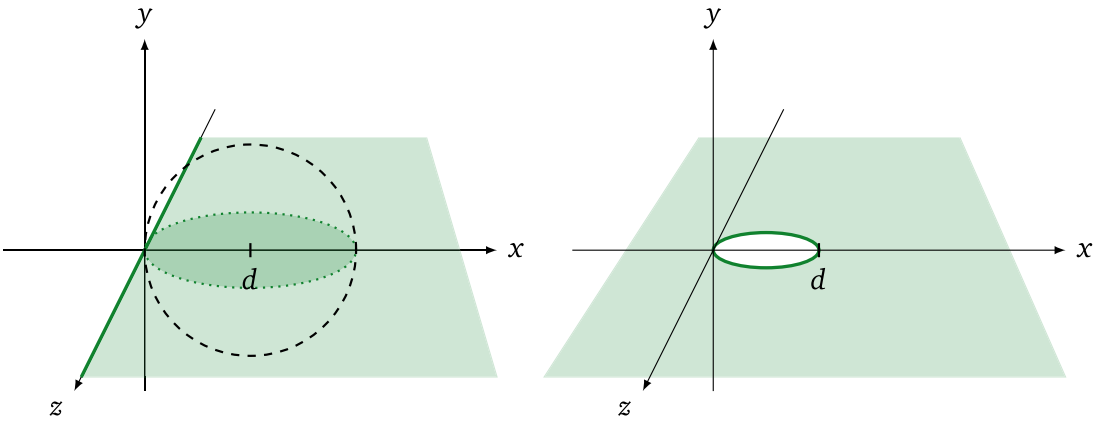

Fig. 16. Kelvin inversion of a half-plane into a plate with a hole (see Ref. [114]).

where $\mathbf{E}(\mathbf{r})$ are the fields of the relevant modes (which are found via an eigenfrequency search), and the sum runs over their complex frequencies.

5.4. Fully numerical methods

In cases where the above approximations do not apply, the Green's tensor must be calculated in a more numerical fashion. Two of the most prominent and general methods are finite-difference time-domain and volume integral methods which we will discuss in turn.

5.4.1. Finite difference time-domain

The finite-difference time domain (FDTD) technique is popular in nanophotonics due to its simplicity, versatility and suitability for sub-wavelength problems. At the core of the method is discretisation of the differential statements of Maxwell's equations in both space and time, with derivatives replaced by finite difference approximations. Spatial discretisation onto a cubic lattice allows an arbitrary structures to easily be included by changing the relative permittivity and/or permeability of a given set of cells.

The starting point for FDTD is the two time-dependent Maxwell equations in media [Eqs. (35) and (117)], in the absence of sources;

$$\nabla \times \mathbf{E} = -\dot{\mathbf{B}} \tag{254}$$

$$\nabla \times \mathbf{H} = \dot{\mathbf{D}} \tag{255}$$

If central difference approximations are used in the time-dependent Maxwell equations, the resulting expressions are second-order accurate in the temporal and spatial steps. This leads to a method for discretising fields on a lattice introduced by Yee [295] and illustrated in Fig. 17a, where the fields are defined at the centres of various edges/facets of a cubic unit cell. The electric-type fields ($\mathbf{E}$ and $\mathbf{D}$) are defined along the edges of the lattice cell at half-integer time steps (Fig. 17b), while the magnetic-type fields ($\mathbf{B}$ and $\mathbf{H}$) are defined on points shifted half a grid cell in all directions (effectively placing them in the middle of each face of the cell) at integer timesteps. The values of each component of the fields are stored on one edge/face only, so for example the value of E_x is only stored at the point halfway along the x axis and H_y is at the centre point of the facet of constant y, with corresponding definitions for the remaining four field components. The size of each Yee cell is the key to achieving sufficient numerical accuracy — a standard recommendation is that no dimension of the cell should exceed around 5% of the shortest wavelength involved [296]. This means that in principle a large spatial grid is required to simulate far-field behaviour, although this problem can be circumvented by only calculating the near fields and using a near-to-far field transformation (see e.g. [76]. Sec 4.6). Care must also be taken at the edge of the grid to minimise unphysical reflections, these can be dealt with using perfectly-matched layers [297]. Dispersion (which of course is most conveniently expressed in the frequency domain) is also relatively cumbersome to introduce in the FDTD method compared to others, for example necessitating an additional convolution in time [298].

The FDTD algorithm above calculates electric and magnetic fields in real space in the time domain — this is not necessarily what a particular application demands. Inspection of Eq. (174) for the spontaneous decay rate and Eq. (186) for resonance energy transfer (and indeed anticipating Eq. (280) for the Rabi frequency) shows that for atomic processes we generally need the Green's tensor $\mathbb{G}$ in (angular) frequency space. The Fourier components of the electric field of a point current source is $\mathbf{j}(\omega)$ at $\mathbf{r}_s$ are given by;

$$\mathbf{E}(\mathbf{r}, \omega) = i\mu_0\omega\mathbb{G}(\mathbf{r}, \mathbf{r}_s, \omega) \cdot \mathbf{j}(\omega). \tag{256}$$

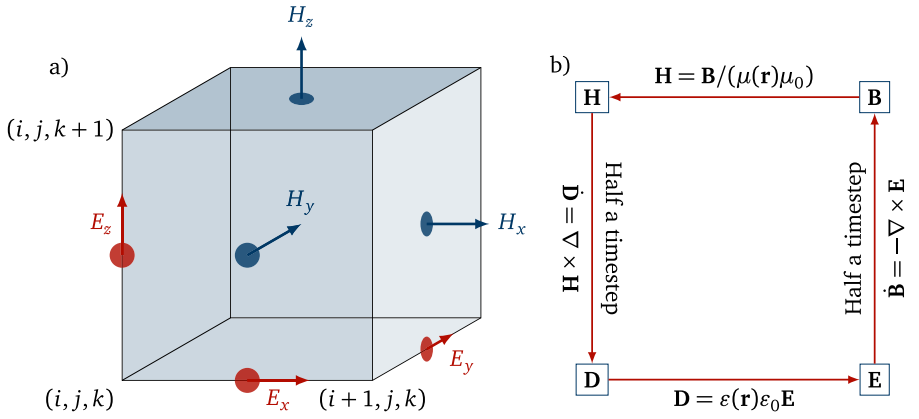

Fig. 17. (a) Illustration of a single cell of the Yee lattice (b) Main loop of calculations carried out during one time step of the FDTD algorithm.

Simulating the electric field of, for example, an x-polarised point source in the time domain, Fourier transforming the result and dividing by $i\mu_0\omega j_y$ then gives $\mathbb{G}_{xy}$ (as discussed in, for example, Ref. [268]). The other components of $\mathbb{G}$ can then be built up in an analogous way.

FDTD is a well-established and mature algorithm, meaning that while it is useful to understand its fundamentals, it is usually unnecessary to implement it from the ground up in order to carry out a calculation in nanophotonics. Various commercial and free FDTD solvers exist in both command-line and graphical user interface (GUI) forms — these include Meep [299] (free, command-line), Optiwave [300] (commercial with limited free version, GUI), Lumerical [301] (commercial, GUI), CST Studio [302] (commercial, GUI), COMSOL [303] (commercial, GUI) and JCMWave [304] (commercial, GUI).[21]

5.4.2. Volume integral methods

An alternative way of numerically calculating dyadic Green's tensors is the volume integral method [305–307]. Instead of working with the differential form of Maxwell's equations like the FDTD approach, volume integral methods transform Maxwell's equations into an integral form so that the field in a given volume can be solved for. In a similar spirit to the discussion after Eq. (256), the quantity that is actually calculated is the electric field of a point source, then the source strength is divided out to give the components of the Green's tensor. For convenience we will find the volume integral equations for the electric field by beginning from our Born-series expanded Green's tensor (237):

$$\mathbb{G}(\mathbf{r},\mathbf{r}',\omega) = \bar{\mathbb{G}}(\mathbf{r},\mathbf{r}',\omega) + \frac{\omega^2}{c^2}\int \mathrm{d}^3 s \bar{\mathbb{G}}(\mathbf{r},\mathbf{s},\omega)\delta\varepsilon(\mathbf{s},\omega)\cdot\mathbb{G}(\mathbf{s},\mathbf{r}',\omega), \tag{257}$$

Taking the scalar product of both sides with a source current $\mathbf{j}(\mathbf{r}'',\omega)$ and integrating over $\mathbf{r}''$, we have;

$$\begin{aligned}\int \mathrm{d}^3 r'' \mathbb{G}(\mathbf{r},\mathbf{r}'',\omega)\cdot\mathbf{j}(\mathbf{r}'',\omega) = &\int \mathrm{d}^3 r'' \bar{\mathbb{G}}(\mathbf{r},\mathbf{r}'',\omega)\cdot\mathbf{j}(\mathbf{r}'',\omega) \\ &+ \frac{\omega^2}{c^2}\int \mathrm{d}^3 r'' \int \mathrm{d}^3 s\, \bar{\mathbb{G}}(\mathbf{r},\mathbf{s},\omega)\delta\varepsilon(\mathbf{s},\omega)\cdot\mathbb{G}(\mathbf{s},\mathbf{r}'',\omega)\cdot\mathbf{j}(\mathbf{r}'',\omega),\end{aligned} \tag{258}$$

giving the standard volume integral form of the electric field (see, e.g. [76]. Sec 16.2);

$$\mathbf{E}(\mathbf{r},\omega) = \bar{\mathbf{E}}(\mathbf{r},\omega) + \frac{\omega^2}{c^2}\int \mathrm{d}^3 s\, \bar{\mathbb{G}}(\mathbf{r},\mathbf{s},\omega)\delta\varepsilon(\mathbf{s},\omega)\cdot\mathbf{E}(\mathbf{s},\omega), \tag{259}$$

where $\bar{\mathbf{E}}(\mathbf{r},\omega)$ is the electric field in the presence of only the unperturbed structure. The volume integral on the right hand side of (259) can then be discretised by assuming that the electric field is constant within each elementary volume, which reduces the system to a set of matrix equations which can be solved directly for small systems. For larger systems, the equations can be re-expressed as discrete convolutions, which can be solved via Fast Fourier Transform (FFT) methods combined with any algorithm for solution of system of linear equations (see, e.g., Chapter 6 of [233] for an overview of such methods). An advantage over the FDTD method discussed in the previous section is that the elementary volumes making up the scatterer can be of arbitrary shape — choice of a suitable meshing function increases the geometrical accuracy of the representation. A disadvantage however is that volume integral methods converge quite poorly for highly scattering materials [296].

[21] Licensing and feature information correct to the authors' knowledge at time of submission.

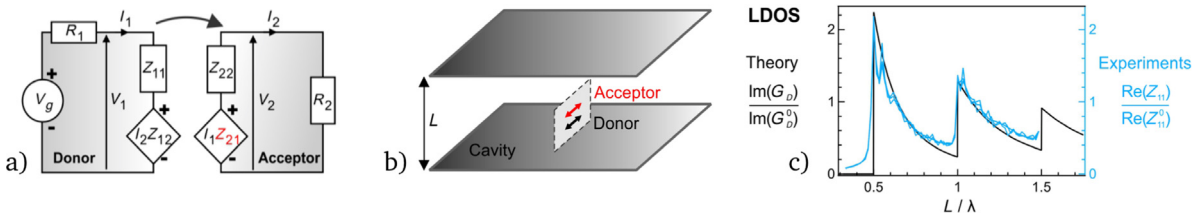

Fig. 18. (a) Microwave circuit used for measuring LDOS [Eq. (178)], CDOS [Eq. (181)] and RET [Eq. (186)]. The source voltage V_g drives the donor, which is placed near a similar acceptor circuit (but without driving). The mutual impedance Z_{21} is proportional to the voltage V_2, which is itself proportional to the electric field over the acceptor antenna length (much shorter than the wavelength, so assumed constant), which in turn is proportional to the relevant elements of the Green's tensor $\mathbb{G}$. (b) External environment of the donor–acceptor pair, which is removed to find free-space quantities used as normalisations. (c) Comparison of the theoretically predicted LDOS with that measured in the experiment, showing close agreement.
Source: All reproduced from [89].

5.5. Experimental reconstruction of the Green's tensor

Aside from being relevant to a wide variety of atomic and molecular processes, the Green's tensor itself has been the subject of recent experimental interest. In Ref. [89], the authors measure the mutual impedance between two dipolar antenna at microwave frequencies as shown in Fig. 18. Even though the majority of photonics applications work at optical frequencies, the scaling properties of electromagnetism can be used to transfer results from the microwave to optical regime, with various scale-transforming techniques existing to mimic molecular aggregates [308] and optical phenomena (loss, plasmons) [309,310] at microwave frequencies by carefully structured surfaces.

6. Design

6.1. Inverse design in nanophotonics

The problem of how best to guide light through a structure with sub-wavelength features is an extremely complex one. Historically, this and related problems have been dominated by intuition-based approaches, where a designer uses a template which is known to work for a specific application, then adjusts a small number of parameters to tune the device to a specific outcome. At a certain level of complexity, this kind of approach becomes infeasible as multiple interacting parameters must be simultaneously optimised, leading to the development of free-form inverse design approaches which also take advantage of recent growth in computing power.

The basic idea of inverse design is to work backwards from a desired set of device characteristics, allowing an algorithm to 'grow' or modify a structure which satisfies those constraints. While this has found tremendous application in nanophotonics, it predates the existence of that field, being a standard tool in the field of mechanics [311–313], before early optical applications in photonic crystals [314]. Its first applications in nanophotonics came with the use of evolutionary (genetic) algorithms in the design of a fibre-to-waveguide coupler [315] and to gradient methods in bandgap optimisation [316]. Several related works on band structure [317,318], and waveguides [319–323] appeared soon after.

The above studies relied on tuning a relatively small number of parameters. The extension to truly freeform design in optics came later with the introduction of the *adjoint method* [329,330], originating in fluid dynamics [331] and first being applied to optimisation problems in Ref. [332]. In free-form optimisation the space of possible designs is overwhelmingly large, so any brute force method is doomed to fail. The adjoint method makes it possible to iterate efficiently using the gradient of some objective (merit) function with respect to design parameters. While it will not be known in general if the resulting devices are globally optimal (unless they can be compared to a fundamental performance bound, see e.g. Ref. [333]), huge performance gains relative to intuition-based approaches have been found as summarised in a number of recent reviews of the state of the art in inverse design. These include summaries of its use in nanophotonics [334], flat optics [335] and tuneable metasurfaces [336], surveys of its relationship with deep learning [337–340], as well as pedagogical tutorials explaining the underlying methods [341,342]. Here we will summarise recent developments[22] in selected areas, but the explosive growth of the field means the accounts below will not be exhaustive.

- **Waveguides and dispersion engineering**. Continuing the lines of research discussed above, studies are ongoing in on-chip resonators, for example Ref. [343] where problems inherent in designing a resonant structure are overcome by mapping to a set of non-resonant problems. Studies in dispersion engineering include the dispersion suppression in graded optical fibres proposed in [344], and the fully three-dimensional couplers detailed in [345]. Purcell

22 Broadly speaking those since 2018 when the comprehensive review [334] was published.

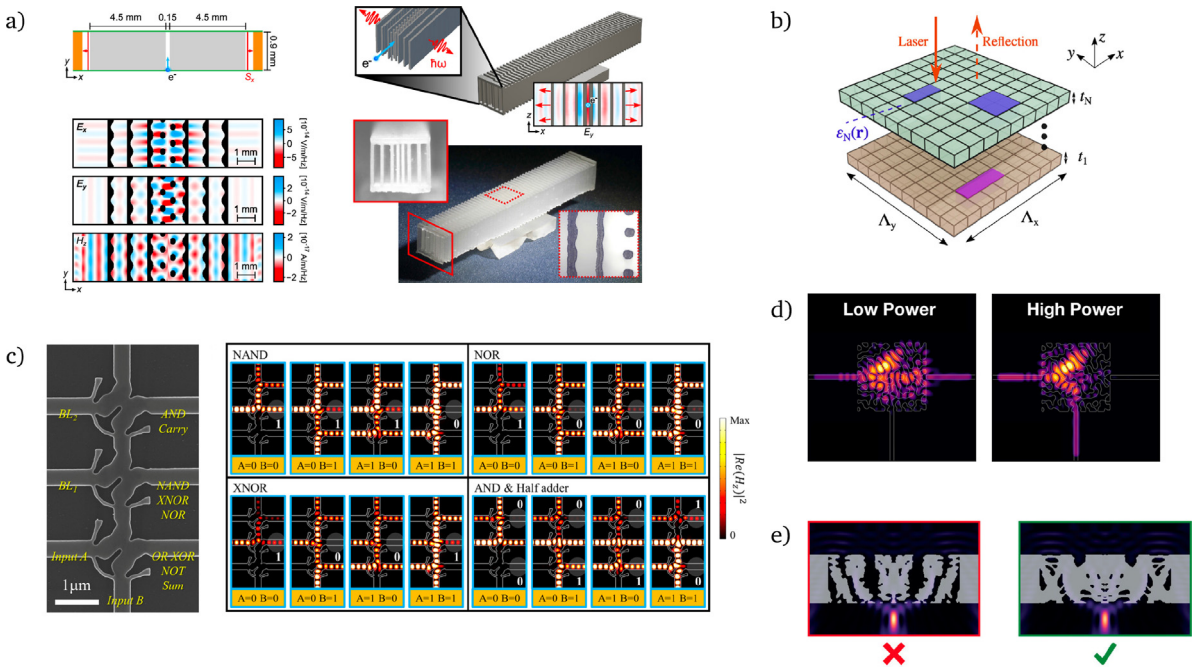

Fig. 19. Selected recent applications of inverse design (a) generation of THz radiation via the Smith–Purcell effect (from [324]), where an electron beam passes a periodic structure and resulting in synchronous radiation. (b) reflectors for relativistic lightsail propulsion (from [325]) (c) cascaded all-optical logic devices (from [326]), demonstrating integration into silicon photonic platforms (d) nonlinear nanophotonic devices (from [327]) (e) inclusion of structural integrity (from [328]).

enhancements of more than three orders of magnitude have been predicted for inverse-designed dielectric nanostructures [346], passive photonic components for mid-IR photonics have been proposed [347], periodic structures for sub-wavelength focusing have been suggested to out-perform photonic crystals [348] and Mie scattering based metasurfaces have been shown to produce helical focusing patterns [349].

- **Metasurfaces**: Very recent applications of the inverse design methodology have included using neural networks to generate dielectric metasurfaces [350,351], 'divide and conquer' approaches based on stitching together different metasurface sections [352] and even meta-optics for virtual reality [353]. Ultra-high efficiency metamaterial polarisers were designed and manufactured in [354], while metagratings for beam steering have been designed and manufactured in [355], with metasurfaces also being proposed for similar problems [356] and designed using genetic-type tree optimisation [357]. Recently a metasurface based on non-local media was designed and manufactured [358], resulting in the thinnest visible-range transmissive meta-lens to date. A general software platform for designing metadevices capable of polarisation splitting, beam bending and focusing was detailed in [359]. Other metamaterial problems to which inverse design has been applied include manufacture of transmission-mode colour filters [360] and metastructures for beam collimation [361], as well as a proposal for metasurfaces for frequency conversion [362]. Performance gains by cascaded metasurfaces were investigated in Refs. [363,364], and the feasibility of reconfigurable metasurfaces was investigated in [365]. Studies also continue into metasurfaces for solar collection efficiency, which began with varying the geometrical properties of silicon arrays to reduce reflection and transmission losses between photovoltaic devices [366,367] as well as introducing periodic nanostructures [368], textured surfaces [369] and diffractive optical elements [370,371] on top of the collection region. More recent solar collection research has been towards quasi-random silicon nanostructures [372] and multilayer dielectric stacks [373].
- **Non-linearity** Techniques of inverse design have recently found applications in non-linear devices, producing photonic switches in [327,374] (see Fig. 19d), second- and third-harmonic generation in fibres and metasurfaces [362], and switches in neural networks [375]. Non-linear response has applications in non-reciprocal devices (see, e.g., [376]), this phenomenon was taken advantage of in the same setup as an inverse designed (linear) in/out coupler in Ref. [377].
- **Novel systems and materials**: Emerging fields of application include proposals for magnonic circuit elements [378], for performance increases of ion-based devices (e.g. electron microscopes and mass spectrometers) [379], passive generation of complex optical lattices from only one or a few beams [380], topology-optimised topological insulators [381] and topological waveguides [382], Raman scattering [383], spontaneous parametric down-conversion [384], environment-induced coherence [385], interfacing with nuclear physics [386], and even lightsail

propulsion [325] (see Fig. 19b). Resonators and gratings for ultrarelativistic electrons were designed and manufactured in Refs. [324,387] (see Fig. 19a), as were optimised scintillating nanostructures [388], photon extractors from NV centres [389] and all-optical logic gates in [326] (as shown in Fig. 19a) and [390]. While many of the inverse-designed devices proposed and manufactured so far rely on silicon, studies are beginning to explore other materials, including diamond [391] (due to its hosting of colour centres) and indium phosphide [392] due to its more comprehensive range of photonic functionality (see, e.g., [393]).

Spanning all of these applications and directions are the practical aspects of actually manufacturing the inverse-designed devices. These were investigated in general in Ref. [394] and in detail in works where fabrication constraints were explicitly built in to the optimisation algorithm [328,395–399] (see Fig. 19e). Related advances include the introduction of energy constraints to propose [400] and then manufacture [401] a robust, integrated demultiplexer. Another issue which is pervasive across the field is that not all processes are particularly amenable to inverse design, as was noticed in [385,402], and also that some fundamental bounds exist even for optimised devices as discussed in general terms in [403,404]. Some specific bounds are known for extinction cross sections [333], near-field radiative heat transfer [405] and the reflection/transmission properties of metasurfaces [406].

6.2. Inverse design of light–matter interactions via the dyadic Green's tensor

So far this review will hopefully have made it clear that a central object in the study of light–matter interactions is the dyadic Green's tensor $\mathbb{G}$ — indeed all the examples given in the previous subsection could in principle have been expressed at least partly in terms of it. Hidden within the Green's tensor are all of the geometrical and material properties of any scatterers that may be present in the environment. It therefore stands to reason that a designer could simply choose a specific $\mathbb{G}$ that is optimal for a given situation. Unfortunately, such generality comes hand-in-hand with an astonishing amount of hidden complexity — as discussed in Section 5 the full (general distance, general material properties) Green's tensor is only analytically known for the very simplest of geometries. These only represent a tiny proportional of the vast space of device geometries so are almost certainly not optimal — the remainder must either be approximated as discussed in Section 5.3, or accessed numerically as in Section 5.4. This means that brute force optimisation in order to find the optimal $\mathbb{G}$ (and thereby the optimal structure) is normally computationally infeasible, so a more judicious approach is needed — this is provided by the *adjoint method*.

6.3. Adjoint method

To introduce the adjoint method we follow Ref. [268], and begin by defining a merit function F that is assumed to be a real-valued functional f of the Green's tensor $\mathbb{G}$;

$$F = f[\mathbb{G}(\mathbf{r}, \mathbf{r}', \omega)], \tag{260}$$

which we will aim to maximise. In principle we could integrate over source and observation positions, as well as frequency, in order to take into account delocalised sources and sinks as well as multimode effects. This will not be done here since it has essentially no effect on the core of the method, and can easily be added back in afterwards (see Ref. [268]). The question we seek to answer is "what change of $\mathbb{G}$ will cause a maximal increase in F?". This is analogous to the problem of finding out what change of x will cause a maximum increase in $f = y(x)$. The answer is of course that we would differentiate y with respect to x and look for the x at which this is maximal. Doing the same thing for our merit function F corresponds to taking a functional derivative, as f is a functional of $\mathbb{G}$. Note that $\mathbb{G}$ in general has complex-valued entries, meaning in principle that one would have to take functional derivatives with respect to the real and imaginary parts of $\mathbb{G}$ separately. However, it turns out to be more convenient to consider $\mathbb{G}$ and its complex conjugate $\mathbb{G}^*$ separately, as is often done in field theory, giving for the required derivative:

$$\begin{aligned}\delta F &= \frac{\partial F}{\partial \mathbb{G}}(\mathbf{r}, \mathbf{r}', \omega) \odot \delta\mathbb{G}(\mathbf{r}, \mathbf{r}', \omega) + \frac{\partial F}{\partial \mathbb{G}^*}(\mathbf{r}, \mathbf{r}', \omega) \odot \delta\mathbb{G}^*(\mathbf{r}, \mathbf{r}', \omega) \\ &= 2\mathrm{Re}\left[\frac{\partial F}{\partial \mathbb{G}}(\mathbf{r}, \mathbf{r}', \omega) \odot \delta\mathbb{G}(\mathbf{r}, \mathbf{r}', \omega)\right],\end{aligned} \tag{261}$$

where $\odot$ denotes the Frobenius product; $\mathbb{A} \odot \mathbb{B} = \sum_{ij} A_{ij}B_{ij}$. Eq. (261) still contains the unknown quantity $\delta\mathbb{G}(\mathbf{r}, \mathbf{r}', \omega)$, representing an infinitesimal change in $\mathbb{G}$. This is precisely the situation for which the Born series introduced earlier in Section 5.3.1 is suited;

$$\delta\mathbb{G}(\mathbf{r}, \mathbf{r}', \omega) = \mu_0\omega^2 n\alpha(\omega) \int_V d^3r'' \mathbb{G}(\mathbf{r}, \mathbf{r}'', \omega) \cdot \mathbb{G}(\mathbf{r}'', \mathbf{r}', \omega) = \mu_0\omega^2 n\alpha(\omega) V \mathbb{G}(\mathbf{r}, \mathbf{s}, \omega) \cdot \mathbb{G}(\mathbf{s}, \mathbf{r}', \omega). \tag{262}$$

where we have assumed a homogeneous scattering body in the second step [see Eq. (240)]. Using this in Eq. (261) we have

$$\delta F = 2\mu_0\omega^2 n\alpha(\omega)\mathrm{Re}\left[\frac{\partial F}{\partial \mathbb{G}}(\mathbf{r}, \mathbf{r}', \omega) \odot \int_V d^3r'' \mathbb{G}(\mathbf{r}, \mathbf{r}'', \omega) \cdot \mathbb{G}(\mathbf{r}'', \mathbf{r}', \omega)\right]. \tag{263}$$

In principle calculating δF given by the above expression is enough to find the optimal position $\mathbf{s}$ of a small inclusion that will maximally increase F. However, there is a serious computational problem. In any numerical method, the field is calculated throughout the simulation domain with a given set of sources. Observing the field at a particular point simply means choosing a particular spatial point in the resulting dataset, so changing the *observation* point is trivial. Changing the *source* distribution, however, entails doing a whole *new* simulation. Looking back at Eq. (263), we can see that the optimisation position $\mathbf{s}$ appears in the source (second) position in the Green's tensor $\mathbb{G}$, meaning that changing the optimisation position entails doing a whole new simulation. Use of Eq. (263) is therefore no better than simple brute-force calculation of the relevant observable for all possible optimisation points, which for a realistic problem will be unfeasibly numerous.

To get around this, there is one very neat trick that leads to huge computational gain. This is to take advantage of the source-observer symmetry of Maxwell's equations, which, in terms of $\mathbb{G}$ translates to;

$$\mathbb{G}(\mathbf{r}, \mathbf{r}', \omega) = \mathbb{G}^{\mathrm{T}}(\mathbf{r}', \mathbf{r}, \omega), \tag{264}$$

also known as the Lorentz reciprocity condition. This constraint holds in any medium that is reciprocal, with non-reciprocal media including for example Faraday media under the influence of an external magnetic field (the basis of magneto-optical isolators). Therefore, by making the broadly-applicable assumption that the material at hand is reciprocal media we can use (264) to rewrite (263) as:

$$\delta F = \mathrm{Re}\left[\frac{\partial F}{\partial \mathbb{G}}(\mathbf{r}, \mathbf{r}', \omega) \odot \int_V d^3 r'' \mathbb{G}^{\mathrm{T}}(\mathbf{r}'', \mathbf{r}, \omega) \cdot \mathbb{G}(\mathbf{r}'', \mathbf{r}', \omega)\right] \tag{265}$$

where we have also dropped the factor $2\mu_0\omega^2 n\alpha(\omega)$ since these (positive) constants will have no effect on the spatial position of the maximum of δF. This can be further approximated if V is sufficiently small that the integral can be approximated by its value at the centre, taken to be at $\mathbf{s}$;

$$\delta F = \mathrm{Re}\left[\frac{\partial F}{\partial \mathbb{G}}(\mathbf{r}, \mathbf{r}', \omega) \odot \left(\mathbb{G}^{\mathrm{T}}(\mathbf{s}, \mathbf{r}, \omega) \cdot \mathbb{G}(\mathbf{s}, \mathbf{r}', \omega)\right)\right], \tag{266}$$

where a factor V has again been dropped. Eq. (266) is the central formula of Green's tensor based optimisation. The positions appearing in the second arguments of the Green's tensor are $\mathbf{r}$ and $\mathbf{r}'$ which are both fixed, meaning that only *two* simulations are required to produce δF for the whole space for any given F. After this a computationally trivial data processing step identifies the position of the maximum of the δF found by combining those two Green's tensors via Eq. (266). Equations playing the role of (266) are sometimes known as topological derivatives, especially in the mathematics literature (e.g. [407,408]).

The version of the adjoint method used above is particularly suited for working with the statements of atomic emission/absorption rates and processes dealt with in Section 4, as these work directly and only with the Green's tensor. If the desired observable is, for example, the electric field itself in an extended region, the direct Green's tensor method becomes unwieldy. This is because a spatial integral needs to be taken to calculate the electric field from the Green's tensor, which ordinarily will have been calculated by first simulating an electric field anyway. In such situations it is more natural to work with the version of the adjoint method based on electric fields, as was done in the original formulations of nanophotonic inverse design upon which the completely Green's tensor based version was built. In the electric field case the equivalent of (266) for an observation position $\mathbf{r}'$ is [330]

$$\delta F_E \propto \mathrm{Re}\left[\alpha \mathbf{E}(\mathbf{s}) \cdot \mathbf{E}^{\mathrm{A}}(\mathbf{s})\right], \tag{267}$$

where α is the polarisability of the chosen building block (a cube, a sphere, etc.), $\mathbf{E}(\mathbf{s})$ is the electric field and $\mathbf{E}^{\mathrm{A}}$ is the adjoint electric field, which is the field that a dipole placed at position $\mathbf{r}'$ would radiate.

6.3.1. Merit function example: spontaneous decay

A simple and pedagogical example of how to use the Green's tensor merit function gradient expression (266) is provided by spontaneous decay, as discussed in Section 4.1. The rate of spontaneous decay for a two-level atom with transition frequency ω_{A} and dipole moment $\mathbf{d}_{\mathrm{A}}$, placed at position $\mathbf{r}$ is given by Eq. (174) as;

$$\Gamma = \frac{2\mu_0\omega_{\mathrm{A}}^2}{\hbar}\mathbf{d} \cdot \mathrm{Im}\mathbb{G}(\mathbf{r}_{\mathrm{A}}, \mathbf{r}_{\mathrm{A}}, \omega_{\mathrm{A}}) \cdot \mathbf{d} = \frac{2\mu_0\omega_{\mathrm{A}}^2}{\hbar}\frac{1}{2i} d_i \left[\mathbb{G}_{ij}(\mathbf{r}_{\mathrm{A}}, \mathbf{r}_{\mathrm{A}}, \omega_{\mathrm{A}}) - \mathbb{G}_{ij}^*(\mathbf{r}_{\mathrm{A}}, \mathbf{r}_{\mathrm{A}}, \omega_{\mathrm{A}})\right] d_j. \tag{268}$$

We can therefore take our spontaneous decay merit function as;

$$F_{\mathrm{SD}} = \mathbf{d} \cdot \mathrm{Im}\mathbb{G}(\mathbf{r}_{\mathrm{A}}, \mathbf{r}_{\mathrm{A}}, \omega_{\mathrm{A}}) \cdot \mathbf{d} = \frac{1}{2i} d_i \left[\mathbb{G}_{ij}(\mathbf{r}_{\mathrm{A}}, \mathbf{r}_{\mathrm{A}}, \omega_{\mathrm{A}}) - \mathbb{G}_{ij}^*(\mathbf{r}_{\mathrm{A}}, \mathbf{r}_{\mathrm{A}}, \omega_{\mathrm{A}})\right] d_j. \tag{269}$$

The derivative with respect to G can then be taken, giving

$$\frac{\partial F_{\mathrm{SD}}}{\partial G_{kl}} = \frac{1}{2i} d_i d_j \delta_{ik} \delta_{jl}. \tag{270}$$

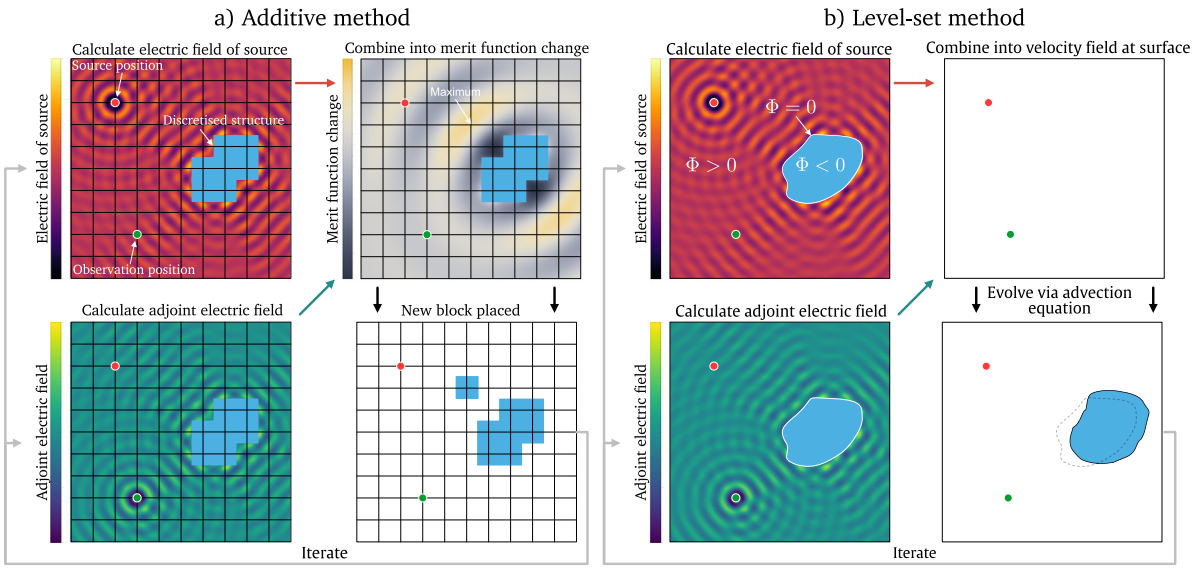

Fig. 20. Schematic representation of (a) the additive inverse design process based on the topological derivative (266) and (b) the level set inverse design process based on the shape derivative (279).

Using this in Eq. (266), we have:

$$\begin{aligned}\delta F_{\mathrm{SD}} &= \mathrm{Re}\left[\frac{\partial F_{\mathrm{SD}}}{\partial \mathbb{G}_{kl}}(\mathbf{r}_{\mathrm{A}}, \mathbf{r}_{\mathrm{A}}, \omega_{\mathrm{A}})\mathbb{G}^{\mathrm{T}}_{km}(\mathbf{s}, \mathbf{r}_{\mathrm{A}}, \omega_{\mathrm{A}})\mathbb{G}_{ml}(\mathbf{s}, \mathbf{r}_{\mathrm{A}}, \omega_{\mathrm{A}})\right] \\ &= \mathrm{Re}\left[\frac{1}{2i}d_i d_j \delta_{ik}\delta_{jl}\mathbb{G}^{\mathrm{T}}_{km}(\mathbf{s}, \mathbf{r}_{\mathrm{A}}, \omega_{\mathrm{A}})\mathbb{G}_{ml}(\mathbf{s}, \mathbf{r}_{\mathrm{A}}, \omega_{\mathrm{A}})\right] \\ &= \frac{1}{2}\mathrm{Im}\left[d_i d_j \mathbb{G}^{\mathrm{T}}_{im}(\mathbf{s}, \mathbf{r}_{\mathrm{A}}, \omega_{\mathrm{A}})\mathbb{G}_{mj}(\mathbf{s}, \mathbf{r}_{\mathrm{A}}, \omega_{\mathrm{A}})\right] \end{aligned} \tag{271}$$

giving

$$\delta F_{\mathrm{SD}} = \frac{1}{2}\mathrm{Im}\left\{\left[\mathbf{d}\cdot\mathbb{G}^{\mathrm{T}}(\mathbf{s}, \mathbf{r}_{\mathrm{A}}, \omega_{\mathrm{A}})\right]\cdot\left[\mathbb{G}(\mathbf{s}, \mathbf{r}_{\mathrm{A}}, \omega_{\mathrm{A}})\cdot\mathbf{d}\right]\right\} \tag{272}$$

in agreement with Ref. [268]. This expression could be used, for example, to design nanophotonic cavities for Purcell enhancement.

6.4. Practical implementation

Given a merit function gradient, there are a number of ways to implement a practical optimisation scheme. Here we will concentrate on two of these, a simple additive method and the more complex level-set approach.

The additive approach is conceptually the simplest, being based on adding a small block of dielectric material at the position of maximal δF as illustrated schematically in Fig. 20a. Such an approach can naturally build fabrication constraints via the size and shape of the added blocks, but takes a large number of iterations to build up a complex structure (see, e.g. [268,385]).

A more sophisticated approach is one where the geometry is encoded via function Φ, known as the level set function as introduced by Osher and Sethian in 1988 [409] and subsequently applied to photonics in Ref. [410]. Here, the boundary of a geometry is represented by the contour $\Phi = 0$, with $\Phi < 0$ representing the interior and $\Phi > 0$ the exterior. The level set function Φ is defined in one higher dimension than the geometry at hand, so that for example a circle in a 2D simulation is represented by the values of a 3D function as shown in Fig. 21(a) and (b). In order to implement the optimisation, a formal 'time' parameter t is introduced, which represents the iteration number. The surface of the geometry at a given time is therefore defined by;

$$\Phi(\mathbf{r}(t), t) = 0. \tag{273}$$

Taking a total time derivative of this equation yields

$$\frac{\partial}{\partial t}\Phi(\mathbf{r}(t), t) + \nabla\Phi(\mathbf{r}(t), t)\cdot\frac{\partial \mathbf{r}(t)}{\partial t} = 0, \tag{274}$$

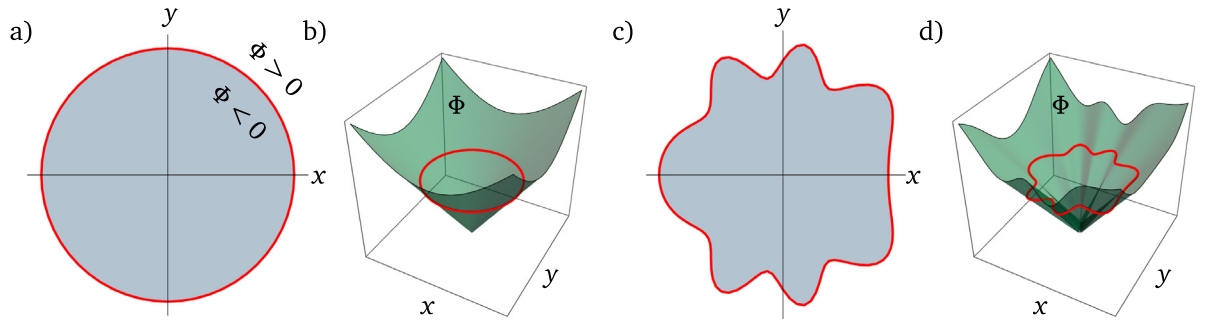

Fig. 21. Two two-dimensional geometries [(a) and (c)], and two possible three-dimensional level set functions [(b) and (d)] corresponding to them.

which is the advection equation, well-studied in fluid dynamics where it governs, for example, the motion of clouds in a velocity field given by the wind. Since only deformations perpendicular to the boundary are relevant (those along the boundary just represent a reparameterisation of the shape), we can simplify this by introducing a scalar velocity field v_n, normal to the surface

$$\frac{\partial}{\partial t}\Phi(\mathbf{r}(t),t)+v_n(\mathbf{r}(t))|\nabla\Phi(\mathbf{r}(t),t)|=0. \tag{275}$$

The boundaries of the geometry should be varied in such a way that F increases, meaning we have to choose an appropriate v_n that ensures this. Rewriting the volume integral in Eq. (265) as the product of an area integral over dA and infinitesimal change δx in the boundary in the normal direction, we have

$$\int_V \mathrm{d}^3r'' \rightarrow \int_{\partial V}\mathrm{d}A\delta x(\mathbf{r}'')=\int_{\partial V}\mathrm{d}Av_n(\mathbf{r}'')\delta t, \tag{276}$$

where in the second step the normal perturbation δx has been replaced by the product of the velocity v_n and the time step δt. The merit function change is now;

$$\delta F=\mathrm{Re}\left[\frac{\partial F}{\partial \mathbb{G}}(\mathbf{r},\mathbf{r}',\omega)\odot\int_{\partial V}\mathrm{d}A\, v_n(\mathbf{r}'')\delta t\mathbb{G}^{\mathrm{T}}(\mathbf{r}'',\mathbf{r},\omega)\cdot\mathbb{G}(\mathbf{r}'',\mathbf{r}',\omega)\right]. \tag{277}$$

By choosing the velocity field as;

$$v_n(\mathbf{r}'')=\frac{\partial F}{\partial \mathbb{G}}(\mathbf{r},\mathbf{r}',\omega)\odot\mathbb{G}^{\mathrm{T}}(\mathbf{r}'',\mathbf{r},\omega)\cdot\mathbb{G}(\mathbf{r}'',\mathbf{r}',\omega)\delta t, \tag{278}$$

we have

$$\delta F=\int_{\partial V}\mathrm{d}A\, v_n^2(\mathbf{r}'')\delta, \tag{279}$$

which ensures a positive change in the merit function at each timestep, and is known as a shape derivative. The process of level-set inverse design is schematically illustrated in Fig. 20b. This process is finding wide use across nanophotonics [399,411] including in fabrication-constrained settings [398] and in terms of its relation to explainable machine learning [412]. Very recent designs based on level-set methods have included CMOS-compatible waveguide bends [413], random meta-atoms [414], fabrication-constrained multiplexers [415], solar energy concentrators [416], modal switches [417] directional routing of light using dielectric nanorods [418] and polarisation rotators [419,420].

7. Frontiers

7.1. Strong coupling and polaritonic chemistry

All of the atomic processes discussed in Section 4 were considered in the weak-coupling, perturbative regime. What happens beyond this? To answer this question we have to first consider what determines whether a light–matter system is strongly or weakly coupled. The key quantity is the Rabi frequency Ω_{R}, which is expressed in terms of the Green's tensor as (see, e.g., [43]);

$$\Omega_{\mathrm{R}}^2(\mathbf{r})=\frac{2\mu_0\gamma\omega^2}{\hbar}\mathbf{d}\cdot\mathrm{Im}\mathbb{G}(\mathbf{r},\mathbf{r},\omega)\cdot\mathbf{d}. \tag{280}$$

where γ is the frequency width of a resonant mode of frequency ω, and $\mathbf{d}$ is the expectation value of the dipole moment operator for the relevant atomic transition. The strong coupling regime is entered when the Rabi frequency is much larger

than both the free space decay rate and the dissipation rate of any cavity present (such a dissipation rate could itself be worked out from $\mathbb{G}$, in which case one could identify strong coupling from $\mathbb{G}$ alone). In other words, the strong coupling regime is entered when the coherent exchange of energy between a quantum emitter and light becomes faster than the decay rates of the atom and the cavity.

In the weak-coupling treatments shown so far we have, without necessarily realising it, used the idea of weak coupling to effect a clear separation between light and matter. This, alongside many of the other qualitative features of the strong coupling regime, can be encapsulated by considering a simple model of coupled harmonic oscillators as is done in the pedagogical treatment in Ref. [421]. Consider two independent oscillators of equal mass m with eigenfrequencies $\omega_\mathrm{A} = \sqrt{k/m}$ and $\omega_\mathrm{B} = \sqrt{(k+\Delta k)/m}$. Defining ω_0 as $\sqrt{k/m}$, we have;

$$\frac{\omega_\mathrm{A}}{\omega_0} = 1 \qquad \frac{\omega_\mathrm{B}}{\omega_0} = \sqrt{1+\frac{\Delta k}{k}} \tag{281}$$

which are plotted in panel of Fig. 22a, where we emphasise that the eigenfrequency of oscillator A is independent of any of the properties of B. When coupling is introduced, the two equations describing the motion of the two oscillators are;

$$m\ddot{x}_\mathrm{A} + kx_\mathrm{A} + \Omega(x_\mathrm{A} - x_\mathrm{B}) = 0, \tag{282}$$

$$m\ddot{x}_\mathrm{B} + kx_\mathrm{B} + \Omega(x_\mathrm{B} - x_\mathrm{A}) = 0. \tag{283}$$

Seeking solutions of the form $x_{\mathrm{A/B}} = x^0_{\mathrm{A/B}} e^{i\omega t}$, this pair of coupled equations can be rewritten as a matrix equation:

$$\begin{pmatrix} -m\omega^2 + k + \Omega & -\Omega \\ -\Omega & -m\omega^2 + k + \Delta k + \Omega \end{pmatrix} \begin{pmatrix} x^0_\mathrm{A} \\ x^0_\mathrm{B} \end{pmatrix} = 0. \tag{284}$$

Non-trivial solutions are given by the values of $\omega_\pm$ for which the matrix on the left hand side has zero determinant;

$$\omega_\pm = \sqrt{\frac{1}{2}\left(\bar{\omega}^2_\mathrm{A} + \bar{\omega}^2_\mathrm{B} \pm \sqrt{\left(\bar{\omega}^2_\mathrm{A} - \bar{\omega}^2_\mathrm{B}\right)^2 + 4\Omega^2/m^2}\right)} \tag{285}$$

with $\bar{\omega}_\mathrm{A} = \sqrt{(k+\Omega)/m}$ and $\bar{\omega}_\mathrm{B} = \sqrt{(k+\Delta k+\Omega)/m}$. The frequencies $\omega_\pm$ are shown in panel (b) of Fig. 22, where the characteristic 'avoided crossing' feature of coupled systems appears. The model can be extended by incorporating a constant[23] damping coefficient γ, corresponding to the introduction of terms $\gamma\dot{x}_\mathrm{A}$ to the left hand side of Eq. (282) and $\gamma\dot{x}_\mathrm{B}$ to the left hand side of Eq. (283). The eigenfrequencies then become complex (and far too unwieldy to write down explicitly here), with the imaginary parts corresponding to the widths of the two states. This has the effect of 'blurring' the lines in panels (a) and (b) in Fig. 22, leading to panels (c) and (d) where the magnitude of the imaginary part of the eigenfrequencies is shown as an error band either side of the real parts. If the coupling is small enough the spectrum may not be spectroscopically distinguishable from the uncoupled case as shown in panel (c) of Fig. 22. If the coupling is larger, the two lines are distinguishable even in the presence of finite linewidth, which is an indication that the system is in the strong coupling regime as shown in panel (d) of Fig. 22.

Strong coupling between light and matter can be reached by a combination of light being restricted to a resonator (either by high confinement or low leakage, or both), and use of emitters with large transition dipole moments (high Rabi frequency). The former can be achieved by using highly localised surface plasmon modes, while the latter is frequently found by using organic materials. The resulting mixed light–matter excitations are known as polaritons[24] which have applications in polaritonic devices that take advantage of their strong intrinsic nonlinearities and ability to be selectively excited [422]. In the last ten years or so there has been an increasing focus on using strong coupling to affect the rate of chemical reactions, beginning with photoisomerisation from spiropyran to merocyanine [423]. This inspired the burgeoning field of polaritonic chemistry, which is reviewed in detail [424–426] and very recently surveyed in terms of theoretical challenges [427]. The main issue is that modelling of cavity molecular polaritons is a fundamentally multi-scale problem — wavelengths in optical cavities are much larger than molecular sizes, leading to a large number of participating molecules. Conversely, sub-wavelength cavities are much harder to construct and model accurately, and generally have large associated losses. Taking this to the extreme, 'picocavities' where atom-scale features are manipulated have been the subject of proposals [428] and demonstrations [429] in other contexts — an open question in polaritonic chemistry is whether similar techniques can be applied to control of chemical reactions at single-molecule level.

7.2. Quantum electrodynamical density functional theory

As mentioned near the end of Section 4.3, the QED theory of resonance energy transfer and interatomic Coulombic decay has a frontier at very short distances, in particular when wave function overlap becomes significant. Such short-range problems are solved by density-functional theories (DFTs) have found wide applicability in ab initio quantum

[23] In reality the damping term would depend on the coupling strength itself, but for the features to be highlighted in this simple model here it suffices to consider a constant.

[24] The polaritons should be carefully distinguished from the other type of polaritonic excitations introduced in Section 3, see discussion following Eq. (161).

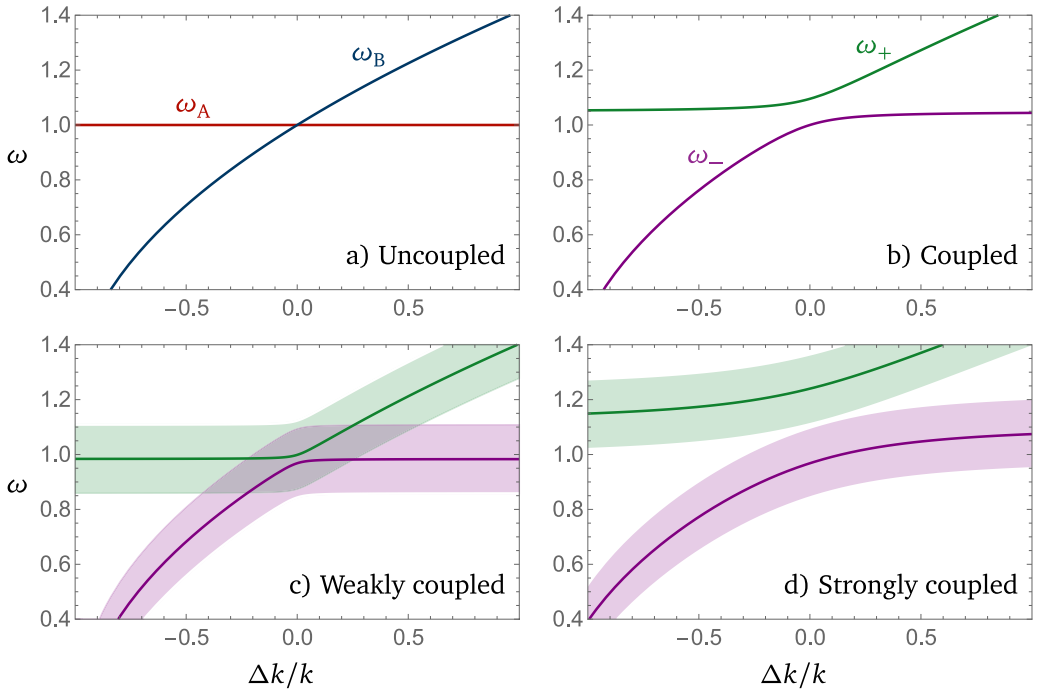

Fig. 22. Uncoupled and coupled oscillators, in weak and strong coupling regimes. Panel (a) shows the eigenfrequencies of two undamped, uncoupled oscillators while panel (b) adds coupling. Panel (c) shows the eigenfrequencies of damped coupled oscillators, but where the coupling is weak enough that they can effectively be considered as uncoupled. Finally, panel (d) shows two damped coupled oscillators but the coupling strength is large enough (or the damping small enough) that this can be unambiguously discriminated from the weak- or no-coupling case – this is the strong coupling regime.

chemistry calculations but are incapable of capturing the longer-range behaviour of the QED theory due to the lack of photonic degrees of freedom. Quantum electrodynamical density functional theory (QEDFT) provides a bridge between the two theories.

DFTs are capable of treating a many-electron problem, which is ordinarily infeasible due to the 'curse of dimensionality' that prevents wave functions from being stored on a realistic medium for any systems other than the tiniest ones. DFT avoids this by considering instead the electron density (depending on only one coordinate), with an appropriate effective potential (a unique functional of the electron density) that ensures the many-body problem and the fictitious one-body problem have the same electron density, in principle given exact results. This is known as the Kohn–Sham construction and is illustrated schematically in Fig. 23.

The Kohn–Sham fields can be calculated uniquely from a given charge density, depending on three terms; the potential generated by the charged density itself, the Hartree energy of the charge density (both known exactly), and the potential associated with exchange and correlation effects. The latter takes into account all the complex quantum-mechanical mutual interactions of the electrons, and has to be accessed via approximations, for which there are several sophisticated approaches in the DFT literature.

Standard DFT as outlined above is wildly successful at electronic structure calculations, but does not include the quantum nature of light. Conversely, in quantum optics the quantum nature of light is treated in full generality, while simple approximations are used for the charged particles (e.g. two- or few-levels, dipole approximation as taken in the examples shown in this review). As mentioned above, the goal of quantum electrodynamical density (QEDFT) [424,430,431] is to bridge this gap, providing a way of treating the quantum natures of particles and light on an equal footing. This is achieved by applying a 'density functionalisation' process, analogous to that shown in Fig. 23, in which internal variables and external variables are identified (in standard DFT these are the charge density and the Kohn–Sham potentials, respectively). If a one-to-one mapping between a given internal variable (or set of them) and an external variable can be found, then analogous processes to those illustrated in Fig. 24 to find observables that are exact in principle.

In QEDFT the internal/external variables are actually pairs of quantities, representing current and vector potential. Just as in standard DFT, finding the relevant Kohn–Sham fields for a given internal pair is a non-trivial task requiring approximations [432–434]. In the non-relativistic limit, multipolar gauge and dipole approximation the relevant external variables turn out to be the electronic external potential and the time derivative of a classical current, which can be shown to be in one-to-one correspondence with the internal variables of electron density and the mode resolved displacement coordinate of a photon (the latter essentially proportional to the displacement field **D** [435]).

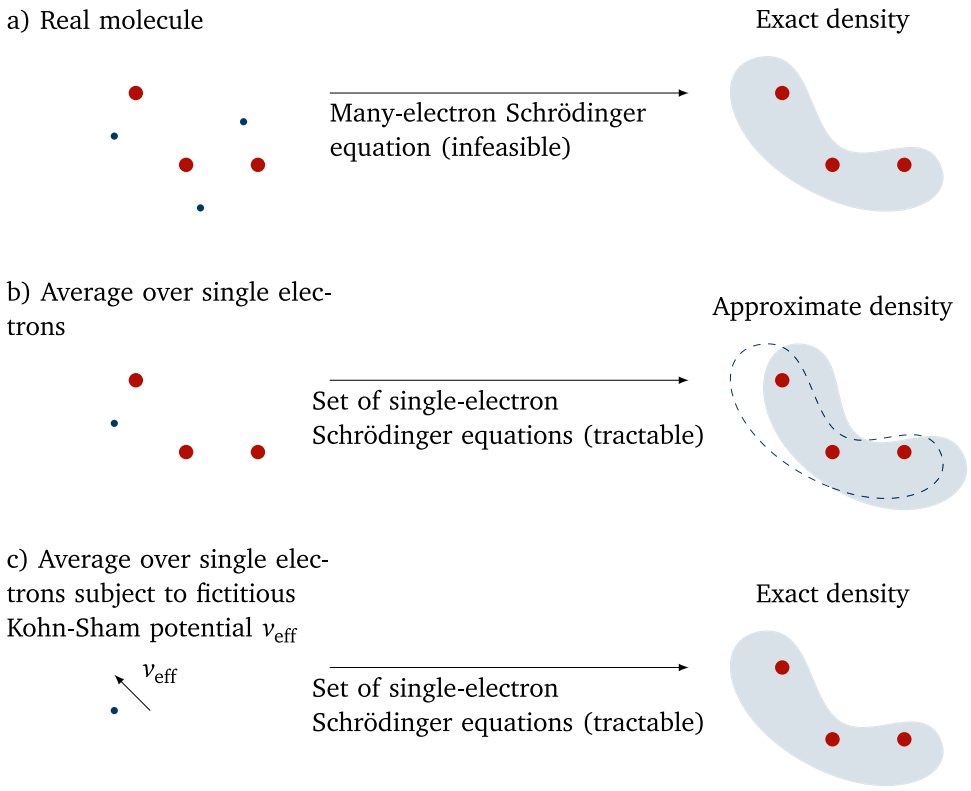

Fig. 23. Schematic illustration of the general principles of the Kohn–Sham construction in density-functional theory.

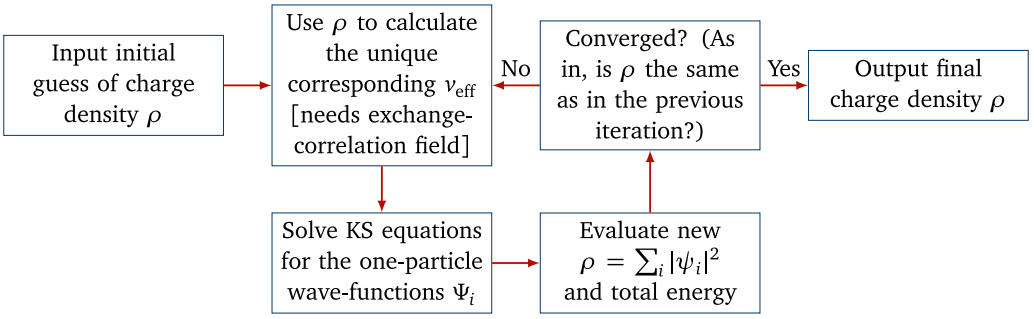

Fig. 24. Computational process for DFT calculations, representing the canonical example of 'density functionalisation' which was later applied to produce QEDFT.

The QEDFT formalism is still in its early stages of development, with explicit numerical results demonstrated for model systems such as a two-site Hubbard model coupled to a single cavity mode [430] or a GaAs ring model restricted to two dimensions and interacting with one mode of the electromagnetic field [434]. Calculations relevant to real systems include dynamic observables of carbon dioxide [436] and electron–photon interaction-distorted ground densities of an isolated azulene molecule and chains of sodium dimers [434], all located within optical cavities. More recent extensions to the QEDFT formalism have been introduction of dissipative dynamics [437] and combination with macroscopic QED [438].

8. Conclusions and outlook

The quantum electrodynamical theory of light–matter interactions is old, well-understood and, as far as we know, a complete description of all electromagnetic phenomena with its predictions having been experimentally confirmed to remarkable accuracy. So why are light–matter interactions such an active field of research? The answer, of course, is that while we have a complete set of equations describing the theory, exact practical solution of them is impossible except in the very simplest of situations. The various sub-fields dealing with light–matter interaction are usually defined

by the way in which this difficulty is circumvented — for example in macroscopic QED the atomic nature of a medium is approximated away, while in density functional theory the photonic degree of freedom is normally ignored. Recent advances have been made in bridging these gaps, for example the polaritonic chemistry techniques discussed in Section 7.1 bring quantum-optical ideas to the study of chemical reactions. Open questions still remain in these new realms of application, for example it is still unclear whether polaritonic chemistry can be used to modify chemical reactions at the single-molecule level. Quantum electrodynamical density functional theory as discussed in Section 7.2 is still in its infancy, but its unification of quantum optics and density functional theory is expected to provide a consistent description of the fundamental light–matter interaction process at a wide range of energy scales.

Even within the framework of a certain theory, the overwhelming complexity of real systems still persists. For example, in macroscopic QED there quite some restrictive assumptions made (linear response, normally point-like dipolar atoms, validity of macroscopic constitutive relations), but even with these one still runs into the problem that the Green's tensor for almost any realistic geometry or material response cannot be found analytically. Some of the ways around this were discussed in Section 5.3, ranging from the Born series for dilute media, techniques from transformation optics, quasi-normal modes and finally fully numerical approaches. The latter allow completely general structures to be described, which is the basis of the free-form optimisation techniques discussed in Section 6. Such techniques circumvent the difficulties encountered when designing sub-wavelength structures for nanophotonics applications by reversing the design process — a goal is specified and an algorithm does the rest.

The next decades are sure to see further unifications between the various realms of applicability of various theories, as is the case across the history of physics. The ability to accurately describe ever more complex quantum electrodynamical systems will lead to applications which cannot be predicted with certainty, but will continue to represent an active and fruitful field of research for some time yet.

Declaration of competing interest

The authors declare that they have no known competing financial interests or personal relationships that could have appeared to influence the work reported in this paper.

Acknowledgements

R.B. acknowledges the UK Research and Innovation Council grants EP/V048449/1 and EP/W016486/1, and N.W. acknowledges funding and support from the Royal Commission for the Exhibition of 1851, United Kingdom.

Appendix. Gradient of multipolar gauge generator

In this appendix we will prove that the right hand sides of Eqs. (81) and (82) are equivalent. We begin by making use of the following vector calculus identity;

$$\nabla(\mathbf{a}\cdot\mathbf{b}) = (\mathbf{a}\cdot\nabla)\mathbf{b} + (\mathbf{b}\cdot\nabla)\mathbf{a} + \mathbf{a}\times(\nabla\times\mathbf{b}) + \mathbf{b}\times(\nabla\times\mathbf{a}) \tag{A.1}$$

Noting that $\mathbf{A}(\mathbf{r}')$ is independent of $\mathbf{r}$, Eq. (81) becomes;

$$\nabla\chi_{\mathrm{M}}(\mathbf{r}) = -\int \mathrm{d}^3r' \int_0^1 \mathrm{d}\lambda \left\{ \left[\mathbf{A}(\mathbf{r}')\cdot\nabla\right]\mathbf{r}\delta(\mathbf{r}'-\lambda\mathbf{r}) + \mathbf{A}(\mathbf{r}')\times\{\nabla\times[\mathbf{r}\delta(\mathbf{r}'-\lambda\mathbf{r})]\}\right\} \tag{A.2}$$

Considering the first term in the integrand, we have;

$$\begin{aligned}\left[\mathbf{A}(\mathbf{r}')\cdot\nabla\right]\mathbf{r}\delta(\mathbf{r}'-\lambda\mathbf{r}) &= \mathbf{A}(\mathbf{r}')\delta(\mathbf{r}'-\lambda\mathbf{r}) + \mathbf{r}\left[\mathbf{A}(\mathbf{r}')\cdot\nabla\right]\delta(\mathbf{r}'-\lambda\mathbf{r}) \\ &= \mathbf{A}(\mathbf{r}')\delta(\mathbf{r}'-\lambda\mathbf{r}) - \lambda\mathbf{r}\left[\mathbf{A}(\mathbf{r}')\cdot\nabla'\right]\delta(\mathbf{r}'-\lambda\mathbf{r})\end{aligned} \tag{A.3}$$

where we used the following relation;

$$\nabla\delta(\mathbf{r}'-\lambda\mathbf{r}) = -\lambda\nabla'\delta(\mathbf{r}'-\lambda\mathbf{r}) \tag{A.4}$$

which can be directly proved by using the Fourier representation of the delta function

$$\delta(\mathbf{r}'-\lambda\mathbf{r}) = \frac{1}{(2\pi)^3}\int d^3k e^{\mathrm{i}\mathbf{k}\cdot(\mathbf{r}'-\lambda\mathbf{r})} \tag{A.5}$$

Then;

$$\nabla\chi_{\mathrm{M}}(\mathbf{r}) = -\int \mathrm{d}^3r' \int_0^1 \mathrm{d}\lambda \left\{ \mathbf{A}(\mathbf{r}')\delta(\mathbf{r}'-\lambda\mathbf{r}) - \lambda\mathbf{r}\left[\mathbf{A}(\mathbf{r}')\cdot\nabla'\right]\delta(\mathbf{r}'-\lambda\mathbf{r}) + \mathbf{A}(\mathbf{r}')\times\{\nabla\times[\mathbf{r}\delta(\mathbf{r}'-\lambda\mathbf{r})]\}\right\} \tag{A.6}$$

Now considering the final term;

$$\nabla\times[\mathbf{r}\delta(\mathbf{r}'-\lambda\mathbf{r})] = \delta(\mathbf{r}'-\lambda\mathbf{r})\nabla\times\mathbf{r} - \mathbf{r}\times[\nabla\delta(\mathbf{r}'-\lambda\mathbf{r})] = \lambda\mathbf{r}\times[\nabla'\delta(\mathbf{r}'-\lambda\mathbf{r})] \tag{A.7}$$

where a vector calculus identity and $\nabla \times \mathbf{r} = \mathbf{0}$ were used. This means Eq. (A.2) becomes;

$$\nabla\chi_{\mathrm{M}}(\mathbf{r}) = -\int \mathrm{d}^3r' \int_0^1 \mathrm{d}\lambda \left\{ \mathbf{A}(\mathbf{r}')\delta(\mathbf{r}' - \lambda\mathbf{r}) - \lambda\mathbf{r}\left[\mathbf{A}(\mathbf{r}')\cdot\nabla'\right]\delta(\mathbf{r}' - \lambda\mathbf{r}) + \mathbf{A}(\mathbf{r}') \times \{\lambda\mathbf{r} \times [\nabla'\delta(\mathbf{r}' - \lambda\mathbf{r})]\} \right\} \tag{A.8}$$

We can use the Jacobi identity:

$$\mathbf{a} \times (\mathbf{b} \times \mathbf{c}) + \mathbf{b} \times (\mathbf{c} \times \mathbf{a}) + \mathbf{c} \times (\mathbf{a} \times \mathbf{b}) \equiv \mathbf{0} \tag{A.9}$$

on the final term

$$\begin{aligned}\nabla\chi_{\mathrm{M}}(\mathbf{r}) = -\int \mathrm{d}^3r' \int_0^1 \mathrm{d}\lambda \Big\{ & \mathbf{A}(\mathbf{r}')\delta(\mathbf{r}' - \lambda\mathbf{r}) - \lambda\mathbf{r}\left[\mathbf{A}(\mathbf{r}')\cdot\nabla'\right]\delta(\mathbf{r}' - \lambda\mathbf{r}) \\ & - \lambda\mathbf{r} \times \{[\nabla'\delta(\mathbf{r}' - \lambda\mathbf{r})] \times \mathbf{A}(\mathbf{r}')\} - \lambda[\nabla'\delta(\mathbf{r}' - \lambda\mathbf{r})] \times [\mathbf{A}(\mathbf{r}') \times \mathbf{r}] \Big\}\end{aligned} \tag{A.10}$$

The first term on the second line can be simplified by noting that;

$$\int d^3r'[\nabla'\delta(\mathbf{r}' - \lambda\mathbf{r})] \times \mathbf{A}(\mathbf{r}') = -\int d^3r'\delta(\mathbf{r}' - \lambda\mathbf{r})\nabla' \times \mathbf{A}(\mathbf{r}') = -\int d^3r'\delta(\mathbf{r}' - \lambda\mathbf{r})\mathbf{B}(\mathbf{r}') \tag{A.11}$$

where integration by parts has been used in the first step. To simplify the second term on the second line we go into index notation

$$\begin{aligned}\left\{[\nabla'\delta(\mathbf{r}' - \lambda\mathbf{r})] \times [\mathbf{A}(\mathbf{r}') \times \mathbf{r}]\right\}_i &= \varepsilon_{ijk}[\nabla'_j\delta(\mathbf{r}' - \lambda\mathbf{r})][\mathbf{A}(\mathbf{r}') \times \mathbf{r}]_k \\ &= \varepsilon_{ijk}[\nabla'_j\delta(\mathbf{r}' - \lambda\mathbf{r})]\varepsilon_{klm}A_l(\mathbf{r}')r_m \\ &= \left(\delta_{il}\delta_{jm} - \delta_{im}\delta_{jl}\right)[\nabla'_j\delta(\mathbf{r}' - \lambda\mathbf{r})]A_l(\mathbf{r}')r_m \\ &= [\nabla'_j\delta(\mathbf{r}' - \lambda\mathbf{r})]A_i(\mathbf{r}')r_j - [\nabla'_j\delta(\mathbf{r}' - \lambda\mathbf{r})]A_j(\mathbf{r}')r_i \\ &= [\mathbf{r}\cdot\nabla'\delta(\mathbf{r}' - \lambda\mathbf{r})]A_i(\mathbf{r}') - r_i[\mathbf{A}(\mathbf{r}')\cdot\nabla']\delta(\mathbf{r}' - \lambda\mathbf{r})\end{aligned} \tag{A.12}$$

So

$$\begin{aligned}\nabla\chi_{\mathrm{M}}(\mathbf{r}) = -\int \mathrm{d}^3r' \int_0^1 \mathrm{d}\lambda \Big\{ & \mathbf{A}(\mathbf{r}')\delta(\mathbf{r}' - \lambda\mathbf{r}) - \lambda\mathbf{r}\left[\mathbf{A}(\mathbf{r}')\cdot\nabla'\right]\delta(\mathbf{r}' - \lambda\mathbf{r}) \\ & + \lambda\mathbf{r} \times \delta(\mathbf{r}' - \lambda\mathbf{r})\mathbf{B}(\mathbf{r}') - \lambda[\mathbf{r}\cdot\nabla'\delta(\mathbf{r}' - \lambda\mathbf{r})]\mathbf{A}(\mathbf{r}') + \lambda\mathbf{r}[\mathbf{A}(\mathbf{r}')\cdot\nabla']\delta(\mathbf{r}' - \lambda\mathbf{r}) \Big\}\end{aligned} \tag{A.13}$$

The second and final terms cancel out, so we are left with;

$$\begin{aligned}\nabla\chi_{\mathrm{M}}(\mathbf{r}) &= -\int \mathrm{d}^3r' \int_0^1 \mathrm{d}\lambda \left\{ \mathbf{A}(\mathbf{r}')\delta(\mathbf{r}' - \lambda\mathbf{r}) + \lambda\mathbf{r} \times \delta(\mathbf{r}' - \lambda\mathbf{r})\mathbf{B}(\mathbf{r}') - \lambda[\mathbf{r}\cdot\nabla'\delta(\mathbf{r}' - \lambda\mathbf{r})]\mathbf{A}(\mathbf{r}') \right\} \\ &= -\int \mathrm{d}^3r' \int_0^1 \mathrm{d}\lambda \left\{ \mathbf{A}(\mathbf{r}')\left\{\delta(\mathbf{r}' - \lambda\mathbf{r}) - \lambda[\mathbf{r}\cdot\nabla'\delta(\mathbf{r}' - \lambda\mathbf{r})]\right\} + \lambda\mathbf{r} \times \delta(\mathbf{r}' - \lambda\mathbf{r})\mathbf{B}(\mathbf{r}') \right\}\end{aligned} \tag{A.14}$$

Again using the Fourier representation of the delta function, it is straightforward to show that;

$$\int_0^1 \mathrm{d}\lambda \left[\delta(\mathbf{r}' - \lambda\mathbf{r}) - \lambda\mathbf{r}\cdot\nabla'\delta(\mathbf{r}' - \lambda\mathbf{r})\right] = \delta(\mathbf{r}' - \mathbf{r}) \tag{A.15}$$

giving

$$\nabla\chi_{\mathrm{M}}(\mathbf{r}) = -\mathbf{A}(\mathbf{r}) - \int \mathrm{d}^3r' \int_0^1 \mathrm{d}\lambda\, \lambda\mathbf{r} \times \delta(\mathbf{r}' - \lambda\mathbf{r})\mathbf{B}(\mathbf{r}') \tag{A.16}$$

If we now define

$$\boldsymbol{\theta}(\mathbf{r}', \mathbf{r}) = -e\int_0^1 \mathrm{d}\lambda\, \lambda\mathbf{r}\delta(\mathbf{r}' - \lambda\mathbf{r}) \tag{A.17}$$

we are left with;

$$\nabla\chi_{\mathrm{M}}(\mathbf{r}) = \mathbf{A}(\mathbf{r}) + \frac{1}{e}\int \mathrm{d}^3r'\, \boldsymbol{\theta}(\mathbf{r}', \mathbf{r}) \times \mathbf{B}(\mathbf{r}') \tag{A.18}$$

which is Eq. (82) in the main text.

References

[1] X. Fan, T.G. Myers, B.A.D. Sukra, G. Gabrielse, Measurement of the electron magnetic moment, Phys. Rev. Lett. 130 (7) (2023) 071801, http://dx.doi.org/10.1103/PhysRevLett.130.071801.

[2] B. Bazak, J. Kirscher, S. König, M.P. Valderrama, N. Barnea, U. van Kolck, Four-body scale in universal few-boson systems, Phys. Rev. Lett. 122 (14) (2019) 143001, http://dx.doi.org/10.1103/PhysRevLett.122.143001.

[3] M.E. Peskin, D.V. Schroeder, An Introduction to Quantum Field Theory, Avalon Publishing, 1995.

[4] R. Banerjee, D. Chatterjee, Non-relativistic reduction of spinors, new currents and their algebra, Nuclear Phys. B 954 (2020) 114994, http://dx.doi.org/10.1016/j.nuclphysb.2020.114994.

[5] P.W. Milonni, The Quantum Vacuum : An Introduction to Quantum Electrodynamics, Academic Press, San Diego, 1994.

[6] M. Babiker, R. Loudon, Derivation of the Power-Zienau-Woolley Hamiltonian in quantum electrodynamics by gauge transformation, Proc. R. Soc. Lond. Ser. A Math. Phys. Eng. Sci. 385 (1789) (1983) 439–460, http://dx.doi.org/10.1098/rspa.1983.0022.

[7] M.O. Scully, A.A. Svidzinsky, The Lamb shift—yesterday, today, and tomorrow, Science 328 (5983) (2010) 1239–1241, http://dx.doi.org/10.1126/science.1190737.

[8] A.S. Prasad, J. Hinney, S. Mahmoodian, K. Hammerer, S. Rind, P. Schneeweiss, A.S. Sørensen, J. Volz, A. Rauschenbeutel, Correlating photons using the collective nonlinear response of atoms weakly coupled to an optical mode, Nat. Photonics 14 (12) (2020) 719–722, http://dx.doi.org/10.1038/s41566-020-0692-z.

[9] R.W. Boyd, Nonlinear Optics, Academic Press, 2003.

[10] G. Barton, Elements of Green's Functions and Propagation: Potential, Diffusion, and Waves, in: Oxford Science Publications, Clarendon Press, Oxford, 1989.

[11] P. Johansson, Electromagnetic Green's function for layered systems: Applications to nanohole interactions in thin metal films, Phys. Rev. B 83 (19) (2011) 195408, http://dx.doi.org/10.1103/PhysRevB.83.195408.

[12] E.A. Muljarov, Full electromagnetic Green's dyadic of spherically symmetric open optical systems and elimination of static modes from the resonant-state expansion, Phys. Rev. A 101 (5) (2020) 053854, http://dx.doi.org/10.1103/PhysRevA.101.053854.

[13] M. Paulus, P. Gay-Balmaz, O.J.F. Martin, Accurate and efficient computation of the Green's tensor for stratified media, Phys. Rev. E 62 (4) (2000) 5797–5807, http://dx.doi.org/10.1103/PhysRevE.62.5797.

[14] T.G. Philbin, Canonical quantization of macroscopic electromagnetism, New J. Phys. 12 (12) (2010) 123008, http://dx.doi.org/10.1088/1367-2630/12/12/123008.

[15] C.-T. Tai, Dyadic Green's Functions in Electromagnetic Theory, IEEE Press, New York, 1994.

[16] A. Hörl, A. Trügler, U. Hohenester, Full three-dimensonal reconstruction of the dyadic green tensor from electron energy loss spectroscopy of plasmonic nanoparticles, ACS Photonics 2 (10) (2015) 1429–1435, http://dx.doi.org/10.1021/acsphotonics.5b00256.

[17] A. Cerjan, A.D. Stone, Why the laser linewidth is so narrow: A modern perspective, Phys. Scr. 91 (1) (2015) 013003, http://dx.doi.org/10.1088/0031-8949/91/1/013003.

[18] C.M. Bender, S. Boettcher, Real spectra in non-Hermitian Hamiltonians having $\mathscr{P}\mathscr{T}$ symmetry, Phys. Rev. Lett. 80 (24) (1998) 5243–5246, http://dx.doi.org/10.1103/PhysRevLett.80.5243.

[19] R. El-Ganainy, M. Khajavikhan, D.N. Christodoulides, S.K. Ozdemir, The dawn of non-Hermitian optics, Commun. Phys. 2 (1) (2019) 1–5, http://dx.doi.org/10.1038/s42005-019-0130-z.

[20] J.M. Elson, R.H. Ritchie, Photon interactions at a rough metal surface, Phys. Rev. B 4 (12) (1971) 4129–4138, http://dx.doi.org/10.1103/PhysRevB.4.4129.

[21] M. Babiker, G. Barton, Quantum frequency shifts near a plasma surface, J. Phys. A: Math. Gen. 9 (1) (1976) 129–144, http://dx.doi.org/10.1088/0305-4470/9/1/018.

[22] R.J. Glauber, M. Lewenstein, Quantum optics of dielectric media, Phys. Rev. A 43 (1) (1991) 467–491, http://dx.doi.org/10.1103/PhysRevA.43.467.

[23] H. Haken, in: S.M. Kay, A. Maitland (Eds.), Quantum Optics, Academic Press, New York, 1970, p. 201.

[24] J. Gea-Banacloche, N. Lu, L.M. Pedrotti, S. Prasad, M.O. Scully, K. Wódkiewicz, Treatment of the spectrum of squeezing based on the modes of the universe. I. Theory and a physical picture, Phys. Rev. A 41 (1) (1990) 369–380, http://dx.doi.org/10.1103/PhysRevA.41.369.

[25] C.K. Carniglia, L. Mandel, Quantization of evanescent electromagnetic waves, Phys. Rev. D 3 (2) (1971) 280–296, http://dx.doi.org/10.1103/PhysRevD.3.280.

[26] P. Grossel, J.M. Vigoureux, D. Van Labeke, Static dipole moment of an atom or a centrosymmetric molecule near a perfect metallic surface, Phys. Rev. A 28 (2) (1983) 524–531, http://dx.doi.org/10.1103/PhysRevA.28.524.

[27] J.-M. Vigoureux, P. Grossel, D. Van Labeke, C. Girard, Quantum electrodynamics near an interface: Polarizability of a pair of adsorbed molecules, Phys. Rev. A 35 (4) (1987) 1493–1502, http://dx.doi.org/10.1103/PhysRevA.35.1493.

[28] L. Allen, S. Stenholm, Quantum effects at a dielectric interface, Opt. Commun. 93 (3) (1992) 253–264, http://dx.doi.org/10.1016/0030-4018(92)90537-2.

[29] M. Janowicz, W. Żakowicz, Quantum radiation of a harmonic oscillator near the planar dielectric-vacuum interface, Phys. Rev. A 50 (5) (1994) 4350–4364, http://dx.doi.org/10.1103/PhysRevA.50.4350.

[30] R. Gütig, C. Eberlein, Quantum radiation from moving dielectrics in two, three, and more spatial dimensions, J. Phys. A: Math. Gen. 31 (32) (1998) 6819–6838, http://dx.doi.org/10.1088/0305-4470/31/32/006.

[31] C. Eberlein, R. Zietal, Interaction of an atom with layered dielectrics, Phys. Rev. A 82 (6) (2010) 062506, http://dx.doi.org/10.1103/PhysRevA.82.062506.

[32] N. Bartolo, R. Messina, D.A.R. Dalvit, F. Intravaia, Nonequilibrium Casimir-Polder plasmonic interactions, Phys. Rev. A 93 (4) (2016) 042111, http://dx.doi.org/10.1103/PhysRevA.93.042111.

[33] T. Haug, S.Y. Buhmann, R. Bennett, Casimir-Polder potential in the presence of a Fock state, Phys. Rev. A 99 (1) (2019) 012508, http://dx.doi.org/10.1103/PhysRevA.99.012508.

[34] C. Eberlein, D. Robaschik, Quantum electrodynamics near a dielectric half-space, Phys. Rev. D 73 (2) (2006) 025009, http://dx.doi.org/10.1103/PhysRevD.73.025009.

[35] R. Bennett, C. Eberlein, Quantum electrodynamics of a free particle near dispersive dielectric or conducting boundaries, Phys. Rev. A 86 (6) (2012) 062505, http://dx.doi.org/10.1103/PhysRevA.86.062505.

[36] G. Pieplow, C. Henkel, Cherenkov friction on a neutral particle moving parallel to a dielectric, J. Phys. Condens. Matter : Inst. Phys. J. 27 (21) (2015) 214001, http://dx.doi.org/10.1088/0953-8984/27/21/214001.

[37] R. Bennett, C. Eberlein, Magnetic moment of an electron near a surface with dispersion, New J. Phys. 14 (12) (2012) 123035, http://dx.doi.org/10.1088/1367-2630/14/12/123035.

[38] R. Bennett, C. Eberlein, Anomalous magnetic moment of an electron near a dispersive surface, Phys. Rev. A 88 (1) (2013) 012107, http://dx.doi.org/10.1103/PhysRevA.88.012107.

[39] T. Gruner, D.-G. Welsch, Correlation of radiation-field ground-state fluctuations in a dispersive and lossy dielectric, Phys. Rev. A 51 (4) (1995) 3246–3256, http://dx.doi.org/10.1103/PhysRevA.51.3246.
[40] H.T. Dung, L. Knöll, D.-G. Welsch, Three-dimensional quantization of the electromagnetic field in dispersive and absorbing inhomogeneous dielectrics, Phys. Rev. A 57 (5) (1998) 3931–3942, http://dx.doi.org/10.1103/PhysRevA.57.3931.
[41] S. Scheel, S.Y. Buhmann, Macroscopic QED - concepts and applications, Acta Phys. Slovaca 58 (5) (2009) 675–809.
[42] S.Y. Buhmann, Dispersion Forces I - Macroscopic Quantum Electrodynamics and Ground-State Casimir, Casimir-Polder and Van der Waals Forces, Vol. 247, Springer, Berlin, 2012, http://dx.doi.org/10.1007/978-3-642-32484-0.
[43] S.Y. Buhmann, Dispersion Forces II - Many-Body Effects, Excited Atoms, Finite Temperature and Quantum Friction, Vol. 248, Springer, Berlin, 2012, http://dx.doi.org/10.1007/978-3-642-32466-6.
[44] E. Lifshitz, The theory of molecular attractive forces between solids, J. Exp. Theor. Phys. 2 (1) (1956) 73–83.
[45] L.D. Landau, E.M. Lifshitz, Electrodynamics of Continuous Media, Pergamon, 1984.
[46] C. Eberlein, R. Zietal, Quantum electrodynamics near a dispersive and absorbing dielectric, Phys. Rev. A 86 (2) (2012) 022111, http://dx.doi.org/10.1103/PhysRevA.86.022111.
[47] L.G. Suttorp, A.J. van Wonderen, Fano diagonalization of a polariton model for an inhomogeneous absorptive dielectric, Europhys. Lett. 67 (5) (2004) 766, http://dx.doi.org/10.1209/epl/i2004-10131-8.
[48] L.G. Suttorp, M. Wubs, Field quantization in inhomogeneous absorptive dielectrics, Phys. Rev. A 70 (1) (2004) 013816, http://dx.doi.org/10.1103/PhysRevA.70.013816.
[49] H.-P. Breuer, F. Petruccione, The Theory of Open Quantum Systems, Oxford University Press, 2002.
[50] S. Rotter, S. Gigan, Light fields in complex media: Mesoscopic scattering meets wave control, Rev. Modern Phys. 89 (1) (2017) 015005, http://dx.doi.org/10.1103/RevModPhys.89.015005.
[51] O. Zaitsev, L. Deych, Recent developments in the theory of multimode random lasers, J. Opt. 12 (2) (2010) 024001, http://dx.doi.org/10.1088/2040-8978/12/2/024001.
[52] S.M. Dutra, Cavity Quantum Electrodynamics: The Strange Theory of Light in a Box, John Wiley & Sons, 2005.
[53] J.D. Jackson, Classical Electrodynamics, Wiley, 1975.
[54] O.D. Stefano, S. Savasta, R. Girlanda, Microscopic calculation of noise current operators for electromagnetic field quantization in absorbing material systems, J. Opt. B: Quantum Semiclass. Opt. 3 (4) (2001) 288–292, http://dx.doi.org/10.1088/1464-4266/3/4/314.
[55] A. Drezet, Quantizing polaritons in inhomogeneous dissipative systems, Phys. Rev. A 95 (2) (2017) 023831, http://dx.doi.org/10.1103/PhysRevA.95.023831.
[56] V. Dorier, J. Lampart, S. Guérin, H.R. Jauslin, Canonical quantization for quantum plasmonics with finite nanostructures, Phys. Rev. A 100 (4) (2019) 042111, http://dx.doi.org/10.1103/PhysRevA.100.042111.
[57] V. Dorier, S. Guérin, H.-R. Jauslin, Critical review of quantum plasmonic models for finite-size media, Nanophotonics 9 (12) (2020) 3899–3907, http://dx.doi.org/10.1515/nanoph-2020-0061.
[58] G.W. Hanson, F. Lindel, S.Y. Buhmann, S.Y. Buhmann, Langevin noise approach for lossy media and the lossless limit, J. Opt. Soc. Amer. B 38 (3) (2021) 758–768, http://dx.doi.org/10.1364/JOSAB.404295.
[59] S. Scheel, L. Knöll, D.-G. Welsch, QED commutation relations for inhomogeneous Kramers-Kronig dielectrics, Phys. Rev. A 58 (1) (1998) 700–706, http://dx.doi.org/10.1103/PhysRevA.58.700.
[60] T.G. Philbin, Damped vacuum states of light, J. Opt. 18 (9) (2016) 095201, http://dx.doi.org/10.1088/2040-8978/18/9/095201.
[61] A. Asenjo-Garcia, J.D. Hood, D.E. Chang, H.J. Kimble, Atom-light interactions in quasi-one-dimensional nanostructures: A Green's-function perspective, Phys. Rev. A 95 (3) (2017) 033818, http://dx.doi.org/10.1103/PhysRevA.95.033818.
[62] S.J. Masson, A. Asenjo-Garcia, Atomic-waveguide quantum electrodynamics, Phys. Rev. Res. 2 (4) (2020) 043213, http://dx.doi.org/10.1103/PhysRevResearch.2.043213.
[63] J. Klaers, J. Schmitt, F. Vewinger, M. Weitz, Bose-Einstein condensation of photons in an optical microcavity, Nature 468 (7323) (2010) 545–548, http://dx.doi.org/10.1038/nature09567.
[64] J. Franz, R. Bennett, S.Y. Buhmann, Auger decay in dispersing and absorbing environments, Phys. Rev. A 104 (1) (2021) 013103, http://dx.doi.org/10.1103/PhysRevA.104.013103.
[65] S. Saravi, A.N. Poddubny, T. Pertsch, F. Setzpfandt, A.A. Sukhorukov, Atom-mediated spontaneous parametric down-conversion in periodic waveguides, Opt. Lett. 42 (22) (2017) 4724, http://dx.doi.org/10.1364/OL.42.004724.
[66] A. Einstein, Strahlungs-emission und absorption nach der quantentheorie, Dtsch. Phys. Ges. 18 (1916) 318–323.
[67] P.W. Milonni, Why spontaneous emission? Amer. J. Phys. 52 (4) (1984) 340–343, http://dx.doi.org/10.1119/1.13886.
[68] D. Dzsotjan, A.S. Sørensen, M. Fleischhauer, Quantum emitters coupled to surface plasmons of a nanowire: A Green's function approach, Phys. Rev. B 82 (7) (2010) 075427, http://dx.doi.org/10.1103/PhysRevB.82.075427.
[69] V.D. Karanikolas, C.A. Marocico, P.R. Eastham, A.L. Bradley, Near-field relaxation of a quantum emitter to two-dimensional semiconductors: Surface dissipation and exciton polaritons, Phys. Rev. B 94 (19) (2016) 195418, http://dx.doi.org/10.1103/PhysRevB.94.195418.
[70] J. Sakurai, Modern Quantum Mechanics, Addison-Wesley, 1994.
[71] J.M. Zhang, Y. Liu, Fermi's golden rule: Its derivation and breakdown by an ideal model, Eur. J. Phys. 37 (6) (2016) 065406, http://dx.doi.org/10.1088/0143-0807/37/6/065406.
[72] S.Y. Buhmann, L. Knöll, D.-G. Welsch, H.T. Dung, Casimir-Polder forces: A nonperturbative approach, Phys. Rev. A 70 (5) (2004) 052117, http://dx.doi.org/10.1103/PhysRevA.70.052117.
[73] W.E. Lamb, R.C. Retherford, Fine structure of the hydrogen atom by a microwave method, Phys. Rev. 72 (3) (1947) 241–243, http://dx.doi.org/10.1103/PhysRev.72.241.
[74] E.M. Purcell, Spontaneous emission probabilities at radio frequences, Bull. Am. Phys. Soc. 69 (11–12) (1946) 674.
[75] K. Joulain, R. Carminati, J.-P. Mulet, J.-J. Greffet, Definition and measurement of the local density of electromagnetic states close to an interface, Phys. Rev. B 68 (24) (2003) 245405, http://dx.doi.org/10.1103/PhysRevB.68.245405.
[76] L. Novotny, B. Hecht, Principles of Nano-Optics, Cambridge University Press, Cambridge, 2006, http://dx.doi.org/10.1017/CBO9780511813535.
[77] R. Carminati, A. Cazé, D. Cao, F. Peragut, V. Krachmalnicoff, R. Pierrat, Y. De Wilde, Electromagnetic density of states in complex plasmonic systems, Surf. Sci. Rep. 70 (1) (2015) 1–41, http://dx.doi.org/10.1016/j.surfrep.2014.11.001.
[78] W.L. Barnes, S.A.R. Horsley, W.L. Vos, Classical antennas, quantum emitters, and densities of optical states, J. Opt. 22 (7) (2020) 073501, http://dx.doi.org/10.1088/2040-8986/ab7b01.
[79] A. Cazé, R. Pierrat, R. Carminati, Spatial coherence in complex photonic and plasmonic systems, Phys. Rev. Lett. 110 (6) (2013) 063903, http://dx.doi.org/10.1103/PhysRevLett.110.063903.
[80] C. Sauvan, J.P. Hugonin, R. Carminati, P. Lalanne, Modal representation of spatial coherence in dissipative and resonant photonic systems, Phys. Rev. A 89 (4) (2014) 043825, http://dx.doi.org/10.1103/PhysRevA.89.043825.
[81] J. de Rosny, M. Davy, Green's function retrieval and fluctuations of cross density of states in multiple-scattering media, Europhys. Lett. 106 (5) (2014) 54004, http://dx.doi.org/10.1209/0295-5075/106/54004.

[82] R. Carminati, R. Carminati, M. Gurioli, M. Gurioli, Purcell effect with extended sources: The role of the cross density of states, Opt. Express 30 (10) (2022) 16174–16183, http://dx.doi.org/10.1364/OE.454992.
[83] K. Drexhage, Influence of a dielectric interface on fluorescence decay time, J. Lumin. 1–2 (1970) 693–701, http://dx.doi.org/10.1016/0022-2313(70)90082-7.
[84] D. Kleppner, Inhibited spontaneous emission, Phys. Rev. Lett. 47 (4) (1981) 233–236, http://dx.doi.org/10.1103/PhysRevLett.47.233.
[85] P. Goy, J.M. Raimond, M. Gross, S. Haroche, Observation of cavity-enhanced single-atom spontaneous emission, Phys. Rev. Lett. 50 (24) (1983) 1903–1906, http://dx.doi.org/10.1103/PhysRevLett.50.1903.
[86] E. Yablonovitch, Inhibited spontaneous emission in solid-state physics and electronics, Phys. Rev. Lett. 58 (20) (1987) 2059–2062, http://dx.doi.org/10.1103/PhysRevLett.58.2059.
[87] J.M. Gérard, B. Sermage, B. Gayral, B. Legrand, E. Costard, V. Thierry-Mieg, Enhanced spontaneous emission by quantum boxes in a monolithic optical microcavity, Phys. Rev. Lett. 81 (5) (1998) 1110–1113, http://dx.doi.org/10.1103/PhysRevLett.81.1110.
[88] K. Rustomji, R. Abdeddaim, C.M. de Sterke, B. Kuhlmey, S. Enoch, Measurement and simulation of the polarization-dependent Purcell factor in a microwave fishnet metamaterial, Phys. Rev. B 95 (3) (2017) 035156, http://dx.doi.org/10.1103/PhysRevB.95.035156.
[89] K. Rustomji, M. Dubois, P. Jomin, S. Enoch, J. Wenger, C.M. de Sterke, R. Abdeddaim, Complete electromagnetic dyadic green function characterization in a complex environment—resonant dipole-dipole interaction and cooperative effects, Phys. Rev. X 11 (2) (2021) 021004, http://dx.doi.org/10.1103/PhysRevX.11.021004.
[90] F.J. Garcia de Abajo, M. Kociak, Probing the photonic local density of states with electron energy loss spectroscopy, Phys. Rev. Lett. 100 (10) (2008) 106804, http://dx.doi.org/10.1103/PhysRevLett.100.106804.
[91] V. Krachmalnicoff, D. Cao, A. Cazé, E. Castanié, R. Pierrat, N. Bardou, S. Collin, R. Carminati, Y.D. Wilde, Towards a full characterization of a plasmonic nanostructure with a fluorescent near-field probe, Opt. Express 21 (9) (2013) 11536–11545, http://dx.doi.org/10.1364/OE.21.011536.
[92] D. Cao, A. Cazé, M. Calabrese, R. Pierrat, N. Bardou, S. Collin, R. Carminati, V. Krachmalnicoff, Y. De Wilde, Mapping the radiative and the apparent nonradiative local density of states in the near field of a metallic nanoantenna, ACS Photonics 2 (2) (2015) 189–193, http://dx.doi.org/10.1021/ph500431g.
[93] E.J.W. Verwey, J.T.G. Overbeek, K. van Nes, Theory of the Stability of Lyophobic Colloids: The Interaction of Sol Particles Having an Electric Double Layer, Elsevier Publishing Company, 1948.
[94] H.B.G. Casimir, D. Polder, The influence of retardation on the London-van der Waals forces, Phys. Rev. 73 (4) (1948) 360–372, http://dx.doi.org/10.1103/PhysRev.73.360.
[95] M. Könne, R. Bennett, T. Reisinger, S.Y. Buhmann, Impact of dispersion forces on matter-wave scattering near a dielectric disk, Phys. Rev. A 96 (1) (2017) 013626, http://dx.doi.org/10.1103/PhysRevA.96.013626.
[96] R. Higa, J.F. Babb, Few-neutron systems with the long-range Casimir-Polder force, Braz. J. Phys. 51 (2) (2021) 231–237, http://dx.doi.org/10.1007/s13538-020-00849-5.
[97] V.M. Mostepanenko, J.F. Babb, A.O. Caride, G.L. Klimchitskaya, S.I. Zanette, Dependence of the Casimir–Polder interaction between an atom and a cavity wall on atomic and material properties, J. Phys. A: Math. Gen. 39 (21) (2006) 6583–6587, http://dx.doi.org/10.1088/0305-4470/39/21/S57.
[98] A. Salam, Non-Relativistic QED Theory of the Van Der Waals Dispersion Interaction, Springer, 2016.
[99] P.W. Milonni, Casimir forces without the vacuum radiation field, Phys. Rev. A 25 (3) (1982) 1315–1327, http://dx.doi.org/10.1103/PhysRevA.25.1315.
[100] H.B.G. Casimir, On the attraction between two perfectly conducting plates, Proc. K. Ned. Akad. 360 (1948) 793–795, doi:citeulike-article-id:8810715.
[101] P. Barcellona, R. Bennett, S.Y. Buhmann, Lateral interatomic dispersion forces, Phys. Rev. A 102 (2) (2020) 020802, http://dx.doi.org/10.1103/physreva.102.020802.
[102] G. Barton, Frequency shifts near an interface: Inadequacy of two-level atomic models, J. Phys. B: At. Mol. Phys. 7 (16) (1974) 2134–2142, http://dx.doi.org/10.1088/0022-3700/7/16/012.
[103] E.A. Power, T. Thirunamachandran, Quantum electrodynamics in a cavity, Phys. Rev. A 25 (5) (1982) 2473–2484, http://dx.doi.org/10.1103/PhysRevA.25.2473.
[104] J.M. Wylie, J.E. Sipe, Quantum electrodynamics near an interface. II, Phys. Rev. A 32 (4) (1985) 2030–2043, http://dx.doi.org/10.1103/PhysRevA.32.2030.
[105] H. Safari, D.G. Welsch, S.Y. Buhmann, S. Scheel, Van der Waals potentials of paramagnetic atoms, Phys. Rev. A 78 (6) (2008) 062901, http://dx.doi.org/10.1103/PhysRevA.78.062901.
[106] H. Haakh, F. Intravaia, C. Henkel, S. Spagnolo, R. Passante, B. Power, F. Sols, Temperature dependence of the magnetic Casimir-Polder interaction, Phys. Rev. A 80 (6) (2009) 062905, http://dx.doi.org/10.1103/PhysRevA.80.062905.
[107] S.Y. Buhmann, H. Safari, S. Scheel, A. Salam, Body-assisted dispersion potentials of diamagnetic atoms, Phys. Rev. A 87 (1) (2013) 012507, http://dx.doi.org/10.1103/PhysRevA.87.012507.
[108] T. Nakajima, P. Lambropoulos, H. Walther, Level shift and depopulation by blackbody radiation of a Rydberg atom between two metallic plates, Phys. Rev. A 56 (6) (1997) 5100–5110, http://dx.doi.org/10.1103/PhysRevA.56.5100.
[109] S.-T. Wu, C. Eberlein, Quantum electrodynamics of an atom in front of a non–dispersive dielectric half–space. II. Effects of finite temperature, Proc. R. Soc. Lond. Ser. A Math. Phys. Eng. Sci. 456 (2000) (2000) 1931–1951, http://dx.doi.org/10.1098/rspa.2000.0595.
[110] M.-P. Gorza, M. Ducloy, Van der Waals interactions between atoms and dispersive surfaces at finite temperature, Eur. Phys. J. D 40 (3) (2006) 343–356, http://dx.doi.org/10.1140/epjd/e2006-00239-3.
[111] S. Fuchs, S.Y. Buhmann, Purcell-Dicke enhancement of the Casimir-Polder potential, Europhys. Lett. 124 (3) (2018) http://dx.doi.org/10.1209/0295-5075/124/34003.
[112] K. Sinha, B.P. Venkatesh, P. Meystre, Collective effects in Casimir-Polder forces, Phys. Rev. Lett. 121 (18) (2018) 183605, http://dx.doi.org/10.1103/PhysRevLett.121.183605.
[113] A. Laliotis, B.-S. Lu, M. Ducloy, D. Wilkowski, Atom-surface physics: A review, AVS Quantum Sci. 3 (4) (2021) 043501, http://dx.doi.org/10.1116/5.0063701.
[114] C. Eberlein, R. Zietal, Casimir-Polder interaction between a polarizable particle and a plate with a hole, Phys. Rev. A 83 (5) (2011) 052514, http://dx.doi.org/10.1103/PhysRevA.83.052514.
[115] J.L. Hemmerich, R. Bennett, T. Reisinger, S. Nimmrichter, J. Fiedler, H. Hahn, H. Gleiter, S.Y. Buhmann, Impact of Casimir-Polder interaction on Poisson-spot diffraction at a dielectric sphere, Phys. Rev. A 94 (2) (2016) 023621, http://dx.doi.org/10.1103/PhysRevA.94.023621.
[116] H. Bender, C. Stehle, C. Zimmermann, S. Slama, J. Fiedler, S. Scheel, S.Y. Buhmann, V.N. Marachevsky, Probing atom-surface interactions by diffraction of Bose-Einstein condensates, Phys. Rev. X 4 (1) (2014) 011029, http://dx.doi.org/10.1103/PhysRevX.4.011029.
[117] D.A.R. Dalvit, P.A.M. Neto, A. Lambrecht, S. Reynaud, Lateral Casimir–Polder force with corrugated surfaces, J. Phys. A 41 (16) (2008) 164028, http://dx.doi.org/10.1088/1751-8113/41/16/164028.
[118] R. Bennett, D.H.J. O'Dell, Revealing short-range non-Newtonian gravity through Casimir-Polder shielding, New J. Phys. 21 (3) (2019) 033032, http://dx.doi.org/10.1088/1367-2630/ab0ca6.

[119] S. Ribeiro, S. Scheel, Shielding vacuum fluctuations with graphene, Phys. Rev. A 88 (4) (2013) 042519, http://dx.doi.org/10.1103/PhysRevA.88.042519.
[120] D.T. Butcher, S.Y. Buhmann, S. Scheel, Casimir-Polder forces between chiral objects, New J. Phys. 14 (11) (2012) 113013, http://dx.doi.org/10.1088/1367-2630/14/11/113013.
[121] A. Shih, D. Raskin, P. Kusch, Investigation of the interaction potential between a neutral molecule and a conducting surface, Phys. Rev. A 9 (2) (1974) 652–662, http://dx.doi.org/10.1103/PhysRevA.9.652.
[122] D. Raskin, P. Kusch, Interaction between a neutral atomic or molecular beam and a conducting surface, Phys. Rev. 179 (3) (1969) 712–721, http://dx.doi.org/10.1103/PhysRev.179.712.
[123] A. Shih, V.A. Parsegian, Van der Waals forces between heavy alkali atoms and gold surfaces: Comparison of measured and predicted values, Phys. Rev. A 12 (3) (1975) 835–841, http://dx.doi.org/10.1103/PhysRevA.12.835.
[124] D.J. Heinzen, M.S. Feld, Vacuum radiative level shift and spontaneous-emission linewidth of an atom in an optical resonator, Phys. Rev. Lett. 59 (23) (1987) 2623–2626, http://dx.doi.org/10.1103/PhysRevLett.59.2623.
[125] A. Anderson, S. Haroche, E.A. Hinds, W. Jhe, D. Meschede, Measuring the van der Waals forces between a Rydberg atom and a metallic surface, Phys. Rev. A 37 (9) (1988) 3594–3597, http://dx.doi.org/10.1103/PhysRevA.37.3594.
[126] M. Marrocco, M. Weidinger, R.T. Sang, H. Walther, Quantum electrodynamic shifts of Rydberg energy levels between parallel metal plates, Phys. Rev. Lett. 81 (26) (1998) 5784–5787, http://dx.doi.org/10.1103/PhysRevLett.81.5784.
[127] A. Shih, Van der Waals forces between a Cs atom or a CsCl molecule and metal or dielectric surfaces, Phys. Rev. A 9 (4) (1974) 1507–1514, http://dx.doi.org/10.1103/PhysRevA.9.1507.
[128] A. Anderson, S. Haroche, E.A. Hinds, W. Jhe, D. Meschede, L. Moi, Reflection of thermal Cs atoms grazing a polished glass surface, Phys. Rev. A 34 (4) (1986) 3513–3516, http://dx.doi.org/10.1103/PhysRevA.34.3513.
[129] V. Sandoghdar, C.I. Sukenik, E.A. Hinds, S. Haroche, Direct measurement of the van der Waals interaction between an atom and its images in a micron-sized cavity, Phys. Rev. Lett. 68 (23) (1992) 3432–3435, http://dx.doi.org/10.1103/PhysRevLett.68.3432.
[130] R.E. Grisenti, W. Schöllkopf, J.P. Toennies, G.C. Hegerfeldt, T. Köhler, Determination of atom-surface van der Waals potentials from transmission-grating diffraction intensities, Phys. Rev. Lett. 83 (9) (1999) 1755–1758, http://dx.doi.org/10.1103/PhysRevLett.83.1755.
[131] B. Brezger, L. Hackermüller, S. Uttenthaler, J. Petschinka, M. Arndt, A. Zeilinger, Matter-wave interferometer for large molecules, Phys. Rev. Lett. 88 (10) (2002) 100404, http://dx.doi.org/10.1103/PhysRevLett.88.100404.
[132] J.D. Perreault, A.D. Cronin, T.A. Savas, Using atomic diffraction of Na from material gratings to measure atom-surface interactions, Phys. Rev. A 71 (5) (2005) 053612, http://dx.doi.org/10.1103/PhysRevA.71.053612.
[133] J.D. Perreault, A.D. Cronin, Observation of atom wave phase shifts induced by van der Waals atom-surface interactions, Phys. Rev. Lett. 95 (13) (2005) 133201, http://dx.doi.org/10.1103/PhysRevLett.95.133201.
[134] N. Gack, C. Reitz, J.L. Hemmerich, M. Könne, R. Bennett, J. Fiedler, H. Gleiter, S.Y. Buhmann, H. Hahn, T. Reisinger, Signature of short-range van der Waals forces observed in Poisson spot diffraction with indium atoms, Phys. Rev. Lett. 125 (5) (2020) 050401, http://dx.doi.org/10.1103/PhysRevLett.125.050401.
[135] C.I. Sukenik, M.G. Boshier, D. Cho, V. Sandoghdar, E.A. Hinds, Measurement of the Casimir-Polder force, Phys. Rev. Lett. 70 (5) (1993) 560–563, http://dx.doi.org/10.1103/PhysRevLett.70.560.
[136] F. Shimizu, Specular reflection of very slow metastable neon atoms from a solid surface, Phys. Rev. Lett. 86 (6) (2001) 987–990, http://dx.doi.org/10.1103/PhysRevLett.86.987.
[137] V. Druzhinina, M. DeKieviet, Experimental observation of quantum reflection far from threshold, Phys. Rev. Lett. 91 (19) (2003) 193202, http://dx.doi.org/10.1103/PhysRevLett.91.193202.
[138] H. Oberst, Y. Tashiro, K. Shimizu, F. Shimizu, Quantum reflection of He* on silicon, Phys. Rev. A 71 (5) (2005) 052901, http://dx.doi.org/10.1103/PhysRevA.71.052901.
[139] H. Bender, P.W. Courteille, C. Marzok, C. Zimmermann, S. Slama, Direct measurement of intermediate-range Casimir-Polder potentials, Phys. Rev. Lett. 104 (8) (2010) 083201, http://dx.doi.org/10.1103/PhysRevLett.104.083201.
[140] M.A. Wilson, P. Bushev, J. Eschner, F. Schmidt-Kaler, C. Becher, R. Blatt, U. Dorner, Vacuum-field level shifts in a single trapped ion mediated by a single distant mirror, Phys. Rev. Lett. 91 (21) (2003) 213602, http://dx.doi.org/10.1103/PhysRevLett.91.213602.
[141] P. Bushev, A. Wilson, J. Eschner, C. Raab, F. Schmidt-Kaler, C. Becher, R. Blatt, Forces between a single atom and its distant mirror image, Phys. Rev. Lett. 92 (22) (2004) 223602, http://dx.doi.org/10.1103/PhysRevLett.92.223602.
[142] D.M. Harber, J.M. Obrecht, J.M. McGuirk, E.A. Cornell, Measurement of the Casimir-Polder force through center-of-mass oscillations of a Bose-Einstein condensate, Phys. Rev. A 72 (3) (2005) 033610, http://dx.doi.org/10.1103/PhysRevA.72.033610.
[143] J.M. Obrecht, R.J. Wild, M. Antezza, L.P. Pitaevskii, S. Stringari, E.A. Cornell, Measurement of the temperature dependence of the Casimir-Polder force, Phys. Rev. Lett. 98 (6) (2007) 063201, http://dx.doi.org/10.1103/PhysRevLett.98.063201.
[144] A. Laliotis, T.P. De Silans, I. Maurin, M. Ducloy, D. Bloch, Casimir-Polder interactions in the presence of thermally excited surface modes, Nature Commun. 5 (2014) http://dx.doi.org/10.1038/ncomms5364.
[145] C. Garcion, N. Fabre, H. Bricha, F. Perales, S. Scheel, M. Ducloy, G. Dutier, Intermediate-range Casimir-Polder interaction probed by high-order slow atom diffraction, Phys. Rev. Lett. 127 (17) (2021) 170402, http://dx.doi.org/10.1103/PhysRevLett.127.170402.
[146] D.L. Dexter, A theory of sensitized luminescence in solids, J. Chem. Phys. 21 (5) (1953) 836–850, http://dx.doi.org/10.1063/1.1699044.
[147] G.A. Jones, D.S. Bradshaw, Resonance energy transfer: From fundamental theory to recent applications, Front. Phys. 7 (2019) http://dx.doi.org/10.3389/fphy.2019.00100.
[148] G. Cario, J. Franck, Über zerlegung von wasserstoffmolekülen durch angeregte quecksilberatome, Z. Phys. 11 (1) (1922) 161–166, http://dx.doi.org/10.1007/BF01328410.
[149] G. Carlo, Über entstehung wahrer lichtabsorption und scheinbare koppelung von quantensprüngen, Z. Phys. 10 (1) (1922) 185–199, http://dx.doi.org/10.1007/BF01332559.
[150] J. Franck, Einige aus der theorie von Klein und Bosseland zu ziehende folgerungen über fluoreszenz, photochemische prozesse und die elektronenemission glühender körper, Z. Phys. 9 (1) (1922) 259–266, http://dx.doi.org/10.1007/BF01326976.
[151] F. Perrin, La fluorescence des solutions - Induction moléculaire. – polarisation et durée d'émission. – photochimie, Ann. Phys. 10 (12) (1929) 169–275, http://dx.doi.org/10.1051/anphys/192910120169.
[152] T. Forster, Energiewanderung und fluoreszenz, Naturwissenschaften 33 (6) (1946) 166–175, http://dx.doi.org/10.1007/BF00585226.
[153] T. Förster, Zwischenmolekulare energiewanderung und fluoreszenz, Ann. Phys. 437 (1–2) (1948) 55–75, http://dx.doi.org/10.1002/andp.19484370105.
[154] S.A. Latt, H.T. Cheung, E.R. Blout, Energy transfer. A system with relatively fixed donor-acceptor separation, J. Am. Chem. Soc. 87 (1965) 995–1003, http://dx.doi.org/10.1021/ja01083a011.
[155] L. Stryer, R.P. Haugland, Energy transfer: A spectroscopic ruler, Proc. Natl. Acad. Sci. USA 58 (2) (1967) 719–726, http://dx.doi.org/10.1073/pnas.58.2.719.
[156] R.B. Sekar, A. Periasamy, Fluorescence resonance energy transfer (FRET) microscopy imaging of live cell protein localizations, J. Cell Biol. 160 (5) (2003) 629–633, http://dx.doi.org/10.1083/jcb.200210140.

[157] E.A. Jares-Erijman, T.M. Jovin, Imaging molecular interactions in living cells by FRET microscopy, Curr. Opin. Chem. Biol. 10 (5) (2006) 409–416, http://dx.doi.org/10.1016/j.cbpa.2006.08.021.
[158] H. Sahoo, D. Roccatano, A. Hennig, W.M. Nau, A 10-Å spectroscopic ruler applied to short polyprolines, J. Am. Chem. Soc. 129 (31) (2007) 9762–9772, http://dx.doi.org/10.1021/ja072178s.
[159] S. Chatterjee, J.B. Lee, N.V. Valappil, D. Luo, V.M. Menon, Investigating the distance limit of a metal nanoparticle based spectroscopic ruler, Biomed. Opt. Express 2 (6) (2011) 1727–1733, http://dx.doi.org/10.1364/BOE.2.001727.
[160] A. Pietraszewska-Bogiel, T. Gadella, FRET microscopy: From principle to routine technology in cell biology, J. Microsc. 241 (2) (2011) 111–118, http://dx.doi.org/10.1111/j.1365-2818.2010.03437.x.
[161] A. Periasamy, R. Day, Molecular Imaging: FRET Microscopy and Spectroscopy, Elsevier, 2011.
[162] B. Schuler, E.A. Lipman, P.J. Steinbach, M. Kumke, W.A. Eaton, Polyproline and the "spectroscopic ruler" revisited with single-molecule fluorescence, Proc. Natl. Acad. Sci. 102 (8) (2005) 2754–2759, http://dx.doi.org/10.1073/pnas.0408164102.
[163] E. Sobakinskaya, M. Schmidt am Busch, T. Renger, Theory of FRET "spectroscopic ruler" for short distances: Application to polyproline, J. Phys. Chem. B 122 (1) (2018) 54–67, http://dx.doi.org/10.1021/acs.jpcb.7b09535.
[164] A. Niggas, S. Creutzburg, J. Schwestka, B. Wöckinger, T. Gupta, P.L. Grande, D. Eder, J.P. Marques, B.C. Bayer, F. Aumayr, R. Bennett, R.A. Wilhelm, Peeling graphite layer by layer reveals the charge exchange dynamics of ions inside a solid, Commun. Phys. 4 (1) (2021) 180, http://dx.doi.org/10.1038/s42005-021-00686-1.
[165] J.S. Avery, The retarded dipole-dipole interaction in exciton theory, Proc. Phys. Soc. 89 (3) (1966) 677–682, http://dx.doi.org/10.1088/0370-1328/89/3/321.
[166] L. Gomberoff, E.A. Power, The resonance transfer of excitation, Proc. Phys. Soc. 88 (2) (1966) 281–284, http://dx.doi.org/10.1088/0370-1328/88/2/302.
[167] E.A. Power, T. Thirunamachandran, Quantum electrodynamics with nonrelativistic sources. III. Intermolecular interactions, Phys. Rev. A 28 (5) (1983) 2671–2675, http://dx.doi.org/10.1103/PhysRevA.28.2671.
[168] D.L. Andrews, B.S. Sherborne, Resonant excitation transfer: A quantum electrodynamical study, J. Chem. Phys. 86 (7) (1987) 4011–4017, http://dx.doi.org/10.1063/1.451910.
[169] D.L. Andrews, A unified theory of radiative and radiationless molecular energy transfer, Chem. Phys. 135 (2) (1989) 195–201, http://dx.doi.org/10.1016/0301-0104(89)87019-3.
[170] G.J. Daniels, R.D. Jenkins, D.S. Bradshaw, D.L. Andrews, Resonance energy transfer: The unified theory revisited, J. Chem. Phys. 119 (4) (2003) 2264–2274, http://dx.doi.org/10.1063/1.1579677.
[171] R. Grinter, G.A. Jones, Resonance energy transfer: The unified theory via vector spherical harmonics, J. Chem. Phys. 145 (7) (2016) 074107, http://dx.doi.org/10.1063/1.4960732.
[172] D.L. Andrews, G. Juzeliūnas, Intermolecular energy transfer: Retardation effects, J. Chem. Phys. 96 (9) (1992) 6606–6612, http://dx.doi.org/10.1063/1.462599.
[173] D.P. Craig, E.A. Power, T. Thirunamachandran, The interaction of optically active molecules, Proc. R. Soc. Lond. Ser. A Math. Phys. Eng. Sci. 322 (1549) (1971) 165–179, http://dx.doi.org/10.1098/rspa.1971.0061.
[174] D.P. Craig, T. Thirunamachandran, Chiral discrimination in molecular excitation transfer, J. Chem. Phys. 109 (4) (1998) 1259–1263, http://dx.doi.org/10.1063/1.476676.
[175] J.J. Rodriguez, A. Salam, Effect of medium chirality on the rate of resonance energy transfer, J. Phys. Chem. B 115 (18) (2011) 5183–5190, http://dx.doi.org/10.1021/jp105715z.
[176] K. Nasiri Avanaki, W. Ding, G.C. Schatz, Resonance energy transfer in arbitrary media: Beyond the point dipole approximation, J. Phys. Chem. C 122 (51) (2018) 29445–29456, http://dx.doi.org/10.1021/acs.jpcc.8b07407.
[177] A. Salam, A general formula for the rate of resonant transfer of energy between two electric multipole moments of arbitrary order using molecular quantum electrodynamics, J. Chem. Phys. 122 (4) (2005) 044112, http://dx.doi.org/10.1063/1.1830430.
[178] D.P. Craig, T. Thirunamachandran, Third-body mediation of resonance coupling between identical molecules, Chem. Phys. 135 (1) (1989) 37–48, http://dx.doi.org/10.1016/0301-0104(89)87004-1.
[179] A. Salam, Mediation of resonance energy transfer by a third molecule, J. Chem. Phys. 136 (1) (2012) 014509, http://dx.doi.org/10.1063/1.3673779.
[180] G.J. Daniels, D.L. Andrews, The electronic influence of a third body on resonance energy transfer, J. Chem. Phys. 116 (15) (2002) 6701–6712, http://dx.doi.org/10.1063/1.1461819.
[181] C. Abeywickrama, M. Premaratne, S.D. Gunapala, D.L. Andrews, Impact of a charged neighboring particle on Förster resonance energy transfer (FRET), J. Phys.: Condens. Matter 32 (9) (2020) 095305, http://dx.doi.org/10.1088/1361-648X/ab577a.
[182] D.L. Andrews, J.S. Ford, Resonance energy transfer: Influence of neighboring matter absorbing in the wavelength region of the acceptor, J. Chem. Phys. 139 (1) (2013) 014107, http://dx.doi.org/10.1063/1.4811793.
[183] D. Weeraddana, M. Premaratne, D.L. Andrews, Direct and third-body mediated resonance energy transfer in dimensionally constrained nanostructures, Phys. Rev. B 92 (3) (2015) 035128, http://dx.doi.org/10.1103/PhysRevB.92.035128.
[184] J.S. Ford, A. Salam, G.A. Jones, A quantum electrodynamics description of quantum coherence and damping in condensed-phase energy transfer, J. Phys. Chem. Lett. 10 (18) (2019) 5654–5661, http://dx.doi.org/10.1021/acs.jpclett.9b02183.
[185] D. Green, G.A. Jones, A. Salam, Polariton mediated resonance energy transfer in a fluid, J. Chem. Phys. 153 (3) (2020) 034111, http://dx.doi.org/10.1063/5.0011562.
[186] J.S. Ford, D.L. Andrews, Geometrical effects on resonance energy transfer between orthogonally-oriented chromophores, mediated by a nearby polarisable molecule, Chem. Phys. Lett. 591 (2014) 88–92, http://dx.doi.org/10.1016/j.cplett.2013.11.002.
[187] A. Salam, Near-zone mediation of RET by one and two proximal particles, J. Phys. Chem. A 123 (13) (2019) 2853–2860, http://dx.doi.org/10.1021/acs.jpca.9b00827.
[188] M.C. Waller, R. Bennett, Environment-modified three-body energy transfer, 2022, http://dx.doi.org/10.48550/arXiv.2206.03790, arXiv:2206.03790.
[189] G. Juzeliūnas, D.L. Andrews, Quantum electrodynamics of resonant energy transfer in condensed matter, Phys. Rev. B 49 (13) (1994) 8751–8763, http://dx.doi.org/10.1103/PhysRevB.49.8751.
[190] J.I. Gersten, A. Nitzan, Photophysics and photochemistry near surfaces and small particles, Surf. Sci. 158 (1) (1985) 165–189, http://dx.doi.org/10.1016/0039-6028(85)90293-6.
[191] S.D. Druger, S. Arnold, L.M. Folan, Theory of enhanced energy transfer between molecules embedded in spherical dielectric particles, J. Chem. Phys. 87 (5) (1987) 2649–2659, http://dx.doi.org/10.1063/1.453103.
[192] P.T. Leung, K. Young, Theory of enhanced energy tranfer in an aerosol particle, J. Chem. Phys. 89 (5) (1988) 2894–2899, http://dx.doi.org/10.1063/1.454994.
[193] V.V. Klimov, V.S. Letokhov, Resonance interaction between two atomic dipoles separated by the surface of a dielectric nanosphere, Phys. Rev. A 58 (4) (1998) 3235–3247, http://dx.doi.org/10.1103/PhysRevA.58.3235.

[194] T. Kobayashi, Q. Zheng, T. Sekiguchi, Resonant dipole-dipole interaction in a cavity, Phys. Rev. A 52 (4) (1995) 2835–2846, http://dx.doi.org/10.1103/PhysRevA.52.2835.
[195] T. Kobayashi, Q. Zheng, T. Sekiguchi, Resonance transfer of excitation for molecules between mirrors, Phys. Lett. A 199 (1) (1995) 21–26, http://dx.doi.org/10.1016/0375-9601(95)00028-2.
[196] M. Cho, R.J. Silbey, Excitation transfer in the vicinity of a dielectric surface, Chem. Phys. Lett. 242 (3) (1995) 291–296, http://dx.doi.org/10.1016/0009-2614(95)00737-O.
[197] H.T. Dung, L. Knöll, D.-G. Welsch, Intermolecular energy transfer in the presence of dispersing and absorbing media, Phys. Rev. A 65 (4) (2002) 043813, http://dx.doi.org/10.1103/PhysRevA.65.043813.
[198] D.L. Andrews, T. Thirunamachandran, On three-dimensional rotational averages, J. Chem. Phys. 67 (11) (1977) 5026–5033, http://dx.doi.org/10.1063/1.434725.
[199] K. Rustomji, M. Dubois, B. Kuhlmey, C.M. de Sterke, S. Enoch, R. Abdeddaim, J. Wenger, Direct imaging of the energy-transfer enhancement between two dipoles in a photonic cavity, Phys. Rev. X 9 (1) (2019) 011041, http://dx.doi.org/10.1103/PhysRevX.9.011041.
[200] Y.-C. Wei, M.-W. Lee, P.-T. Chou, G.D. Scholes, G.C. Schatz, L.-Y. Hsu, Can nanocavities significantly enhance resonance energy transfer in a single donor–acceptor pair? J. Phys. Chem. C 125 (33) (2021) 18119–18128, http://dx.doi.org/10.1021/acs.jpcc.1c04623.
[201] D. Martín-Cano, L. Martín-Moreno, F.J. García-Vidal, E. Moreno, Resonance energy transfer and superradiance mediated by plasmonic nanowaveguides, Nano Lett. 10 (8) (2010) 3129–3134, http://dx.doi.org/10.1021/nl101876f.
[202] A. Poudel, X. Chen, M.A. Ratner, Enhancement of resonant energy transfer due to an evanescent wave from the metal, J. Phys. Chem. Lett. 7 (6) (2016) 955–960, http://dx.doi.org/10.1021/acs.jpclett.6b00119.
[203] Y. Choi, Y. Park, T. Kang, L.P. Lee, Selective and sensitive detection of metal ions by plasmonic resonance energy transfer-based nanospectroscopy, Nature Nanotechnol. 4 (11) (2009) 742–746, http://dx.doi.org/10.1038/nnano.2009.258.
[204] J. Bohlen, Á. Cuartero-González, E. Pibiri, D. Ruhlandt, A.I. Fernández-Domínguez, P. Tinnefeld, G.P. Acuna, Plasmon-assisted Förster resonance energy transfer at the single-molecule level in the moderate quenching regime, Nanoscale 11 (16) (2019) 7674–7681, http://dx.doi.org/10.1039/C9NR01204D.
[205] L.M. Folan, S. Arnold, S.D. Druger, Enhanced energy transfer within a microparticle, Chem. Phys. Lett. 118 (3) (1985) 322–327, http://dx.doi.org/10.1016/0009-2614(85)85324-0.
[206] P. Andrew, W.L. Barnes, Förster energy transfer in an optical microcavity, Science 290 (5492) (2000) 785–788, http://dx.doi.org/10.1126/science.290.5492.785.
[207] D.J. Roth, M.E. Nasir, P. Ginzburg, P. Wang, A. Le Marois, K. Suhling, D. Richards, A.V. Zayats, Förster resonance energy transfer inside hyperbolic metamaterials, ACS Photonics 5 (11) (2018) 4594–4603, http://dx.doi.org/10.1021/acsphotonics.8b01083.
[208] J. Yu, M. Sharma, S. Delikanli, M.D. Birowosuto, H.V. Demir, C. Dang, Mutual energy transfer in a binary colloidal quantum well complex, J. Phys. Chem. Lett. 10 (17) (2019) 5193–5199, http://dx.doi.org/10.1021/acs.jpclett.9b01939.
[209] M. Lunz, V.A. Gerard, Y.K. Gun'ko, V. Lesnyak, N. Gaponik, A.S. Susha, A.L. Rogach, A.L. Bradley, Surface plasmon enhanced energy transfer between donor and acceptor CdTe nanocrystal quantum dot monolayers, Nano Lett. 11 (8) (2011) 3341–3345, http://dx.doi.org/10.1021/nl201714y.
[210] M. Sanz-Paz, J. Wenger, N.F. van Hulst, M. Mivelle, M.F. Garcia-Parajo, Nanoscale control of single molecule Förster resonance energy transfer by a scanning photonic nanoantenna, Nanophotonics 9 (12) (2020) 4021–4031, http://dx.doi.org/10.1515/nanoph-2020-0221.
[211] N. Aissaoui, K. Moth-Poulsen, M. Käll, P. Johansson, L.M. Wilhelmsson, B. Albinsson, FRET enhancement close to gold nanoparticles positioned in DNA origami constructs, Nanoscale 9 (2) (2017) 673–683, http://dx.doi.org/10.1039/C6NR04852H.
[212] N.T. Anderson, S. Ren, J. Chao, P.H. Dinolfo, X. Wang, Exploiting plasmon-mediated energy transfer to enhance end-to-end efficiency in a DNA origami energy transfer array, ACS Appl. Nano Mater. 2 (9) (2019) 5563–5572, http://dx.doi.org/10.1021/acsanm.9b01137.
[213] L.S. Cederbaum, J. Zobeley, F. Tarantelli, Giant intermolecular decay and fragmentation of clusters, Phys. Rev. Lett. 79 (24) (1997) 4778–4781, http://dx.doi.org/10.1103/PhysRevLett.79.4778.
[214] F.M. Penning, Über ionisation durch metastabile atome, Naturwissenschaften 15 (40) (1927) 818, http://dx.doi.org/10.1007/BF01505431.
[215] T. Jahnke, U. Hergenhahn, B. Winter, R. Dörner, U. Frühling, P.V. Demekhin, K. Gokhberg, L.S. Cederbaum, A. Ehresmann, A. Knie, A. Dreuw, Interatomic and intermolecular Coulombic decay, Chem. Rev. 120 (20) (2020) 11295–11369, http://dx.doi.org/10.1021/acs.chemrev.0c00106.
[216] R. Thissen, P. Lablanquie, R. Hall, M. Ukai, K. Ito, Photoionization of argon, krypton and xenon clusters in the inner valence shell region, Eur. Phys. J. D 4 (3) (1998) 335–342, http://dx.doi.org/10.1007/s100530050217.
[217] T.D. Thomas, C. Miron, K. Wiesner, P. Morin, T.X. Carroll, L.J. Sæthre, Anomalous natural linewidth in the 2p photoelectron spectrum of SiF_4, Phys. Rev. Lett. 89 (22) (2002) 223001, http://dx.doi.org/10.1103/PhysRevLett.89.223001.
[218] S. Marburger, O. Kugeler, U. Hergenhahn, T. Möller, Experimental evidence for interatomic Coulombic decay in Ne clusters, Phys. Rev. Lett. 90 (20) (2003) 203401, http://dx.doi.org/10.1103/PhysRevLett.90.203401.
[219] M. Mucke, M. Braune, S. Barth, M. Förstel, T. Lischke, V. Ulrich, T. Arion, U. Becker, A. Bradshaw, U. Hergenhahn, A hitherto unrecognized source of low-energy electrons in water, Nat. Phys. 6 (2) (2010) 143–146, http://dx.doi.org/10.1038/nphys1500.
[220] T. Jahnke, H. Sann, T. Havermeier, K. Kreidi, C. Stuck, M. Meckel, M. Schöffler, N. Neumann, R. Wallauer, S. Voss, A. Czasch, O. Jagutzki, A. Malakzadeh, F. Afaneh, T. Weber, H. Schmidt-Böcking, R. Dörner, Ultrafast energy transfer between water molecules, Nat. Phys. 6 (2) (2010) 139–142, http://dx.doi.org/10.1038/nphys1498.
[221] K. Gokhberg, P. Kolorenč, A.I. Kuleff, L.S. Cederbaum, Site- and energy-selective slow-electron production through intermolecular Coulombic decay, Nature 505 (2014) 661–663, http://dx.doi.org/10.1038/nature12936.
[222] B. Boudaiffa, P. Cloutier, D. Hunting, M.A. Huels, L. Sanche, Resonant formation of DNA strand breaks by low-energy (3 to 20 eV) electrons, Science 287 (5458) (2000) 1658–1660.
[223] P. Zhang, C. Perry, T.T. Luu, D. Matselyukh, H.J. Wörner, Intermolecular Coulombic decay in liquid water, Phys. Rev. Lett. 128 (13) (2022) 133001, http://dx.doi.org/10.1103/PhysRevLett.128.133001.
[224] P.H.P. Harbach, M. Schneider, S. Faraji, A. Dreuw, Intermolecular Coulombic decay in biology: The initial electron detachment from $FADH^-$ in DNA photolyases, J. Phys. Chem. Lett. 4 (6) (2013) 943–949, http://dx.doi.org/10.1021/jz400104h.
[225] V. Averbukh, I.B. Müller, L.S. Cederbaum, Mechanism of interatomic Coulombic decay in clusters, Phys. Rev. Lett. 93 (26) (2004) 263002, http://dx.doi.org/10.1103/PhysRevLett.93.263002.
[226] J.L. Hemmerich, R. Bennett, S.Y. Buhmann, The influence of retardation and dielectric environments on interatomic Coulombic decay, Nature Commun. 9 (1) (2018) 2934, http://dx.doi.org/10.1038/s41467-018-05091-x.
[227] T. Miteva, S. Kazandjian, P. Kolorenč, P. Votavová, N. Sisourat, Interatomic Coulombic decay mediated by ultrafast superexchange energy transfer, Phys. Rev. Lett. 119 (8) (2017) 083403, http://dx.doi.org/10.1103/PhysRevLett.119.083403.
[228] R. Bennett, P. Votavová, P. Kolorenč, T. Miteva, N. Sisourat, S.Y. Buhmann, Virtual photon approximation for three-body interatomic Coulombic decay, Phys. Rev. Lett. 122 (15) (2019) 153401, http://dx.doi.org/10.1103/PhysRevLett.122.153401.
[229] S. Kazandjian, J. Rist, M. Weller, F. Wiegandt, D. Aslitürk, S. Grundmann, M. Kircher, G. Nalin, D. Pitters, I. Vela Pérez, M. Waitz, G. Schiwietz, B. Griffin, J.B. Williams, R. Dörner, M. Schöffler, T. Miteva, F. Trinter, T. Jahnke, N. Sisourat, Frustrated Coulomb explosion of small helium clusters, Phys. Rev. A 98 (5) (2018) 050701, http://dx.doi.org/10.1103/PhysRevA.98.050701.

[230] C. Hoffmeister, C. Müller, A.B. Voitkiv, Resonant interatomic Coulombic decay in a laser field, Phys. Rev. A 105 (4) (2022) 042803, http://dx.doi.org/10.1103/PhysRevA.105.042803.
[231] J.D. Asmussen, R. Michiels, U. Bangert, N. Sisourat, M. Binz, L. Bruder, M. Danailov, M. Di Fraia, R. Feifel, L. Giannessi, O. Plekan, K.C. Prince, R.J. Squibb, D. Uhl, A. Wituschek, M. Zangrando, C. Callegari, F. Stienkemeier, M. Mudrich, Time-resolved ultrafast interatomic Coulombic decay in superexcited sodium-doped helium nanodroplets, J. Phys. Chem. Lett. 13 (20) (2022) 4470–4478, http://dx.doi.org/10.1021/acs.jpclett.2c00645.
[232] W. Chew, Waves and Fields in Inhomogeneous Media, IEEE Press, New York, 1995.
[233] T.M. Søndergaard, Green's Function Integral Equation Methods in Nano-Optics, CRC Press, Boca Raton, 2019, http://dx.doi.org/10.1201/9781351260206.
[234] D.L. Mills, A.A. Maradudin, Surface roughness and the optical properties of a semi-infinite material; the effect of a dielectric overlayer, Phys. Rev. B 12 (8) (1975) 2943–2958, http://dx.doi.org/10.1103/PhysRevB.12.2943.
[235] C.E. Reed, J. Giergiel, J.C. Hemminger, S. Ushioda, Dipole radiation in a multilayer geometry, Phys. Rev. B 36 (9) (1987) 4990–5000, http://dx.doi.org/10.1103/PhysRevB.36.4990.
[236] M.S. Tomaš, Green function for multilayers: Light scattering in planar cavities, Phys. Rev. A 51 (3) (1995) 2545–2559, http://dx.doi.org/10.1103/PhysRevA.51.2545.
[237] M.-S. Tomaš, Recursion relations for generalized Fresnel coefficients: Casimir force in a planar cavity, Phys. Rev. A 81 (4) (2010) 044104, http://dx.doi.org/10.1103/PhysRevA.81.044104.
[238] Z. Xiang, Y. Lu, Electromagnetic dyadic Green's function in cylindrically multilayered media, IEEE Trans. Microw. Theory Tech. 44 (4) (1996) 614–621, http://dx.doi.org/10.1109/22.491029.
[239] L.-W. Li, M.-S. Leong, T.-S. Yeo, P.-S. Kooi, Electromagnetic dyadic Green's functions in spectral domain for multilayered cylinders, J. Electromagn. Waves Appl. 14 (7) (2000) 961–985, http://dx.doi.org/10.1163/156939300X00086.
[240] L.-W. Li, P.-S. Kooi, M.-S. Leong, T.-S. Yee, Electromagnetic dyadic Green's function in spherically multilayered media, IEEE Trans. Microw. Theory Tech. 42 (12) (1994) 2302–2310, http://dx.doi.org/10.1109/22.339756.
[241] G. Bimonte, T. Emig, R.L. Jaffe, M. Kardar, Casimir forces beyond the proximity approximation, Europhys. Lett. 97 (5) (2012) 50001, http://dx.doi.org/10.1209/0295-5075/97/50001.
[242] NIST Digital Library of Mathematical Functions (http://dlmf.nist.gov/), http://dlmf.nist.gov/, Release 1.1.6 of 2022-06-30.
[243] W.R. Inc., Mathematica, Version 13.2, Champaign, IL, 2022, URL https://www.wolfram.com/mathematica.
[244] G. Tyras, Radiation and Propagation of Electromagnetic Waves, Academic Press, 1969.
[245] A. Kwan, J. Dudley, E. Lantz, Who really discovered Snell's law? Phys. World 15 (4) (2002) 64, http://dx.doi.org/10.1088/2058-7058/15/4/44.
[246] M.S. Mahoney, The Mathematical Career of Pierre de Fermat, 1601-1665: Second Edition, Princeton University Press, 2018.
[247] M. Born, Quantenmechanik der stoßvorgänge, Z. Phys. 38 (11) (1926) 803–827, http://dx.doi.org/10.1007/BF01397184.
[248] F.J. Dyson, The radiation theories of tomonaga, schwinger, and feynman, Phys. Rev. 75 (3) (1949) 486–502, http://dx.doi.org/10.1103/PhysRev.75.486.
[249] B.A. Lippmann, J. Schwinger, Variational principles for scattering processes. I, Phys. Rev. 79 (3) (1950) 469–480, http://dx.doi.org/10.1103/PhysRev.79.469.
[250] S.Y. Buhmann, D.-G. Welsch, Born expansion of the Casimir-Polder interaction of a ground-state atom with dielectric bodies, Appl. Phys. B 82 (2) (2006) 189–201, http://dx.doi.org/10.1007/s00340-005-2055-3.
[251] R.E. Kleinman, G.F. Roach, P.M. van den Berg, Convergent Born series for large refractive indices, J. Opt. Soc. Amer. A 7 (5) (1990) 890–897, http://dx.doi.org/10.1364/JOSAA.7.000890.
[252] K. Kilgore, S. Moskow, J.C. Schotland, Convergence of the Born and inverse Born series for electromagnetic scattering, Appl. Anal. 96 (10) (2017) 1737–1748, http://dx.doi.org/10.1080/00036811.2017.1292349.
[253] B. Krüger, T. Brenner, A. Kienle, Solution of the inhomogeneous Maxwell's equations using a Born series, Opt. Express 25 (21) (2017) 25165–25182, http://dx.doi.org/10.1364/OE.25.025165.
[254] N.A. Ustimenko, D.F. Kornovan, K.V. Baryshnikova, A.B. Evlyukhin, M.I. Petrov, Multipole Born series approach to light scattering by Mie-resonant nanoparticle structures, J. Opt. 24 (3) (2022) 035603, http://dx.doi.org/10.1088/2040-8986/ac4a21.
[255] K. Kilgore, S. Moskow, J.C. Schotland, Convergence of the Born and inverse Born series for electromagnetic scattering, Appl. Anal. 96 (10) (2017) 1737–1748, http://dx.doi.org/10.1080/00036811.2017.1292349.
[256] R. Bennett, Born-series approach to the calculation of Casimir forces, Phys. Rev. A 89 (6) (2014) 062512, http://dx.doi.org/10.1103/PhysRevA.89.062512.
[257] H.T. Dung, S.Y. Buhmann, D.-G. Welsch, Local-field correction to the spontaneous decay rate of atoms embedded in bodies of finite size, Phys. Rev. A 74 (2) (2006) 023803, http://dx.doi.org/10.1103/PhysRevA.74.023803.
[258] A. Sambale, S.Y. Buhmann, D.-G. Welsch, M.-S. Tomaš, Local-field correction to one- and two-atom van der Waals interactions, Phys. Rev. A 75 (4) (2007) 042109, http://dx.doi.org/10.1103/PhysRevA.75.042109.
[259] S.Y. Buhmann, H. Safari, D.-G. Welsch, H.T. Dung, Microscopic origin of Casimir-Polder forces, Open Syst. Inf. Dyn. 13 (4) (2006) 427–436, http://dx.doi.org/10.1007/s11080-006-9024-0.
[260] F.A. Burger, J. Fiedler, S.Y. Buhmann, Zero-point electromagnetic stress tensor for studying Casimir forces on colloidal particles in media, Europhys. Lett. 121 (2) (2018) 24004, http://dx.doi.org/10.1209/0295-5075/121/24004.
[261] T.A. Nguyen, H.T. Dung, Spontaneous decay of an excited atom placed near a rectangular plate, Eur. Phys. J. D 46 (1) (2008) 173–177, http://dx.doi.org/10.1140/epjd/e2007-00268-4.
[262] R. Bennett, Spontaneous decay rate and Casimir-Polder potential of an atom near a lithographed surface, Phys. Rev. A 92 (2) (2015) 022503, http://dx.doi.org/10.1103/PhysRevA.92.022503.
[263] H.T. Dung, T.M. Hien, Atomic spontaneous decay near a finite-length dielectric cylinder, Opt. Commun. 355 (2015) 27–32, http://dx.doi.org/10.1016/j.optcom.2015.06.019.
[264] N. Dung Chinh, Van der Waals interaction of an atom near a fiber tip, Eur. Phys. J. D 72 (9) (2018) 164, http://dx.doi.org/10.1140/epjd/e2018-90113-0.
[265] R. Golestanian, Casimir-Lifshitz interaction between dielectrics of arbitrary geometry: A dielectric contrast perturbation theory, Phys. Rev. A 80 (1) (2009) 012519, http://dx.doi.org/10.1103/PhysRevA.80.012519.
[266] A. Azari, H.S. Samanta, R. Golestanian, Casimir–Lifshitz interaction between dielectric heterostructures, New J. Phys. 11 (9) (2009) 093023, http://dx.doi.org/10.1088/1367-2630/11/9/093023.
[267] A. Azari, M. Miri, R. Golestanian, Effect of the heterogeneity of metamaterials on the Casimir-Lifshitz interaction, Phys. Rev. A 82 (3) (2010) 032512, http://dx.doi.org/10.1103/PhysRevA.82.032512.
[268] R. Bennett, S.Y. Buhmann, Inverse design of light–matter interactions in macroscopic QED, New J. Phys. 22 (9) (2020) 093014, http://dx.doi.org/10.1088/1367-2630/abac3a.
[269] F. Sun, B. Zheng, H. Chen, W. Jiang, S. Guo, Y. Liu, Y. Ma, S. He, Transformation optics: From classic theory and applications to its new branches, Laser Photonics Rev. 11 (6) (2017) 1700034, http://dx.doi.org/10.1002/lpor.201700034.
[270] W. Thomson, Extracts of two letters to Mr. Liouville, J. Math. Pures Appl. 12 (1845) 256.

[271] P. Barcellona, R. Bennett, S.Y. Buhmann, Manipulating the Coulomb interaction: A Green's function perspective, J. Phys. Commun. 2 (3) (2018) 035027, http://dx.doi.org/10.1088/2399-6528/aaa70a.
[272] R. de Melo e Souza, W.J.M. Kort-Kamp, C. Sigaud, C. Farina, Image method in the calculation of the van der Waals force between an atom and a conducting surface, Amer. J. Phys. 81 (5) (2013) 366–376, http://dx.doi.org/10.1119/1.4798548.
[273] C. Eberlein, R. Zietal, Exact dispersion-force potentials: Interaction of an atom with a conductor-patched dielectric surface, Phys. Rev. A 86 (5) (2012) 052522, http://dx.doi.org/10.1103/PhysRevA.86.052522.
[274] P.P. Abrantes, Y. França, F.S.S. da Rosa, C. Farina, R. de Melo e Souza, Repulsive van der Waals interaction between a quantum particle and a conducting toroid, Phys. Rev. A 98 (1) (2018) 012511, http://dx.doi.org/10.1103/PhysRevA.98.012511.
[275] A.W. Rodriguez, M.T.H. Reid, J. Varela, J.D. Joannopoulos, F. Capasso, S.G. Johnson, Anomalous near-field heat transfer between a cylinder and a perforated surface, Phys. Rev. Lett. 110 (1) (2013) 014301, http://dx.doi.org/10.1103/PhysRevLett.110.014301.
[276] G.H. Low, P.F. Herskind, I.L. Chuang, Finite-geometry models of electric field noise from patch potentials in ion traps, Phys. Rev. A 84 (5) (2011) 053425, http://dx.doi.org/10.1103/PhysRevA.84.053425.
[277] Y. Romach, T. Wasserman, S. Tishby, N. Bar-Gill, Long-range magnetic dipole-dipole interaction mediated by a superconductor, Phys. Rev. Res. 3 (3) (2021) 033280, http://dx.doi.org/10.1103/PhysRevResearch.3.033280.
[278] R. De Melo E Souza, W.J.M. Kort-Kamp, C. Sigaud, C. Farina, Sommerfeld's image method in the calculation of van der Waals forces, Int. J. Mod. Phys.: Conf. Ser. 14 (2012) 281–290, http://dx.doi.org/10.1142/S2010194512007404.
[279] H.M. Lai, P.T. Leung, K. Young, P.W. Barber, S.C. Hill, Time-independent perturbation for leaking electromagnetic modes in open systems with application to resonances in microdroplets, Phys. Rev. A 41 (9) (1990) 5187–5198, http://dx.doi.org/10.1103/PhysRevA.41.5187.
[280] E.S.C. Ching, P.T. Leung, A. Maassen van den Brink, W.M. Suen, S.S. Tong, K. Young, Quasinormal-mode expansion for waves in open systems, Rev. Modern Phys. 70 (4) (1998) 1545–1554, http://dx.doi.org/10.1103/RevModPhys.70.1545.
[281] R.-C. Ge, P.T. Kristensen, J.F. Young, S. Hughes, Quasinormal mode approach to modelling light-emission and propagation in nanoplasmonics, New J. Phys. 16 (11) (2014) 113048, http://dx.doi.org/10.1088/1367-2630/16/11/113048.
[282] S. Franke, S. Hughes, M.K. Dezfouli, P.T. Kristensen, K. Busch, A. Knorr, M. Richter, Quantization of quasinormal modes for open cavities and plasmonic cavity quantum electrodynamics, Phys. Rev. Lett. 122 (21) (2019) 213901, http://dx.doi.org/10.1103/PhysRevLett.122.213901.
[283] S. Franke, J. Ren, S. Hughes, M. Richter, Fluctuation-dissipation theorem and fundamental photon commutation relations in lossy nanostructures using quasinormal modes, Phys. Rev. Res. 2 (3) (2020) 033332, http://dx.doi.org/10.1103/PhysRevResearch.2.033332.
[284] P.Y. Chen, D.J. Bergman, Y. Sivan, Generalizing normal mode expansion of electromagnetic Green's tensor to open systems, Phys. Rev. A 11 (4) (2019) 044018, http://dx.doi.org/10.1103/PhysRevApplied.11.044018.
[285] P.T. Leung, S.Y. Liu, K. Young, Completeness and orthogonality of quasinormal modes in leaky optical cavities, Phys. Rev. A 49 (4) (1994) 3057–3067, http://dx.doi.org/10.1103/PhysRevA.49.3057.
[286] P.T. Leung, K.M. Pang, Completeness and time-independent perturbation of morphology-dependent resonances in dielectric spheres, J. Opt. Soc. Amer. B 13 (5) (1996) 805–817, http://dx.doi.org/10.1364/JOSAB.13.000805.
[287] T. Christopoulos, O. Tsilipakos, O. Tsilipakos, E.E. Kriezis, Perturbation theory for Kerr nonlinear leaky cavities, Opt. Lett. 45 (23) (2020) 6442–6445, http://dx.doi.org/10.1364/OL.408336.
[288] J. Ren, S. Franke, S. Hughes, Quasinormal modes, local density of states, and classical purcell factors for coupled loss-gain resonators, Phys. Rev. X 11 (4) (2021) 041020, http://dx.doi.org/10.1103/PhysRevX.11.041020.
[289] P.T. Leung, S.Y. Liu, S.S. Tong, K. Young, Time-independent perturbation theory for quasinormal modes in leaky optical cavities, Phys. Rev. A 49 (4) (1994) 3068–3073, http://dx.doi.org/10.1103/PhysRevA.49.3068.
[290] C. Sauvan, J.P. Hugonin, I.S. Maksymov, P. Lalanne, Theory of the spontaneous optical emission of nanosize photonic and plasmon resonators, Phys. Rev. Lett. 110 (23) (2013) 237401, http://dx.doi.org/10.1103/PhysRevLett.110.237401.
[291] P. Lalanne, W. Yan, K. Vynck, C. Sauvan, J.-P. Hugonin, Light interaction with photonic and plasmonic resonances, Laser Photonics Rev. 12 (5) (2018) 1700113, http://dx.doi.org/10.1002/lpor.201700113.
[292] C. Tao, J. Zhu, Y. Zhong, H. Liu, Coupling theory of quasinormal modes for lossy and dispersive plasmonic nanoresonators, Phys. Rev. B 102 (4) (2020) 045430, http://dx.doi.org/10.1103/PhysRevB.102.045430.
[293] M.B. Doost, W. Langbein, E.A. Muljarov, Resonant state expansion applied to two-dimensional open optical systems, Phys. Rev. A 87 (4) (2013) 043827, http://dx.doi.org/10.1103/PhysRevA.87.043827.
[294] M.B. Doost, W. Langbein, E.A. Muljarov, Resonant-state expansion applied to three-dimensional open optical systems, Phys. Rev. A 90 (1) (2014) 013834, http://dx.doi.org/10.1103/PhysRevA.90.013834.
[295] K. Yee, Numerical solution of initial boundary value problems involving Maxwell's equations in isotropic media, IEEE Trans. Antennas and Propagation 14 (3) (1966) 302–307, http://dx.doi.org/10.1109/TAP.1966.1138693.
[296] B. Gallinet, J. Butet, O.J.F. Martin, Numerical methods for nanophotonics: Standard problems and future challenges, Laser Photonics Rev. 9 (6) (2015) 577–603, http://dx.doi.org/10.1002/lpor.201500122.
[297] J.P. Berenger, A perfectly matched layer for the absorption of electromagnetic waves, J. Comput. Phys. 114 (2) (1994) 185–200, http://dx.doi.org/10.1006/jcph.1994.1159.
[298] Q. Chen, M. Katsurai, P. Aoyagi, An FDTD formulation for dispersive media using a current density, IEEE Trans. Antennas and Propagation 46 (11) (1998) 1739–1746, http://dx.doi.org/10.1109/8.736632.
[299] A.F. Oskooi, D. Roundy, M. Ibanescu, P. Bermel, J. Joannopoulos, S.G. Johnson, Meep: A flexible free-software package for electromagnetic simulations by the FDTD method, Comput. Phys. Comm. 181 (3) (2010) 687–702, http://dx.doi.org/10.1016/J.CPC.2009.11.008.
[300] Optiwave, 2022, https://optiwave.com/.
[301] Lumerical: High-performance photonic simulation software, 2022, https://www.lumerical.com/.
[302] CST studio suite 3D EM simulation and analysis software, 2022, https://www.3ds.com/products-services/simulia/products/cst-studio-suite/.
[303] COMSOL AB, COMSOL Multiphysics, Comsol AB, Stockholm, Sweden, URL https://www.comsol.com.
[304] JCMWave, JCMWave, Berlin, Germany, URL https://www.jcmwave.com.
[305] V. Shankar, A.H. Mohammadian, W.F. Hall, A time-domain, finite-volume treatment for the Maxwell equations, Electromagnetics 10 (1–2) (1990) 127–145, http://dx.doi.org/10.1080/02726349008908232.
[306] N.K. Madsen, R.W. Ziolkowski, A three-dimensional modified finite volume technique for Maxwell's equations, Electromagnetics 10 (1–2) (1990) 147–161, http://dx.doi.org/10.1080/02726349008908233.
[307] O.J.F. Martin, N.B. Piller, Electromagnetic scattering in polarizable backgrounds, Phys. Rev. E 58 (3) (1998) 3909–3915, http://dx.doi.org/10.1103/PhysRevE.58.3909.
[308] J.B. Pendry, L. Martin-Moreno, F.J. Garcia-Vidal, Mimicking surface plasmons with structured surfaces, Science 305 (5685) (2004) 847–848, http://dx.doi.org/10.1126/science.1098999.
[309] A.P. Hibbins, B.R. Evans, J.R. Sambles, Experimental verification of designer surface plasmons, Science 308 (5722) (2005) 670–672, http://dx.doi.org/10.1126/science.1109043.
[310] M. Baraclough, S.S. Seetharaman, I.R. Hooper, W.L. Barnes, Metamaterial analogues of molecular aggregates, ACS Photonics 6 (11) (2019) 3003–3009, http://dx.doi.org/10.1021/acsphotonics.9b01208.

[311] M.P. Bendsoe, O. Sigmund, Topology Optimization: Theory, Methods, and Applications, Springer Science & Business Media, 2003.
[312] J. Jensen, O. Sigmund, Topology optimization for nano-photonics, Laser Photonics Rev. 5 (2) (2011) 308–321, http://dx.doi.org/10.1002/lpor.201000014.
[313] O. Sigmund, On the usefulness of non-gradient approaches in topology optimization, Struct. Multidiscip. Optim. 43 (5) (2011) 589–596, http://dx.doi.org/10.1007/s00158-011-0638-7.
[314] P.I. Borel, A. Harpøth, L.H. Frandsen, M. Kristensen, P. Shi, J.S. Jensen, O. Sigmund, Topology optimization and fabrication of photonic crystal structures, Opt. Express 12 (9) (2004) 1996, http://dx.doi.org/10.1364/OPEX.12.001996.
[315] M. Spuhler, B. Offrein, G.-L. Bona, R. Germann, I. Massarek, D. Erni, A very short planar silica spot-size converter using a nonperiodic segmented waveguide, J. Lightwave Technol. 16 (9) (1998) 1680–1685, http://dx.doi.org/10.1109/50.712252.
[316] D.C. Dobson, S.J. Cox, Maximizing band gaps in two-dimensional photonic crystals, SIAM J. Appl. Math. 59 (6) (1999) 2108–2120, http://dx.doi.org/10.1137/S0036139998338455.
[317] S.J. Cox, D.C. Dobson, Band structure optimization of two-dimensional photonic crystals in H-polarization, J. Comput. Phys. 158 (2) (2000) 214–224, http://dx.doi.org/10.1006/jcph.1999.6415.
[318] J.M. Geremia, J. Williams, H. Mabuchi, Inverse-problem approach to designing photonic crystals for cavity QED experiments, Phys. Rev. E 66 (6) (2002) 066606, http://dx.doi.org/10.1103/PhysRevE.66.066606.
[319] D. Ernil, Application of evolutionary optimization algorithms in computational optics, Appl. Comput. Electromagn. Soc. J. (ACES) 15 (2) (2000) 43–60.
[320] T. Felici, H.W. Engl, On shape optimization of optical waveguides using inverse problem techniques, Inverse Problems 17 (4) (2001) 1141–1162, http://dx.doi.org/10.1088/0266-5611/17/4/338.
[321] J. Jiang, J. Cai, G.P. Nordin, L. Li, Parallel microgenetic algorithm design for photonic crystal and waveguide structures, Opt. Lett. 28 (23) (2003) 2381–2383, http://dx.doi.org/10.1364/ol.28.002381.
[322] G. Kiziltas, D. Psychoudakis, J. Volakis, N. Kikuchi, Topology design optimization of dielectric substrates for bandwidth improvement of a patch antenna, IEEE Trans. Antennas and Propagation 51 (10) (2003) 2732–2743, http://dx.doi.org/10.1109/TAP.2003.817539.
[323] A. Håkansson, J. Sánchez-Dehesa, Inverse designed photonic crystal de-multiplex waveguide coupler, Opt. Express 13 (14) (2005) 5440–5449, http://dx.doi.org/10.1364/OPEX.13.005440.
[324] B. Hermann, U. Haeusler, G. Yadav, A. Kirchner, T. Feurer, C. Welsch, P. Hommelhoff, R. Ischebeck, Inverse-designed narrowband THz radiator for ultrarelativistic electrons, ACS Photonics 9 (4) (2022) 1143–1149, http://dx.doi.org/10.1021/acsphotonics.1c01932.
[325] W. Jin, W. Li, M. Orenstein, S. Fan, Inverse design of lightweight broadband reflector for relativistic lightsail propulsion, ACS Photonics 7 (9) (2020) 2350–2355, http://dx.doi.org/10.1021/acsphotonics.0c00768.
[326] L. He, F. Zhang, H. Zhang, L.-J. Kong, W. Zhang, X. Xu, X. Zhang, Topology-optimized ultracompact all-optical logic devices on silicon photonic platforms, ACS Photonics 9 (2) (2022) 597–604, http://dx.doi.org/10.1021/acsphotonics.1c01569.
[327] T.W. Hughes, M. Minkov, I.A.D. Williamson, S. Fan, Adjoint method and inverse design for nonlinear nanophotonic devices, ACS Photonics 5 (12) (2018) 4781–4787, http://dx.doi.org/10.1021/acsphotonics.8b01522.
[328] Y. Augenstein, C. Rockstuhl, Inverse design of nanophotonic devices with structural integrity, ACS Photonics 7 (8) (2020) 2190–2196, http://dx.doi.org/10.1021/acsphotonics.0c00699.
[329] J.S. Jensen, O. Sigmund, Systematic design of photonic crystal structures using topology optimization: Low-loss waveguide bends, Appl. Phys. Lett. 84 (12) (2004) 2022–2024, http://dx.doi.org/10.1063/1.1688450.
[330] C.M. Lalau-Keraly, S. Bhargava, O.D. Miller, E. Yablonovitch, Adjoint shape optimization applied to electromagnetic design, Opt. Express 21 (18) (2013) 21693, http://dx.doi.org/10.1364/oe.21.021693.
[331] O. Pironneau, On optimum design in fluid mechanics, J. Fluid Mech. 64 (1) (1974) 97–110, http://dx.doi.org/10.1017/S0022112074002023.
[332] A. Jameson, Aerodynamic design via control theory, J. Sci. Comput. 3 (3) (1988) 233–260, http://dx.doi.org/10.1007/BF01061285.
[333] O.D. Miller, C.W. Hsu, M.T.H. Reid, W. Qiu, B.G. DeLacy, J.D. Joannopoulos, M. Soljačić, S.G. Johnson, Fundamental limits to extinction by metallic nanoparticles, Phys. Rev. Lett. 112 (12) (2014) 123903, http://dx.doi.org/10.1103/PhysRevLett.112.123903.
[334] S. Molesky, Z. Lin, A.Y. Piggott, W. Jin, J. Vucković, A.W. Rodriguez, Inverse design in nanophotonics, Nat. Photonics 12 (11) (2018) 659–670, http://dx.doi.org/10.1038/s41566-018-0246-9.
[335] W.T. Chen, A.Y. Zhu, F. Capasso, Flat optics with dispersion-engineered metasurfaces, Nat. Rev. Mater. 5 (8) (2020) 604–620, http://dx.doi.org/10.1038/s41578-020-0203-3.
[336] T. Badloe, J. Lee, J. Seong, J. Rho, Tunable metasurfaces: The path to fully active nanophotonics, Adv. Photonics Res. 2 (9) (2021) 2000205, http://dx.doi.org/10.1002/adpr.202000205.
[337] S. So, T. Badloe, J. Noh, J. Bravo-Abad, J. Rho, Deep learning enabled inverse design in nanophotonics, Nanophotonics 9 (5) (2020) 1041–1057, http://dx.doi.org/10.1515/nanoph-2019-0474.
[338] W. Ma, Z. Liu, Z.A. Kudyshev, A. Boltasseva, W. Cai, Y. Liu, Deep learning for the design of photonic structures, Nat. Photonics 15 (2) (2021) 77–90, http://dx.doi.org/10.1038/s41566-020-0685-y.
[339] P.R. Wiecha, A. Arbouet, A. Arbouet, C. Girard, C. Girard, O.L. Muskens, O.L. Muskens, Deep learning in nano-photonics: Inverse design and beyond, Photonics Res. 9 (5) (2021) B182–B200, http://dx.doi.org/10.1364/PRJ.415960.
[340] D. Midtvedt, V. Mylnikov, A. Stilgoe, M. Käll, H. Rubinsztein-Dunlop, G. Volpe, Deep learning in light–matter interactions, Nanophotonics 11 (14) (2022) 3189–3214, http://dx.doi.org/10.1515/nanoph-2022-0197.
[341] R.E. Christiansen, R.E. Christiansen, O. Sigmund, O. Sigmund, Inverse design in photonics by topology optimization: Tutorial, J. Opt. Soc. Amer. B 38 (2) (2021) 496–509, http://dx.doi.org/10.1364/JOSAB.406048.
[342] R.E. Christiansen, R.E. Christiansen, O. Sigmund, O. Sigmund, Compact 200 line MATLAB code for inverse design in photonics by topology optimization: Tutorial, J. Opt. Soc. Amer. B 38 (2) (2021) 510–520, http://dx.doi.org/10.1364/JOSAB.405955.
[343] G.H. Ahn, K.Y. Yang, R. Trivedi, A.D. White, L. Su, J. Skarda, J. Vučković, Photonic inverse design of on-chip microresonators, ACS Photonics 9 (6) (2022) 1875–1881, http://dx.doi.org/10.1021/acsphotonics.2c00020.
[344] J. Riishede, O. Sigmund, Inverse design of dispersion compensating optical fiber using topology optimization, J. Opt. Soc. Amer. B 25 (1) (2008) 88–97, http://dx.doi.org/10.1364/JOSAB.25.000088.
[345] D. Vercruysse, N.V. Sapra, L. Su, J. Vuckovic, Dispersion engineering with photonic inverse design, IEEE J. Sel. Top. Quantum Electron. 26 (2) (2020) 1–6, http://dx.doi.org/10.1109/JSTQE.2019.2950803.
[346] Y. Brûlé, Y. Brûlé, P. Wiecha, A. Cuche, V. Paillard, G.C. des Francs, G.C. des Francs, Magnetic and electric Purcell factor control through geometry optimization of high index dielectric nanostructures, Opt. Express 30 (12) (2022) 20360–20372, http://dx.doi.org/10.1364/OE.460168.
[347] N. Lebbe, A. Glière, K. Hassan, C. Dapogny, E. Oudet, Shape optimization for the design of passive mid-infrared photonic components, Opt. Quantum Electron. 51 (5) (2019) 166, http://dx.doi.org/10.1007/s11082-019-1849-1.
[348] D.C. Dobson, L.B. Simeonova, Optimization of periodic composite structures for sub-wavelength focusing, Appl. Math. Optim. 60 (1) (2009) 133–150, http://dx.doi.org/10.1007/s00245-008-9063-8.
[349] A. Zhan, R. Gibson, J. Whitehead, E. Smith, J.R. Hendrickson, A. Majumdar, Controlling three-dimensional optical fields via inverse Mie scattering, Sci. Adv. 5 (10) (2019) eaax4769, http://dx.doi.org/10.1126/sciadv.aax4769.

[350] J. Jiang, J.A. Fan, Global optimization of dielectric metasurfaces using a physics-driven neural network, Nano Lett. 19 (8) (2019) 5366–5372, http://dx.doi.org/10.1021/acs.nanolett.9b01857.
[351] J.A. Fan, Freeform metasurface design based on topology optimization, MRS Bull. 45 (3) (2020) 196–201, http://dx.doi.org/10.1557/mrs.2020.62.
[352] T. Phan, D. Sell, E.W. Wang, S. Doshay, K. Edee, J. Yang, J.A. Fan, High-efficiency, large-area, topology-optimized metasurfaces, Light: Sci. Appl. 8 (1) (2019) 48, http://dx.doi.org/10.1038/s41377-019-0159-5.
[353] Z. Li, R. Pestourie, J.-S. Park, Y.-W. Huang, S.G. Johnson, F. Capasso, Inverse design enables large-scale high-performance meta-optics reshaping virtual reality, Nature Commun. 13 (1) (2022) 2409, http://dx.doi.org/10.1038/s41467-022-29973-3.
[354] B. Shen, P. Wang, R. Polson, R. Menon, Ultra-high-efficiency metamaterial polarizer, Optica 1 (5) (2014) 356–360, http://dx.doi.org/10.1364/OPTICA.1.000356.
[355] D. Sell, J. Yang, S. Doshay, R. Yang, J.A. Fan, Large-angle, multifunctional metagratings based on freeform multimode geometries, Nano Lett. 17 (6) (2017) 3752–3757, http://dx.doi.org/10.1021/acs.nanolett.7b01082.
[356] P. Thureja, G.K. Shirmanesh, K.T. Fountaine, R. Sokhoyan, M. Grajower, H.A. Atwater, Array-level inverse design of beam steering active metasurfaces, ACS Nano 14 (11) (2020) 15042–15055, http://dx.doi.org/10.1021/acsnano.0c05026.
[357] C.-H. Lin, Y.-S. Chen, J.-T. Lin, H.C. Wu, H.-T. Kuo, C.-F. Lin, P. Chen, P.C. Wu, Automatic inverse design of high-performance beam-steering metasurfaces via genetic-type tree optimization, Nano Lett. 21 (12) (2021) 4981–4989, http://dx.doi.org/10.1021/acs.nanolett.1c00720.
[358] H. Cai, S. Srinivasan, D.A. Czaplewski, A.B.F. Martinson, D.J. Gosztola, L. Stan, T. Loeffler, S.K.R.S. Sankaranarayanan, D. López, Inverse design of metasurfaces with non-local interactions, npj Comput. Mater. 6 (1) (2020) 1–8, http://dx.doi.org/10.1038/s41524-020-00369-5.
[359] F. Callewaert, V. Velev, P. Kumar, A.V. Sahakian, K. Aydin, Inverse-designed broadband all-dielectric electromagnetic metadevices, Sci. Rep. 8 (1) (2018) 1358, http://dx.doi.org/10.1038/s41598-018-19796-y.
[360] S.S. Panda, H.S. Vyas, R.S. Hegde, Robust inverse design of all-dielectric metasurface transmission-mode color filters, Opt. Mater. Express 10 (12) (2020) 3145–3159, http://dx.doi.org/10.1364/OME.409186.
[361] R. Singh, Y. Nie, M. Gao, A.M. Agarwal, B.W. Anthony, Inverse design of photonic meta-structure for beam collimation in on-chip sensing, Sci. Rep. 11 (1) (2021) 5343, http://dx.doi.org/10.1038/s41598-021-84841-2.
[362] C. Sitawarin, W. Jin, Z. Lin, A.W. Rodriguez, Inverse-designed photonic fibers and metasurfaces for nonlinear frequency conversion [Invited], Photonics Res. 6 (5) (2018) B82–B89, http://dx.doi.org/10.1364/PRJ.6.000B82.
[363] A.S. Backer, Computational inverse design for cascaded systems of metasurface optics, Opt. Express 27 (21) (2019) 30308–30331, http://dx.doi.org/10.1364/OE.27.030308.
[364] Z. Li, W. Liu, D. Ma, S. Yu, H. Cheng, D.-Y. Choi, J. Tian, S. Chen, Inverse design of few-layer metasurfaces empowered by the matrix theory of multilayer optics, Phys. Rev. A 17 (2) (2022) 024008, http://dx.doi.org/10.1103/PhysRevApplied.17.024008.
[365] P. Camayd-Muñoz, G. Roberts, C. Ballew, M. Debbas, A. Faraon, Inverse designed shape-reconfigurable multifunctional photonics, in: 2020 Conference on Lasers and Electro-Optics (CLEO), 2020, pp. 1–2.
[366] H. Alaeian, A.C. Atre, J.A. Dionne, Optimized light absorption in Si wire array solar cells, J. Opt. 14 (2) (2012) 024006, http://dx.doi.org/10.1088/2040-8978/14/2/024006.
[367] M.B. Dühring, O. Sigmund, Optimization of extraordinary optical absorption in plasmonic and dielectric structures, J. Opt. Soc. Amer. B 30 (5) (2013) 1154–1160, http://dx.doi.org/10.1364/JOSAB.30.001154.
[368] P. Wang, R. Menon, Optimization of periodic nanostructures for enhanced light-trapping in ultra-thin photovoltaics, Opt. Express 21 (5) (2013) 6274–6285, http://dx.doi.org/10.1364/OE.21.006274.
[369] V. Ganapati, O.D. Miller, E. Yablonovitch, Light trapping textures designed by electromagnetic optimization for subwavelength thick solar cells, IEEE J. Photovolt. 4 (1) (2014) 175–182, http://dx.doi.org/10.1109/JPHOTOV.2013.2280340.
[370] G. Kim, J.A. Dominguez-Caballero, H. Lee, D.J. Friedman, R. Menon, Increased photovoltaic power output via diffractive spectrum separation, Phys. Rev. Lett. 110 (12) (2013) 123901, http://dx.doi.org/10.1103/PhysRevLett.110.123901.
[371] T.P. Xiao, O.S. Cifci, S. Bhargava, H. Chen, T. Gissibl, W. Zhou, H. Giessen, K.C. Toussaint, E. Yablonovitch, P.V. Braun, Diffractive spectral-splitting optical element designed by adjoint-based electromagnetic optimization and fabricated by femtosecond 3D direct laser writing, ACS Photonics 3 (5) (2016) 886–894, http://dx.doi.org/10.1021/acsphotonics.6b00066.
[372] W.-K. Lee, S. Yu, C.J. Engel, T. Reese, D. Rhee, W. Chen, T.W. Odom, Concurrent design of quasi-random photonic nanostructures, Proc. Natl. Acad. Sci. 114 (33) (2017) 8734–8739, http://dx.doi.org/10.1073/pnas.1704711114.
[373] X. Jiang, H. Yuan, D. Chen, Z. Zhang, T. Du, H. Ma, J. Yang, Metasurface based on inverse design for maximizing solar spectral absorption, Adv. Opt. Mater. 9 (19) (2021) 2100575, http://dx.doi.org/10.1002/adom.202100575.
[374] Y. Elesin, B.S. Lazarov, J.S. Jensen, O. Sigmund, Design of robust and efficient photonic switches using topology optimization, Photon. Nanostruct.: Fundam. Appl. 10 (1) (2012) 153–165, http://dx.doi.org/10.1016/j.photonics.2011.10.003.
[375] E. Khoram, A. Chen, D. Liu, L. Ying, Q. Wang, M. Yuan, Z. Yu, Nanophotonic media for artificial neural inference, Photonics Res. 7 (8) (2019) 823–827, http://dx.doi.org/10.1364/PRJ.7.000823.
[376] L. Bi, J. Hu, P. Jiang, D.H. Kim, G.F. Dionne, L.C. Kimerling, C.A. Ross, On-chip optical isolation in monolithically integrated non-reciprocal optical resonators, Nat. Photonics 5 (12) (2011) 758–762, http://dx.doi.org/10.1038/nphoton.2011.270.
[377] K.Y. Yang, J. Skarda, M. Cotrufo, A. Dutt, G.H. Ahn, M. Sawaby, D. Vercruysse, A. Arbabian, S. Fan, A. Alù, J. Vučković, Inverse-designed non-reciprocal pulse router for chip-based LiDAR, Nat. Photonics 14 (6) (2020) 369–374, http://dx.doi.org/10.1038/s41566-020-0606-0.
[378] Q. Wang, A.V. Chumak, P. Pirro, Inverse-design magnonic devices, Nature Commun. 12 (1) (2021) 2636, http://dx.doi.org/10.1038/s41467-021-22897-4.
[379] L.T. Neustock, P.C. Hansen, Z.E. Russell, L. Hesselink, Inverse design tool for ion optical devices using the adjoint variable method, Sci. Rep. 9 (1) (2019) 11031, http://dx.doi.org/10.1038/s41598-019-47408-w.
[380] D. Kouznetsov, D. Kouznetsov, D. Kouznetsov, O. Arisev, O. Arisev, P.V. Dorpe, P.V. Dorpe, N. Verellen, N. Verellen, Inverse design assisted coherent optical lattices, Opt. Express 30 (7) (2022) 11384–11393, http://dx.doi.org/10.1364/OE.455466.
[381] R.E. Christiansen, F. Wang, O. Sigmund, Topological insulators by topology optimization, Phys. Rev. Lett. 122 (23) (2019) 234502, http://dx.doi.org/10.1103/PhysRevLett.122.234502.
[382] E. Nussbaum, E. Sauer, S. Hughes, Inverse design of broadband and lossless topological photonic crystal waveguide modes, Opt. Lett. 46 (7) (2021) 1732–1735, http://dx.doi.org/10.1364/OL.420080.
[383] R.E. Christiansen, R.E. Christiansen, J. Michon, M. Benzaouia, O. Sigmund, S.G. Johnson, Inverse design of nanoparticles for enhanced Raman scattering, Opt. Express 28 (4) (2020) 4444–4462, http://dx.doi.org/10.1364/OE.28.004444.
[384] E. Rozenberg, A. Karnieli, O. Yesharim, J. Foley-Comer, S. Trajtenberg-Mills, S. Trajtenberg-Mills, D. Freedman, A.M. Bronstein, A. Arie, Inverse design of spontaneous parametric downconversion for generation of high-dimensional qudits, Optica 9 (6) (2022) 602–615, http://dx.doi.org/10.1364/OPTICA.451115.
[385] R. Bennett, Inverse design of environment-induced coherence, Phys. Rev. A 103 (1) (2021) 013706, http://dx.doi.org/10.1103/PhysRevA.103.013706.
[386] O. Diekmann, D. Lentrodt, J. Evers, Inverse design approach to x-ray quantum optics with Mössbauer nuclei in thin-film cavities, Phys. Rev. A 105 (1) (2022) 013715, http://dx.doi.org/10.1103/PhysRevA.105.013715.

[387] U. Haeusler, M. Seidling, P. Yousefi, P. Hommelhoff, Boosting the efficiency of Smith–Purcell radiators using nanophotonic inverse design, ACS Photonics 9 (2) (2022) 664–671, http://dx.doi.org/10.1021/acsphotonics.1c01687.
[388] C. Roques-Carmes, N. Rivera, A. Ghorashi, S.E. Kooi, Y. Yang, Z. Lin, J. Beroz, A. Massuda, J. Sloan, N. Romeo, Y. Yu, J.D. Joannopoulos, I. Kaminer, S.G. Johnson, M. Soljačić, A framework for scintillation in nanophotonics, Science 375 (6583) (2022) eabm9293, http://dx.doi.org/10.1126/science.abm9293.
[389] S. Chakravarthi, P. Chao, P. Chao, C. Pederson, S. Molesky, A. Ivanov, K. Hestroffer, F. Hatami, A.W. Rodriguez, K.-M.C. Fu, K.-M.C. Fu, Inverse-designed photon extractors for optically addressable defect qubits, Optica 7 (12) (2020) 1805–1811, http://dx.doi.org/10.1364/OPTICA.408611.
[390] B. Neşeli, Y.A. Yilmaz, H. Kurt, M. Turduev, Inverse design of ultra-compact photonic gates for all-optical logic operations, J. Phys. D: Appl. Phys. 55 (21) (2022) 215107, http://dx.doi.org/10.1088/1361-6463/ac5660.
[391] C. Dory, D. Vercruysse, K.Y. Yang, N.V. Sapra, A.E. Rugar, S. Sun, D.M. Lukin, A.Y. Piggott, J.L. Zhang, M. Radulaski, K.G. Lagoudakis, L. Su, J. Vučković, Inverse-designed diamond photonics, Nature Commun. 10 (1) (2019) 3309, http://dx.doi.org/10.1038/s41467-019-11343-1.
[392] M. Perestjuk, H. Boerma, A. Schindler, S. Keyvaninia, P. Runge, M. Schell, Inverse-designed InP-based polarization rotator-splitter, in: Optical Fiber Communication Conference (OFC) 2021 (2021), Paper W6A.49, Optica Publishing Group, 2021, p. W6A.49, http://dx.doi.org/10.1364/OFC.2021.W6A.49.
[393] M. Smit, K. Williams, J. van der Tol, Past, present, and future of InP-based photonic integration, APL Photonics 4 (5) (2019) 050901, http://dx.doi.org/10.1063/1.5087862.
[394] O. Sigmund, Manufacturing tolerant topology optimization, Acta Mech. Sinica 25 (2) (2009) 227–239, http://dx.doi.org/10.1007/s10409-009-0240-z.
[395] P.I. Borel, B. Bilenberg, L.H. Frandsen, T. Nielsen, J. Fage-Pedersen, A.V. Lavrinenko, J.S. Jensen, O. Sigmund, A. Kristensen, Imprinted silicon-based nanophotonics, Opt. Express 15 (3) (2007) 1261–1266, http://dx.doi.org/10.1364/OE.15.001261.
[396] W.R. Frei, H.T. Johnson, K.D. Choquette, Optimization of a single defect photonic crystal laser cavity, J. Appl. Phys. 103 (3) (2008) 033102, http://dx.doi.org/10.1063/1.2838173.
[397] A. Oskooi, A. Mutapcic, S. Noda, J.D. Joannopoulos, S.P. Boyd, S.G. Johnson, Robust optimization of adiabatic tapers for coupling to slow-light photonic-crystal waveguides, Opt. Express 20 (19) (2012) 21558–21575, http://dx.doi.org/10.1364/OE.20.021558.
[398] D. Vercruysse, N.V. Sapra, L. Su, R. Trivedi, J. Vučković, Analytical level set fabrication constraints for inverse design, Sci. Rep. 9 (1) (2019) 8999, http://dx.doi.org/10.1038/s41598-019-45026-0.
[399] A.Y. Piggott, E.Y. Ma, L. Su, G.H. Ahn, N.V. Sapra, D. Vercruysse, A.M. Netherton, A.S. Khope, J.E. Bowers, J. Vučković, Inverse-designed photonics for semiconductor foundries, ACS Photonics 7 (3) (2020) 569–575, http://dx.doi.org/10.1021/acsphotonics.9b01540.
[400] G. Zhang, D.-X. Xu, Y. Grinberg, O. Liboiron-Ladouceur, Topological inverse design of nanophotonic devices with energy constraint, Opt. Express 29 (8) (2021) 12681–12695, http://dx.doi.org/10.1364/OE.421202.
[401] G. Zhang, D.-X. Xu, Y. Grinberg, O. Liboiron-Ladouceur, Experimental demonstration of robust nanophotonic devices optimized by topological inverse design with energy constraint, Photonics Res. 10 (7) (2022) 1787–1802, http://dx.doi.org/10.1364/PRJ.457066.
[402] H. Men, K.Y.K. Lee, R.M. Freund, J. Peraire, S.G. Johnson, Robust topology optimization of three-dimensional photonic-crystal band-gap structures, Opt. Express 22 (19) (2014) 22632–22648, http://dx.doi.org/10.1364/OE.22.022632.
[403] O. Sigmund, K. Hougaard, Geometric properties of optimal photonic crystals, Phys. Rev. Lett. 100 (15) (2008) 153904, http://dx.doi.org/10.1103/PhysRevLett.100.153904.
[404] G. Angeris, J. Vučković, S. Boyd, Heuristic methods and performance bounds for photonic design, Opt. Express 29 (2) (2021) 2827–2854, http://dx.doi.org/10.1364/OE.415052.
[405] O.D. Miller, S.G. Johnson, A.W. Rodriguez, Shape-independent limits to near-field radiative heat transfer, Phys. Rev. Lett. 115 (20) (2015) 204302, http://dx.doi.org/10.1103/PhysRevLett.115.204302.
[406] A. Arbabi, A. Faraon, Fundamental limits of ultrathin metasurfaces, Sci. Rep. 7 (1) (2017) 43722, http://dx.doi.org/10.1038/srep43722.
[407] J. Céa, S. Garreau, P. Guillaume, M. Masmoudi, The shape and topological optimizations connection, Comput. Methods Appl. Mech. Engrg. 188 (4) (2000) 713–726, http://dx.doi.org/10.1016/S0045-7825(99)00357-6.
[408] M. Masmoudi, J. Pommier, B. Samet, The topological asymptotic expansion for the Maxwell equations and some applications, Inverse Problems 21 (2) (2005) 547–564, http://dx.doi.org/10.1088/0266-5611/21/2/008.
[409] S. Osher, J.A. Sethian, Fronts propagating with curvature-dependent speed: Algorithms based on Hamilton-Jacobi formulations, J. Comput. Phys. 79 (1) (1988) 12–49, http://dx.doi.org/10.1016/0021-9991(88)90002-2.
[410] C.Y. Kao, S. Osher, E. Yablonovitch, Maximizing band gaps in two-dimensional photonic crystals by using level set methods, Appl. Phys. B 81 (2–3) (2005) 235–244, http://dx.doi.org/10.1007/s00340-005-1877-3.
[411] N. Lebbe, C. Dapogny, E. Oudet, K. Hassan, A. Gliere, Robust shape and topology optimization of nanophotonic devices using the level set method, J. Comput. Phys. 395 (2019) 710–746, http://dx.doi.org/10.1016/j.jcp.2019.06.057.
[412] C. Yeung, D. Ho, B. Pham, K.T. Fountaine, Z. Zhang, K. Levy, A.P. Raman, Enhancing adjoint optimization-based photonic inverse design with explainable machine learning, ACS Photonics 9 (5) (2022) 1577–1585, http://dx.doi.org/10.1021/acsphotonics.1c01636.
[413] S. Yang, H. Jia, J. Niu, X. Fu, L. Yang, CMOS-compatible ultra-compact silicon multimode waveguide bend based on inverse design method, Opt. Commun. 523 (2022) 128733, http://dx.doi.org/10.1016/j.optcom.2022.128733.
[414] H. Huang, X. Zhang, F. Gan, X. Ni, Fabrication-friendly random meta-atom generation for phase-shifting metasurfaces, IEEE Photonics J. 14 (1) (2022) 1–4, http://dx.doi.org/10.1109/JPHOT.2022.3144434.
[415] E. Khoram, X. Qian, M. Yuan, Z. Yu, Controlling the minimal feature sizes in adjoint optimization of nanophotonic devices using B-spline surfaces, Opt. Express 28 (5) (2020) 7060–7069, http://dx.doi.org/10.1364/OE.384438.
[416] R. Mattoso, L.H. Gabrielli, A.A. Novotny, Topology design optimization of nanophotonic devices for energy concentration, Appl. Math. Model. 104 (2022) 517–530, http://dx.doi.org/10.1016/j.apm.2021.11.030.
[417] S. Yang, S. Yang, H. Jia, J. Niu, J. Niu, X. Fu, X. Fu, L. Yang, L. Yang, Guided-mode based arbitrary signal switching through an inverse-designed ultra-compact mode switching device, Opt. Express 30 (9) (2022) 15446–15457, http://dx.doi.org/10.1364/OE.457842.
[418] J.C. Araújo, E. Wadbro, Shape optimization for the strong directional scattering of dielectric nanorods, Internat. J. Numer. Methods Engrg. 122 (15) (2021) 3683–3704, http://dx.doi.org/10.1002/nme.6677.
[419] N. Lebbe, A. Glière, K. Hassan, High-efficiency and broadband photonic polarization rotator based on multilevel shape optimization, Opt. Lett. 44 (8) (2019) 1960–1963, http://dx.doi.org/10.1364/OL.44.001960.
[420] R.A. de Paula, Y.R.R. Bustamante, I. Aldaya, Broadband and highly efficient integrated polarization rotator designed by topology optimization, Appl. Opt. 61 (2) (2022) 463, http://dx.doi.org/10.1364/AO.444985.
[421] L. Novotny, Strong coupling, energy splitting, and level crossings: A classical perspective, Amer. J. Phys. 78 (11) (2010) 1199–1202, http://dx.doi.org/10.1119/1.3471177.
[422] D. Sanvitto, S. Kéna-Cohen, The road towards polaritonic devices, Nature Mater. 15 (10) (2016) 1061–1073, http://dx.doi.org/10.1038/nmat4668.
[423] J.A. Hutchison, T. Schwartz, C. Genet, E. Devaux, T.W. Ebbesen, Modifying chemical landscapes by coupling to vacuum fields, Angew. Chem. Int. Ed. 51 (7) (2012) 1592–1596, http://dx.doi.org/10.1002/anie.201107033.

[424] J. Flick, N. Rivera, P. Narang, Strong light-matter coupling in quantum chemistry and quantum photonics, Nanophotonics 7 (9) (2018) 1479–1501, http://dx.doi.org/10.1515/nanoph-2018-0067.
[425] J. Feist, J. Galego, F.J. Garcia-Vidal, Polaritonic chemistry with organic molecules, ACS Photonics 5 (1) (2018) 205–216, http://dx.doi.org/10.1021/acsphotonics.7b00680.
[426] F.J. Garcia-Vidal, C. Ciuti, T.W. Ebbesen, Manipulating matter by strong coupling to vacuum fields, Science 373 (6551) (2021) eabd0336, http://dx.doi.org/10.1126/science.abd0336.
[427] J. Fregoni, F.J. Garcia-Vidal, J. Feist, Theoretical challenges in polaritonic chemistry, ACS Photonics 9 (4) (2022) 1096–1107, http://dx.doi.org/10.1021/acsphotonics.1c01749.
[428] M. Urbieta, M. Barbry, Y. Zhang, P. Koval, D. Sánchez-Portal, N. Zabala, J. Aizpurua, Atomic-scale lightning rod effect in plasmonic picocavities: A classical view to a quantum effect, ACS Nano 12 (1) (2018) 585–595, http://dx.doi.org/10.1021/acsnano.7b07401.
[429] F. Benz, M.K. Schmidt, A. Dreismann, R. Chikkaraddy, Y. Zhang, A. Demetriadou, C. Carnegie, H. Ohadi, B. de Nijs, R. Esteban, J. Aizpurua, J.J. Baumberg, Single-molecule optomechanics in "picocavities", Science (2016) http://dx.doi.org/10.1126/science.aah5243.
[430] M. Ruggenthaler, J. Flick, C. Pellegrini, H. Appel, I.V. Tokatly, A. Rubio, Quantum-electrodynamical density-functional theory: Bridging quantum optics and electronic-structure theory, Phys. Rev. A 90 (1) (2014) 012508, http://dx.doi.org/10.1103/PhysRevA.90.012508.
[431] M. Ruggenthaler, N. Tancogne-Dejean, J. Flick, H. Appel, A. Rubio, From a quantum-electrodynamical light–matter description to novel spectroscopies, Nat. Rev. Chem. 2 (3) (2018) 1–16, http://dx.doi.org/10.1038/s41570-018-0118.
[432] C. Pellegrini, J. Flick, I.V. Tokatly, H. Appel, A. Rubio, Optimized effective potential for quantum electrodynamical time-dependent density functional theory, Phys. Rev. Lett. 115 (9) (2015) 093001, http://dx.doi.org/10.1103/PhysRevLett.115.093001.
[433] J. Flick, M. Ruggenthaler, H. Appel, A. Rubio, Kohn–Sham approach to quantum electrodynamical density-functional theory: Exact time-dependent effective potentials in real space, Proc. Natl. Acad. Sci. 112 (50) (2015) 15285–15290, http://dx.doi.org/10.1073/pnas.1518224112.
[434] J. Flick, C. Schäfer, M. Ruggenthaler, H. Appel, A. Rubio, Ab initio optimized effective potentials for real molecules in optical cavities: Photon contributions to the molecular ground state, ACS Photonics 5 (3) (2018) 992–1005, http://dx.doi.org/10.1021/acsphotonics.7b01279.
[435] I.V. Tokatly, Time-dependent density functional theory for many-electron systems interacting with cavity photons, Phys. Rev. Lett. 110 (23) (2013) 233001, http://dx.doi.org/10.1103/PhysRevLett.110.233001.
[436] J. Flick, P. Narang, Cavity-correlated electron-nuclear dynamics from first principles, Phys. Rev. Lett. 121 (11) (2018) 113002, http://dx.doi.org/10.1103/PhysRevLett.121.113002.
[437] D.S. Wang, T. Neuman, J. Flick, P. Narang, Light–matter interaction of a molecule in a dissipative cavity from first principles, J. Chem. Phys. 154 (10) (2021) 104109, http://dx.doi.org/10.1063/5.0036283.
[438] M.K. Svendsen, Y. Kurman, P. Schmidt, F. Koppens, I. Kaminer, K.S. Thygesen, Combining density functional theory with macroscopic QED for quantum light-matter interactions in 2D materials, Nature Commun. 12 (1) (2021) 2778, http://dx.doi.org/10.1038/s41467-021-23012-3.